Reduction in ground vibrations by the use of wave obstacles

Persson, Peter

2013

LUND UNIVERSITY

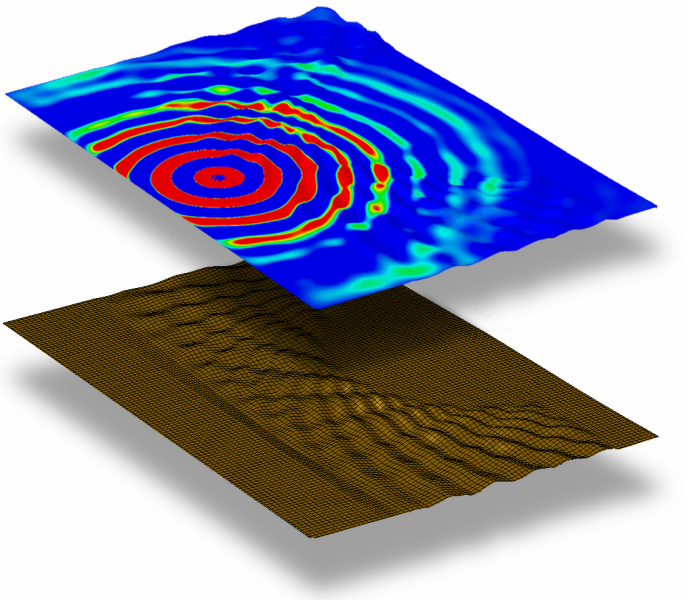

REDUCTION IN GROUND VIBRATIONS BY THE USE OF WAVE OBSTACLES

PETER PERSSON

Structural Mechanics

Licentiate Dissertation

DEPARTMENT OF CONSTRUCTION SCIENCES
DIVISION OF STRUCTURAL MECHANICS

ISRN LUTVDG/TVSM--13/3072--SE (1-102) | ISSN 0281-6679
LICENTIATE DISSERTATION

REDUCTION IN GROUND VIBRATIONS BY THE USE OF WAVE OBSTACLES

PETER PERSSON

Printed by Media-Tryck LU, Lund, Sweden, September 2013 *(Pl)*.

For information, address:
Div. of Structural Mechanics, LTH, Lund University, Box 118, SE-221 00 Lund, Sweden.
Homepage: http://www.byggmek.lth.se

Acknowledgments

The work presented in the thesis was carried out at the Division of Structural Mechanics at Lund University.

I would like to direct gratitude to my supervisors Prof. Göran Sandberg and Ph.D. Kent Persson at the Division of Structural Mechanics for all of their guidance and support during this work, as well as for our interesting and helpful discussions. I would also like to thank the staff at the Department of Construction Sciences for the delightful discussions we have had during lunches and coffee breaks. Mr. Bo Zadig is gratefully acknowledged for his excellent work on various of the figures in the thesis.

The financial support for this work provided by the Silent Spaces project, a part of the EU program Interreg IVA, is gratefully acknowledged.

I would like to thank my parents, Inger Nordeng and Ronny Persson, for always being there for me and for their never-ending patience and their endless support. Special thanks is directed to my father, who has taught me to never be satisfied with less than I can achieve, which has made the thesis possible to carry out and complete.

Lund, August 2013

Peter Persson

Abstract

The increasing size of the population results in that unbuilt spaces needing to be used for the construction of new facilities. Large construction sites can generate disturbing vibrations to nearby buildings, both while construction is underway and afterwards through the operation of subways, for example. The establishment of new areas close to, for example, motorways and railways increases the risk of disturbing vibrations being propagated to the new buildings. It is important that efficient methods for reducing ground vibrations be available when densely built areas are being planned.

Reduction in ground vibrations by use of wave obstacles is investigated here by use of numerical simulations, trenches and shaped landscapes being considered as wave obstacles.

The effects of geometric parameters on open trenches, material parameters in filled trenches, and of infiltrated water in open trenches, were examined in appended Paper A. The finite element method involving use of both finite and infinite elements in the frequency domain was employed. In investigating the effects of the infiltrated water, account was taken of fluid-structure interaction. The finite element model, in which plane strain conditions were assumed, was applied to a road, the bedrock, two layers of soil and a trench. The depth of the trench and the elastic modulus of the solid material that was inserted into it were found to be the most important parameters to consider. The results concerning the infiltration of water into an open trench indicated the presence of water there to increase the vibration levels.

Reduction in traffic-induced ground vibrations by use of shaped landscapes is investigated in appended Paper B, the effects of shaping the landscape surrounding a high-tech facility and using the landscape as a wave obstacle being studied. The effects of the geometric parameters of a shaped landscape were examined in parametric studies. An architectural landscape design was also investigated in terms of its effectiveness in reducing traffic-induced ground vibrations. The finite element method involving use of both finite and infinite elements in the frequency domain was employed, the finite element models employed concerning a layer of soil and the underlying bedrock. It was found that anywhere from an appreciable reduction to an appreciable amplification of the vibrations can occur, depending upon the geometric parameters of the shaped landscape.

Both types of ground modifications that were investigated were shown to be able to achieve an appreciable reduction in the level of vibration. Both the use of a trench filled with a solid material and use of a shaped landscape were found to result in a reduction in the level of vibrations of approximately 35 %. Both these types of methods can thus be regarded as being suitable for making it possible in this respect for buildings to be constructed close to vibration sources.

Contents

Part I

Introduction and overview of the work

1 Introduction

As the population size increases an increase is required too in such facilities as dwellings, subway stations and industrial buildings. This results in that unbuilt spaces both within cities and in areas nearby, as well as motorways and railways, for example, needing to be used for the construction of new facilities. Large urban construction sites can generate disturbing vibrations in residential buildings nearby, both while construction, is underway, and afterwards through the operation of subways, for example. The establishment of new residential areas close to motorways and railways also increases the risk of disturbing vibrations stemming from the latter two sources being propagated to the buildings that are constructed. It is important that efficient methods for reducing ground vibrations be available when densely built areas are being planned.

It is not simply residential buildings that need to be isolated from disturbing vibrations. Occasionally, very strict vibrational requirements are also specified for sensitive equipment in high-tech facilities such as radar towers and synchrotrons. Regardless of whether or not the sensitive equipment in itself is a significant source of vibration, it is important that it be isolated from external vibrations. High-tech facilities are often located in the vicinity of sources of vibrations of significant amplitude, radar towers often being found near rocket-launching facilities, for example, and synchrotrons near heavily trafficked roads, the latter for logistic reasons. Traffic-induced ground vibrations can propagate to facilities nearby and lead to the vibration requirements for sensitive equipment there being exceeded. The vibrations can originate, for example, from irregularities in the asphalt layer, from speed bumps and from vehicles that enter and exit a bridge.

It can be desirable under such conditions to reduce the ground vibrations by use of wave obstacles. The traffic-induced vibrations involved can be reduced by various means. The present thesis deals with two of these methods, the one being shaping of the landscape and the other being the installing of a trench between the road and the facility.

It is known from previous numerical studies [1, 2, 3] concerning the synchrotron facility MAX IV in Lund, Sweden, that the material parameters of the soil there have a strong effect on the vibration levels that occur in sensitive parts of the facility, whereas structural modifications of the facility itself have only, in practice, a slight effect. Most of the vibration energy produced by vibrations induced on the ground surface is transmitted by Rayleigh surface waves that propagate close to the ground surface. Since Rayleigh waves attenuate with horizontal distance, as well as with depth, the ground vibrations can be reduced by constructing a suitable wave obstacle in the ground between the wave source and the facility that is to be protected.

Figure 1.1: The MAX IV facility as it is expected to appear, as rendering in a drawing by the architect bureaus FOJAB and Snøhetta.

1.1 Aims and objectives

The general aim of the thesis is to investigate the use of trenches as well as of shaped landscapes as wave obstacles for reducing the level of incident traffic-induced ground vibrations. Numerical simulations by means of the finite element (FE) method are performed, both two- and three-dimensional dynamic analyses being carried out. The analyses involve parametric studies examining the effects of varying different material and geometric parameters in the FE models employed.

The ultimate objective is to obtain a better understanding of the effectiveness of wave obstacles for reduction of incident ground vibrations. Use of effective wave obstacles enables facilities to be built closer to disturbing vibration sources than would otherwise be possible.

1.2 The synchrotron facility MAX IV

The degree of reduction expected to be achieved in the level of vibration that occur at the new synchrotron facility MAX IV, belonging to MAX-lab, serves as a numerical example in the analyses of vibration reduction involved; see Figure 1.1 for an architectural sketch of the facility. The MAX IV facility is described further, for example, in [4].

The MAX-lab, MAX referring to Microtron Accelerator for X-rays, is a Swedish national laboratory for research concerned with synchrotron radiation. MAX-lab is located in the city of Lund and is operated jointly by the Swedish Research Council and Lund University. On the basis of the electron accelerator LUSY (Lund University Synchrotron) that was present, constructed in 1962, MAX-lab received governmental fundings in 1982 and moved then in 1983 into the current laboratory located at the Faculty of Engineering

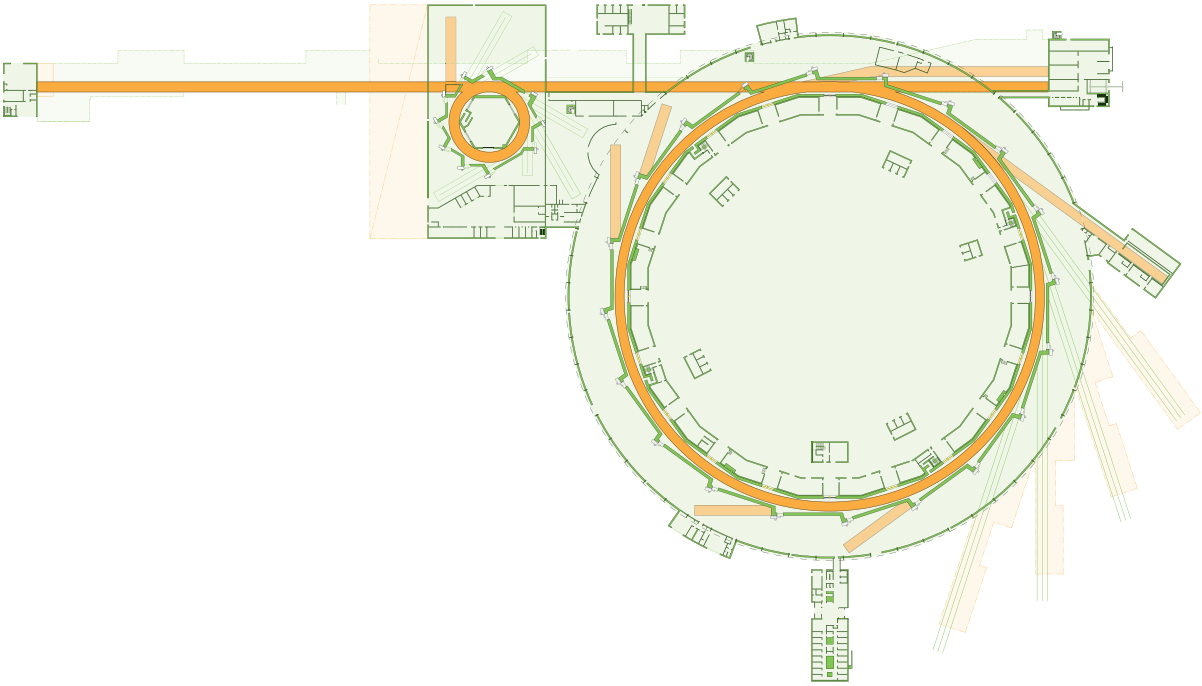

Figure 1.2: Floor plan of the MAX IV facility, a drawing by the company *MAX IV Laboratory*.

of Lund University. The first storage ring, MAX I, became operative in 1987. At present, the facility consists of three storage rings, MAX I, MAX II and MAX III, all of them using the pre-accelerator MAX-injector.

A new storage ring, MAX IV, is needed to increase the possibilities for research in a large number of different areas, such as those of material science, medicine and biology. MAX IV, also in Lund, will basically consist of a main source, a 3 GeV storage ring with a circumference of 528 m, to be used for the production of both soft and hard x-rays the use of which is also to be extended into the free electron laser field. The linear accelerator (Linac), located in an underground tunnel next to the main ring, is to have a width of approximately 10 m and a height of approximately 5 m, being about 400 m in length. There will be two paths in the tunnel, one for installations and the other for logistic and servicing purposes. In the Linac, the electron beam is to be pre-accelerated up to almost the speed of light. The electrons then enter the storage ring, where a magnetic field, one created by a large number of strong magnets distributed along its course, controls the beam of electrons. The electrons emit electromagnetic radiation, synchrotron light as it is called. The storage ring is to have space for 20 experiment stations distributed around the storage ring at equal distances from one another, the electrons being led out tangentially in beam lines for measurement purposes. In Figure 1.2, a 2D plan of the MAX IV area in which the main storage ring (the large ring-shaped building) and the Linac (straight tunnel) can be seen. The structure of the Linac is to consist mainly of concrete, as well as the floor structure of the main building. The ring-shaped building is to have an outer diameter of approximately 200 m, and its roof is to extend to a height of approximately 12 m.

Of major concern is the fact that vibrations of the magnets will result in a ten-fold increase in the level of vibration of the electron beam. Since the quality of the measurements performed in MAX IV will depend upon the precision of the synchrotron light, very strict requirements concerning the level of vibration of the magnets are specified. Strict requirements are placed in particular on the mean vertical vibration level, the aim being for it to be less than 20-30 nm per second within the frequency span of 5-100 Hz. Due both to an active beam-positioning system being employed for the magnets and to the wavelengths being very long at frequencies of less than 5 Hz, vibrations with frequencies of less than 5 Hz will not affect the relative displacements of the magnets in relation to one another to any appreciable extent. Frequencies higher than 100 Hz can be neglected since these are easily damped out in the soil and in the structure.

The buildings at a facility like the MAX IV one is exposed to both harmonic and transient excitations. The harmonic excitations are typically working machines such as pumps, ventilation systems and electrical equipment of other types. Transient excitations are to typically be those due to traffic from nearby roads and human activities in the building, such as walking, the closing of doors and the dropping of objects. On the east side of the MAX IV area there is a smaller road that results in traffic-induced ground vibrations being produced. Additional disturbing vibrations will be those from the motorway E22, which passing 100 m to the west of the main ring-shaped building; see Figure 1.1.

2 Site conditions

In order to be able to achieve results of sufficient accuracy in numerical simulations, it is important to have valid input data, such as reliable material parameters, for example, in the numerical model used for the calculations involved. Trustworthy information about the input data is thus needed and can be obtained in the basis of geotechnical and geophysical measurements. To be able to obtain as reliable data of the ground materials as possible, numerical evaluation of the measurements could be combined with the measurements themselves.

For ground vibrations at a nano-scale level (such as traffic-induced ground vibrations), stresses are usually at a level such that the assumption of linear elasticity is applicable, see Eq. (2.1),

$$\boldsymbol{\sigma} = \mathbf{D}\boldsymbol{\epsilon} \tag{2.1}$$

where the stresses, $\boldsymbol{\sigma}$, and the strains, $\boldsymbol{\epsilon}$, (wrtitten as vectors) have a linear relationship by the constitutive matrix $\mathbf{D}$. Local variations in the soil layer and the bedrock, such as in the strata and granularity involved, can often be assumed to be small as compared with the wavelengths in the low-frequency range. Thus, soil and bedrock can be modelled as being isotropic homogeneous materials, in this case $\mathbf{D}$ being written as

$$\mathbf{D} = \frac{E}{(1+\nu)(1-2\nu)} \begin{bmatrix} 1-\nu & \nu & \nu & 0 & 0 & 0 \\ \nu & 1-\nu & \nu & 0 & 0 & 0 \\ \nu & \nu & 1-\nu & 0 & 0 & 0 \\ 0 & 0 & 0 & \frac{1}{2}(1-2\nu) & 0 & 0 \\ 0 & 0 & 0 & 0 & \frac{1}{2}(1-2\nu) & 0 \\ 0 & 0 & 0 & 0 & 0 & \frac{1}{2}(1-2\nu) \end{bmatrix} \tag{2.2}$$

where E is the elastic modulus and ν is Poisson's ratio.

The goal of the measurements is thus usually to evaluate the material properties needed to describe linear elastic isotropic homogeneous materials, these properties in question those of the mass density, the elastic modulus, Poisson's ratio and the loss factor, information on the layering of the various ground materials being needed as well, for determining the geometry of the FE model to be used.

2.1 Geotechnical measurements

A number of geotechnical and geophysical measurements can be carried out at the construction site of a facility in order to determine the geotechnical and geodynamic material

parameters of the soil and of the bedrock that are located there. The material parameters of both the soil and of the bedrock, as well as their variation with location at the site, are needed as input to the FE models that are employed, so as to enable the FE simulations to provide results of adequate accuracy. Measurements of common types are described briefly in the text that follows.

Two different vibration sources (such as a sledge hammer and explosives) can be used when **surface wave seismic measurements** are carried out. The MASW (Multi-channel Analysis of Surface Waves) approach can be employed for the evaluations carried out, the vertical velocity amplitudes being measured and recorded by geophones and seismographs, respectively. The geophones are usually distributed along a straight line. The obtained data can be processed to obtain depth profiles of shear wave speeds.

VSP (Vertical Seismic Profiling) measurements in cored boreholes can be carried out so as to be able to correlate these with surface wave seismic data (obtained from MASW). A vertical shear and pressure wave speed profile can be obtained by use of recording devices placed in the boreholes so as to record the seismic energy levels there produced by vibration sources at the ground surface.

In **FWD (Falling Weight Deflectometer) tests** that can be performed a weight falls down and hits the ground surface, creating a well-defined impulse load. The peak force amplitude and the frequency content of the load can be adjusted; see Figure 2.1. A seismograph records the vertical velocity amplitude of geophones that are employed, their usually being distributed along a straight line from the location of the FWD. The FWD tests were carried out primarily in order to be able to correlate the results obtained with results of the numerical simulations; see subsection 2.1.1, and also to provide information concerning the attenuation properties of the ground.

The **resistivity measurements** that can be carried out enable plots of the resistivity distribution in the ground to be obtained. Resistivity is a material property, its indicating how strongly a given material opposes the flow of an electric current. Direct current (DC) is injected into the ground between two electrodes, the voltage between two other inner electrodes being measured then so as to be able to measure the electrical resistance of the material between the two inner electrodes. This enables the resistivity to be evaluated. The resistivity is useful primarily for determining the location of various ground materials, such as in the form of strata. The resistivity of different materials can differ considerably, yet different materials can also have the same resistivity. This is why additional reference drilling at the same location (as for the resistivity measurements) is needed in order for the ground stratigraphy along the measured line involved to be interpreted properly.

Geotechnical methods, such as auger drilling and dynamic sounding, can be carried out at different locations at a construction site in order to evaluate various ground material parameters there. Soil samples can be taken at a construction site and be classified both there and in the laboratory. The mass density, the water content and the undrained shear strength can be evaluated, and wave speeds can be measured in the laboratory on cores obtained from boreholes by means of seismic velocity tests. Since soil samples are always somewhat disturbed, the results of measurements of these should be treated with certain caution thereafter.

At the MAX IV construction site measurements of each of the types referred to above were carried out [5].

(a) (b)

Figure 2.1: Photographs of the FWD test setup at the MAX IV site [5]: (a) the FWD machine that generates an impulse load on the ground surface, (b) the seismic measurement station for evaluation of the response due to the FWD impulse load.

2.1.1 Evaluation of material parameters

The mass density can be evaluated mainly through soil sampling. The elastic modulus can be determined from the wave speeds obtained either from soil samples, from correlations between the results of numerical simulations and of FWD tests, or on the basis of relationships between VSP measurements and to surface seismic data. Relating the speed of the pressure wave and of the shear wave to one another enables Poisson's ratio to also be determined. Regarding evaluation of the loss factor, see the example that follows concerned with the MAX IV site.

Simulations in agreement with measurements

Agreement between the results of numerical simulations and measurements can be achieved by carrying out FE calculations and calibrating these to those measurements obtained. The FWD test can be used for such comparisons since, because of the load involved in the FWD tests being known, the tests can be used in conjunction with FE models, by making use of an iterative process in which each of the material properties (the mass density, the elastic modulus, Poisson's ratio and the loss factor) is varied, one at a time while the others are held constant. This enables the sensitivity of the simulation results to the material properties involved to be analysed. Since an interval for each of the material parameters can be determined on the basis of measurements, simulations can be performed to determine the final value of each of the parameters through calibrating the simulation results to the measurements obtained. In the numerical example concerned with MAX IV, this was done for the elastic modulus and for the loss factor in particular, since these were found to have the strongest effect on the response at the ground surface

for the values obtained in the intervals that were evaluated.

Evaluation of damping

The topography of both the soil and the bedrock is somewhat irregular, meaning that the horizontal layering used in the FE models is a simplification. To deal appropriately both with this simplification and with the heterogeneity that exists, account is taken of the loss factor both of the soil and of the bedrock, which in turn takes account of all the attenuation effects that occur, such as those of material damping, variations in the topography and heterogeneity of the material.

The results of the FE simulations carried out are strongly dependent upon the loss factor the model employs. To exemplify how strong the effects of the value of the loss factor on the ground vibration levels at the MAX IV site can be, use was made of an FE model employing material parameters typical for the site; see Figure 2.2. The loss factor for the soil was varied between 0.05 and 0.20, whereas the other material parameters were kept constant. In Figure 2.3, the effects on the displacement response to a harmonic unit load of the variations in the value of the loss factor are shown. As can be seen in the figure, the value of the loss factor which is selected has an appreciable effect on the displacement amplitude.

Although the material damping can be measured in the laboratory, on cores from boreholes, other attenuation effects cannot be assessed. The best estimate of the loss factor that could be obtained was made by taking account of the surface wave seismic measurements and of the results of the FWD tests that were carried out at the MAX IV site, as well as of the results of numerical parameter studies. The best estimate of the loss factor was given a value of between 0.10 and 0.14, depending upon the location in the MAX IV area involved. The loss factor depends upon the location in question, due to the variations in the ground parameters within the MAX IV site.

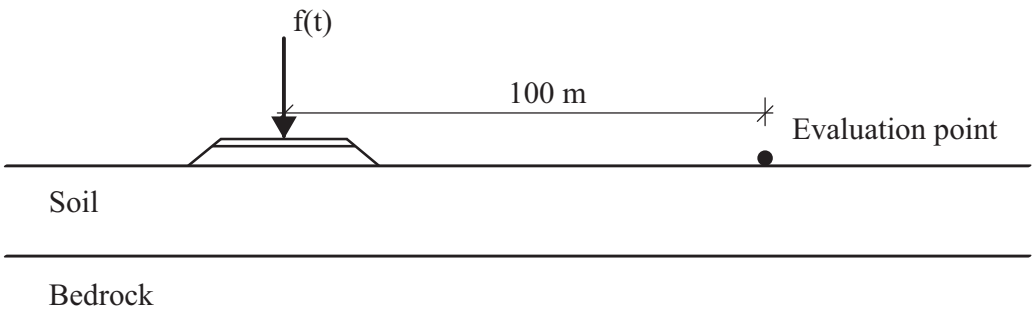

Figure 2.2: FE model. The soil layer is 14 m thick. The evaluation point is located on the ground surface 100 m from the excitation point.

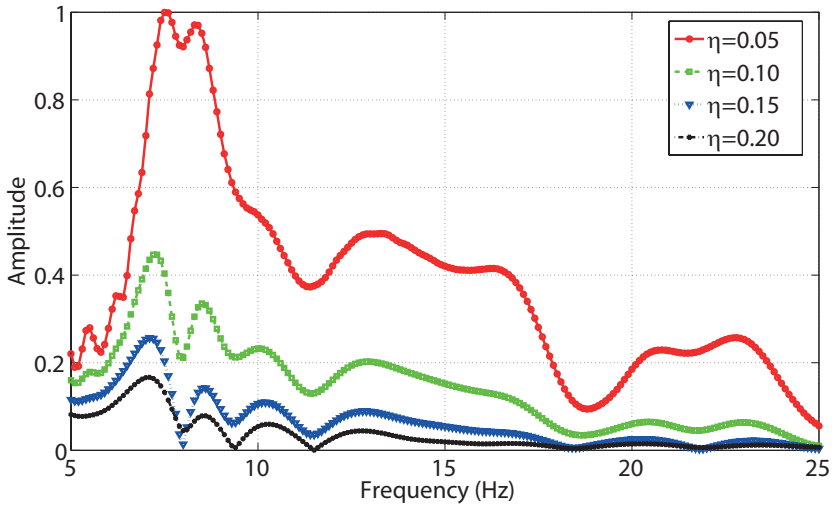

Figure 2.3: The vertical displacement amplitude of the complex magnitude versus the frequency of different values of the loss factor for the soil. The loss factor for the bedrock was kept constant. The amplitude was normalised with respect to the highest amplitude.

2.2 Ground materials

Investigation of the ground at the MAX IV site provided values for the different parameters of the materials involved; see Table 2.1 for values of the material parameters that were considered within the area in which the ring-shaped building is located. The soil properties were found to vary throughout the site. The soil has a depth of between 14 and 16 m and consists mainly of two layers of different clay tills, the softer of the two covering the stiffer one. The soil covers the bedrock consisting mainly of sandstone and shale [5, 16]. In the sections that follow, the types of soil and of bedrock located in the MAX IV area are described in general terms. For further information about soil and bedrock see, for example, [17, 18].

Table 2.1: Ground material parameters

Parameter \ Material	Upper clay layer	Lower clay layer	Bedrock
Depth (m)	2-14	1-12	-
Mass density (kg/m^3)	2125	2125	2600
Elastic modulus (MPa)	215-476	1006-2658	8809
Poisson's ratio	0.48	0.48	0.40
Loss factor	0.10-0.14	0.10-0.14	0.04

2.2.1 Clay tills

In the areas in which sedimentary rocks are found, such a significant amount of clay is present that the till there is denoted as clay till. Clay tills can be problematical to

Figure 2.4: A photograph of the soils at the excavation site for the Linac tunnel.

work with due to the extreme variability of their composition, which can range from their consisting of high proportion of stones and boulders to their consisting almost entirely of clay. Tills are thus a highly unsorted and coarsely graded type of soil having highly varying properties. The properties of tills depend upon how they were formed and how the ice packed them. The soil types that cover the bedrock of the MAX IV site can be identified for the most part as being Low Baltic clay till and Northeast clay till; see Figure 2.4 for a photograph of the soils at the excavation for the Linac tunnel.

Clay tills often have a very low hydraulic conductivity, its taking an extended period of time for water from them to drain during loading. The stress-strain curve for soft clay till usually shows a linear behaviour up until the pre-consolidation pressure is reached, in the over-consolidated state, the soil showing mainly an elastic response when unloading occurs. Soil of this type is thus usually assumed to be linear elastic in the over-consolidated state, i.e. at pressures less than the pre-consolidation pressure. Heavily over-consolidated fine-graded soil and well-compacted coarse-graded soil show mainly an elastic response in shearing when they are exposed to loads of low magnitude. The clay tills at the MAX IV site are regarded as being heavily over-consolidated due to their having a pre-consolidation pressure and to their being exposed to loads of low magnitude. Clay tills are usually water-saturated, which results in the density of natural moisture clay tills and of water-saturated clay tills basically being the same. The density of clay is normally one of between 1400 and 2200 kg/m^3, whereas for a clay till the density is closer to 2200 kg/m^3, due to its being a coarsely graded soil. Since clay tills are normally water-saturated and water is incompressible, Poisson's ratio of it is often close to 0.5. The damping property of the soil, in this case of clay till, is strain-dependent, the damping thus increasing with the strain. The damping value is thus set higher for earthquake analyses than for analyses involving loads of low magnitude (such as traffic loads). The damping ratio for soil can typically vary between approximately 2 and 20 %.

2.2.2 Sandstone and shale

In principle, the formation of sedimentary rocks starts with sediment particles on the ocean bottom. These become packed and undergo biochemical processes of various types for thousands of years, their being transformed so as to create hard formations in the

form of sedimentary rocks. Processes of this sort determine the characteristic features of sedimentary rocks, in particular their layered structure. Sedimentary rocks can be divided into three separate groups on the basis of their manner of being formed, those of clastic, organic and chemical rocks, respectively. Sandstone and shale belong to the clastic rocks.

Sandstone is medium-grained, its consisting mainly of such sand-sized minerals as quartz and feldspar, since these are the most common minerals in the earth's crust. Sandstone is commonly yellow, red, grey or brown in colour. The properties of sandstone can differ, depending on how it was formed.

Shale is fine-grained, its typically being composed of variable amounts of clay minerals and of grains of quartz, their typical being grey in colour. If the clay in it is dominant, the shale is denoted as clay shale which is characterised by its structure of thin lamina or parallel layering.

2.3 Ground vibrations

2.3.1 Distance dependence

At considerable distances from a vibration source, such as a motorway, for example, the attenuation has a stronger effect on the ground vibration levels than it does at short distances. This means that at long distances (the degree of the effect depending upon the load frequency and the ground parameters) the vibrations in the soil (the soil having higher damping than the bedrock) are much more attenuated than the vibrations in the bedrock are. This results in the vibration amplitudes at distances far from the vibration source being higher in the bedrock than in the soil, the damping properties of the materials involved strongly affecting the phenomena that occur and thus which phenomena need to be taken into account.

The results of FE calculations are shown in visualised form in Figure 2.5 so as to exemplify the effects of long distances on the responses obtained. The FE model employed, which involves axisymmetric boundary conditions, was analysed in the frequency domain with use of a harmonic unit point load. The geometry was that of 1000×216 m^2, involving a 16 m deep soil layer and use of infinite (non-reflecting) elements at the boundaries. The material parameters employed were typical for the MAX IV site. As can be seen in Figure 2.5 (lower plot) at a frequency of 12.5 Hz and at a distance of 300 m (or more) from the excitation point the vertical displacement amplitudes are higher in the bedrock than in the soil, whereas this is not the case at a frequency of 7.2 Hz (upper plot). It can also be noted in both plots that the shorter wavelengths in the soil layer are damped out rather quickly and that the motion in the ground that remains is controlled by the bedrock, the wavelengths there being longer.

Another example of the effects of the distance between the excitation point and the evaluation points involved can be seen in the measurements that were carried out at the motorway that runs along adjacent to the MAX IV area; see Figure 2.10 for a schematic presentation of the measurement setup. The velocity was measured at different locations on the ground surface during the passage of what were mainly cars and trucks. An FFT was performed on the velocity-time responses to determine the frequency content of the

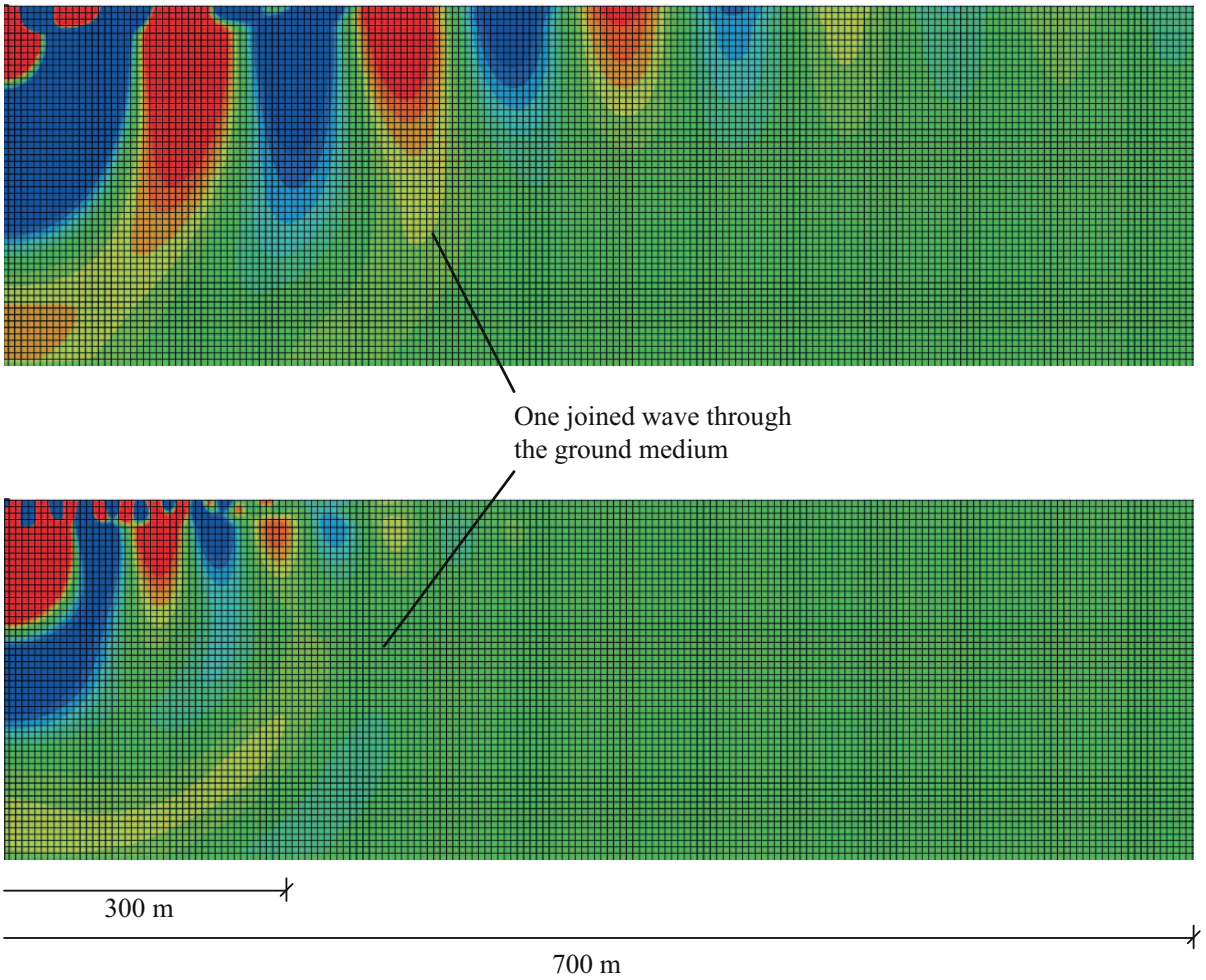

Figure 2.5: Visualisation of the vertical displacements occurring at 7.2 Hz (upper plot) and at 12.5 Hz (lower plot), respectively, showing clearly the differences in wavelength between waves in the soil and in the bedrock. The dimensions shown indicate the distance to the excitation point.

traffic load. As can be seen in Figure 2.6, by comparing (a) with (b) the high frequency content found at an evaluation point at the top of the embankment was already attenuated appreciably 40 m from the motorway.

The effectiveness of a wave obstacle, such as a trench or a shaped landscape, in terms of its reducing incident ground vibrations is also affected by the distance from the load to the area where the vibration amplitudes are of interest. In Figure 2.7, the vertical displacement amplitudes versus the respective frequencies are shown in two separate plots, the one with and the other without consideration of an open trench in the axisymmetric FE model described above. Figure 2.7(a) concerns responses 95 m from the excitation point, whereas Figure 2.7(b) concerns responses 300 m from the excitation point. As can be seen, the degree of effectiveness of a trench is appreciably less at a distance far from the excitation point (300 m from it) than at a distance of 95 m from it. At distances of around 300 m or more from the excitation point, the ground surface motion of the soil

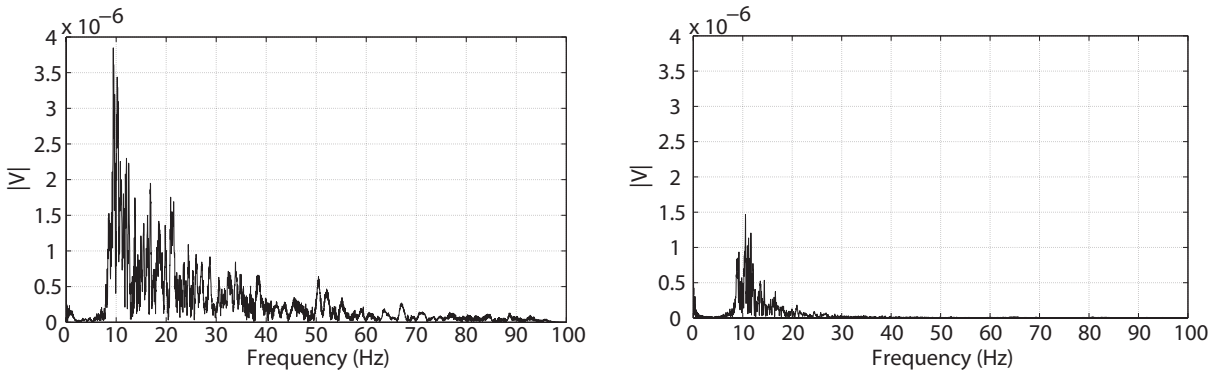

(a) (b)

Figure 2.6: FFT of the time signal at different distances from the E22 motorway: (a) measurements made at the top of the motorway embankment (*MV*). (b) measurements made 40 m from the motorway (*ME*).

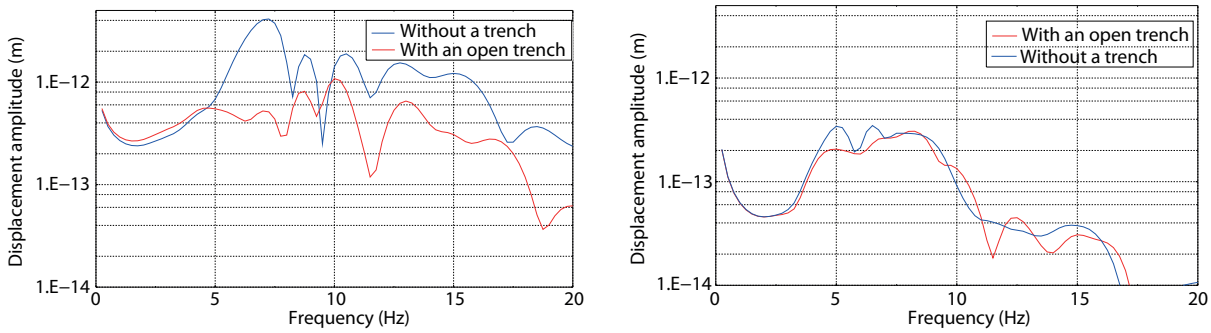

(a) (b)

Figure 2.7: Vertical displacement amplitudes versus frequency, with and without consideration in the FE model of an open trench, located 60 m from the excitation point. The displacements are evaluated at various distances from the excitation point: (a) 95 m from the excitation point, (b) 300 m from it.

tends to be controlled by the bedrock, in the manner described earlier in this section. In Figure 2.8 one can note that the higher frequencies are reduced to a greater extent far (300 m) from the load than those close (95 m) to it. The same tendencies and phenomena as those for the vertical displacements can also be observed for the horizontal ones.

2.3.2 Vertical versus horizontal vibrations

Which of the various vertical and the horizontal components of ground surface vibrations that occur is the dominate one (generates the highest amplitudes) depends in part upon its distance from the excitation point. This can be exemplified by analysing the vertical and the horizontal displacement amplitudes at the MAX IV site.

As can be seen in Figure 2.8(a), the vertical and the horizontal responses, respectively, of the ground surface at a distance of 95 m from the excitation point are somewhat similar

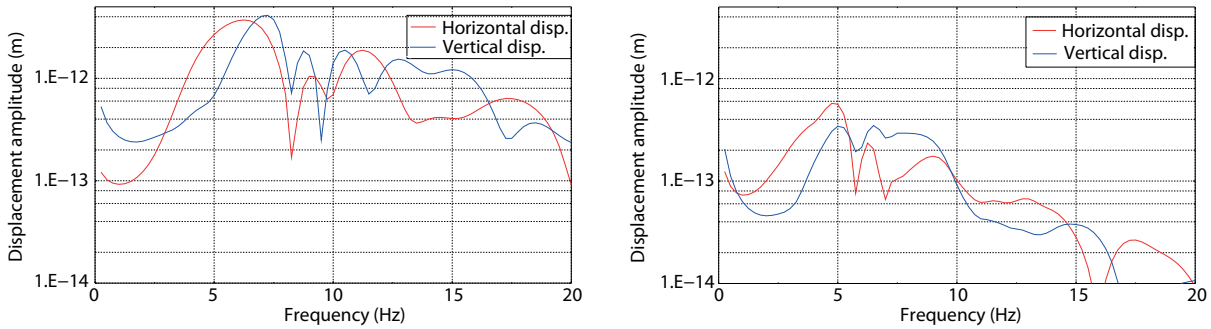

Figure 2.8: Calculated displacement amplitudes versus frequency for the vertical and the horizontal responses, respectively. The displacements are evaluated at various distances from the excitation point: (a) 95 m from the excitation point, (b) 300 m from it.

in terms of the calculated peak displacement amplitudes as obtained on the basis of FE analyses making use of the model described above. As can be seen in Figure 2.8(b), however, at a distance of 300 m from the excitation point the peak amplitude is nearly twice as high for the horizontal response as for the vertical one. The papers that are appended are concerned in particular with vibrations within 300 m of the excitation point.

2.4 Vibration sources

Buildings are often affected by both internal and external vibration sources. Indoor water pumps and fans, people walking inside the building, lifts and the transportation of goods are frequent internal vibration sources. Temporary construction sites, wind loads and traffic primarily involving trains, trams and cars are major external vibration sources.

2.4.1 Traffic loads

Several factors, such as the speed and weight of passing vehicles, as well as irregularities of both the roads and of the wheels of the vehicles involved and inhomogeneous soil conditions, contribute to the vibrations that traffic loads generate [8]. For traffic-induced ground vibrations, the strains involved are usually at a level such that the assumption of linear elasticity is applicable both to soil and to bedrock. In order to account for traffic loads in an FE model, the frequency content of the load can be measured on the road or roads in question. If linearity is assumed, the frequency spectrum can be employed for scaling the load or the calculated displacements, provided a harmonic unit load is employed. Although absolute values of the displacements obtained cannot be achieved in this manner, relative differences in terms of reduction in the level of vibration, in connection with which such differences are usually of interest, can be obtained.

The main building at MAX IV is affected by traffic-induced vibrations from local roads and from the E22 motorway nearby. The ground vibrations that are transmitted and

Figure 2.9: An aerial photograph of the MAX IV area and of the E22 motorway nearby in March 2013. Photographer Perry Nordeng.

originated in the local roads, have been studied, the results obtained being presented in a work report [19]. It was concluded there that since the vibrations originated mainly from irregularities of the road, such as speed bumps, these should be avoided. On the basis of various preliminary investigations it was concluded that traffic from the motorway makes the largest contribution to the level of vibrations found in the main building. Determining how traffic-induced ground vibrations from the motorway could be effectively reduced was of interest in the thesis.

The vibration requirements for MAX IV are especially strict within the frequency span of 5-100 Hz. In various studies of the MAX IV site [1, 2, 3] it has been concluded that vibration source frequencies in excess of 20-25 Hz (the upper frequency depending upon what part of the MAX IV site is involved) have only a negligible effect on the amplitudes of the vibrations at the area in which the buildings are located.

The frequency content of the traffic load on the motorway was assessed on the basis of green-field in-situ measurements; see Figure 2.10 for a schematic plan of the measurement setup. Four seismometers were placed on a granite plate on the ground-level surface, these being used for the data sampling of velocity versus time. In the figure, one of the seismometers (denoted as MV) was placed at the top of the motorway embankment. A second one (ME) was placed 40 m away, perpendicular to the motorway, a third (GB) was placed on a concrete slab located an area area of stabilised soil about 70 m away, and a fourth (OS) was likewise placed about 70 m from the motorway but at some distance from the area of stabilised soil, so as to avoid the effects on the measurement data of the stabilisation of the soil.

Velocity versus time was measured on the embankment (MV) during the passage of vehicles in order to be able to evaluate the frequency content of the traffic load; see Figure 2.11 for a schematic presentation of the measurement setup of the evaluation point that was located on the embankment. As can be seen in Figure 2.12, trucks generated the highest velocities at the measurement point. The peak velocity amplitudes were about six times as high for trucks as for cars. The ten events resulting in the highest velocity

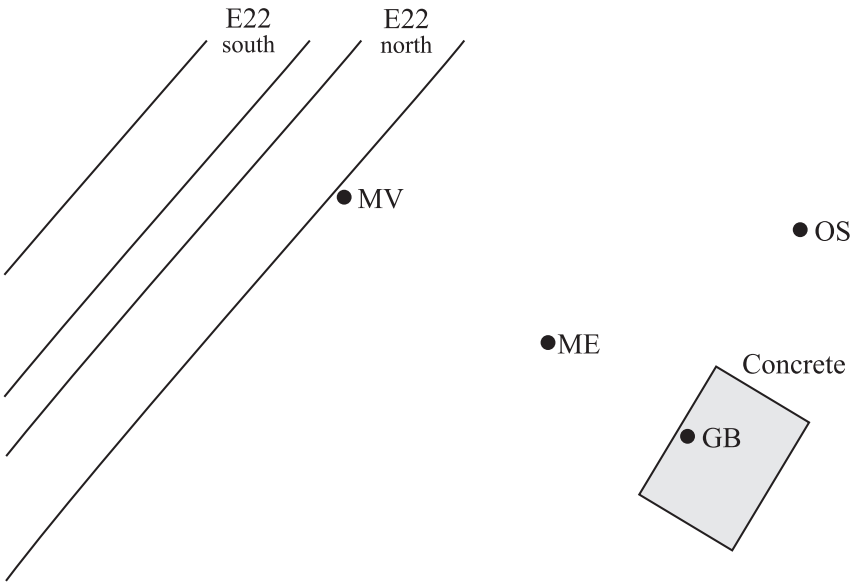

Figure 2.10: Schematic plan of the measurement setup.

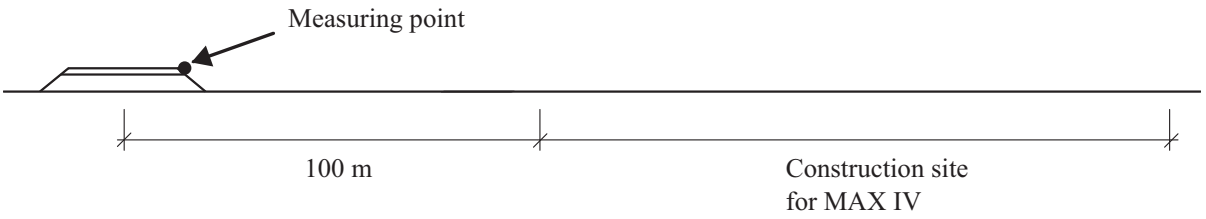

Figure 2.11: Schematic measurement setup.

amplitudes during a one-hour period, all of them involving heavy trucks, were registered. The displacements involved were evaluated and a Fast Fourier Transform (FFT) of the displacement-time curves was performed so as to determine the frequency content of the responses registered at the point in question on the embankment. Since high frequencies tend to be damped out quickly in the soil, the measurements on the embankment do not show the same frequency content as the measurements of the traffic load do. In the frequency range of interest, however, this difference in location was assumed to have only a negligible effect on the frequency content of the load because of the distances between the load (the truck wheels) and the embankment being so short.

In order to evaluate the frequency content of the traffic load, a polynomial was fitted to the experimental data (see Figure 2.13). A second-degree polynomial was used here since it resulted in a good approximation of the experimental data. The second-degree polynomial, which was normalised by its largest magnitude, was considered to be representative of the frequency content of the traffic load.

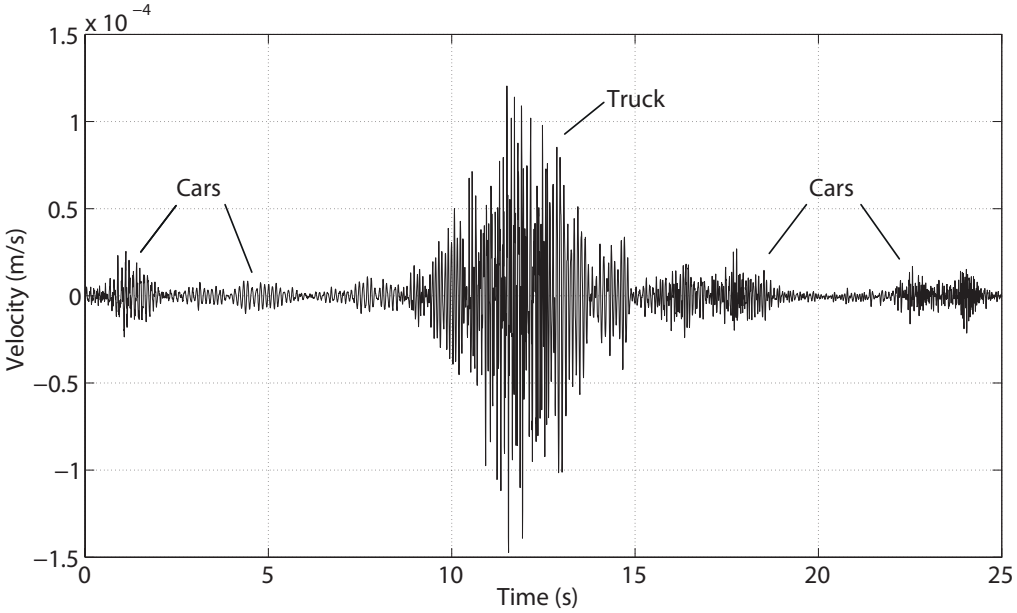

Figure 2.12: Measured vertical velocities versus time of responses at the E22 motorway adjacent to the MAX IV site.

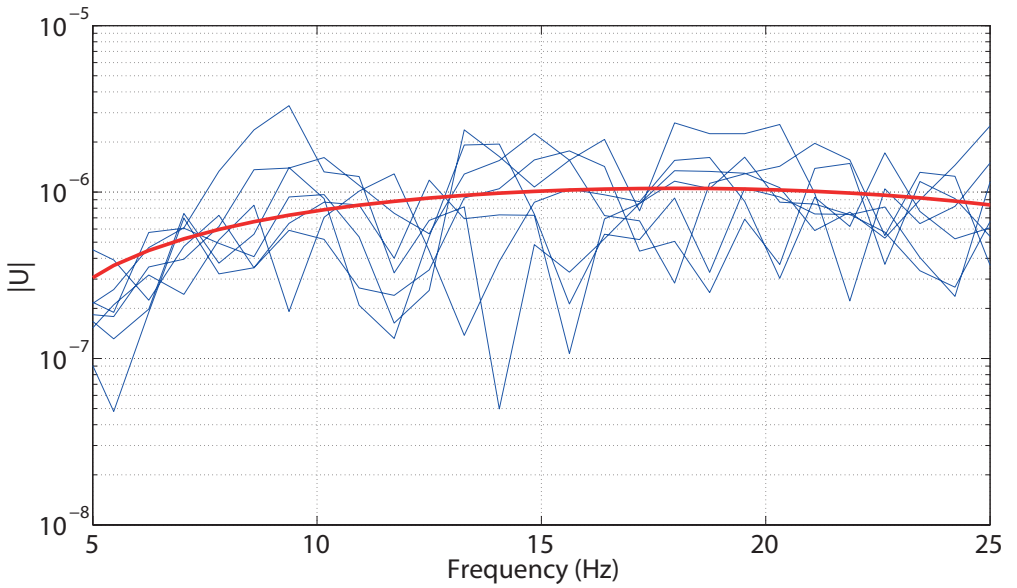

Figure 2.13: The magnitude spectrum of U(t) as obtained on the basis of measurements.

3 Governing theory

Vibrations occur in every building due to time-dependent loading of various kinds. There is a large difference between static and dynamic problems. For static problems, the solution follows natural intuitions, a heavier structure being needed to support heavier loads. For dynamic problems, in contrast, the frequency of a given load needs to be taken into account, since the displacements of the structure are much greater if the frequency of the load is close to the eigenfrequency of the system (a matter to be explained in a later section). A dynamic event can be analysed either in the time domain (in the case of time-dependent responses) or in the frequency domain (in the case of frequency-dependent responses). To convert a signal in the time domain to one in the frequency domain and vice versa, use can be made of a Fast Fourier Transform (FFT) algorithm.

In this section, the following will be described: wave propagation within the ground materials and modelling issues that are involved, formulation of the equation of motion in the frequency domain, together with matters of the eigenfrequencies, their corresponding eigenmodes and the damping involved, formulation of the wave equation for fluid-structure interaction in the frequency domain, the FE method through derivation of the FE formulation in the case of a dynamic problem, and finally the evaluation of the effectiveness of the wave obstacle.

3.1 Propagation of ground borne waves

In the case of a homogeneous halfspace, body waves propagate as a hemispherical wave front, whereas surface (Rayleigh) waves propagate radially as a cylindrical wave front [8]. The geometric attenuation of the body waves is thus proportional to 1/r, whereas in contrast the geometric attenuation of the Rayleigh waves is proportional to $\sqrt{1/r}$. Thus, at a relatively large distance from a vibration source it is the Rayleigh waves that are more likely to become the dominant wave form. In analyses involving both soil and bedrock, which differ significantly in their damping properties and stiffness, wave propagation is more complex. As described in subsection 2.3.1, at distances rather far from the excitation point the body waves in the bedrock can be of considerable importance and control the motion of the soil. Traffic-induced ground vibrations, with which the thesis is primarily concerned, are transmitted as both body and Rayleigh waves. Wave propagation in ground materials are described in detail in, for example, [6, 7, 8].

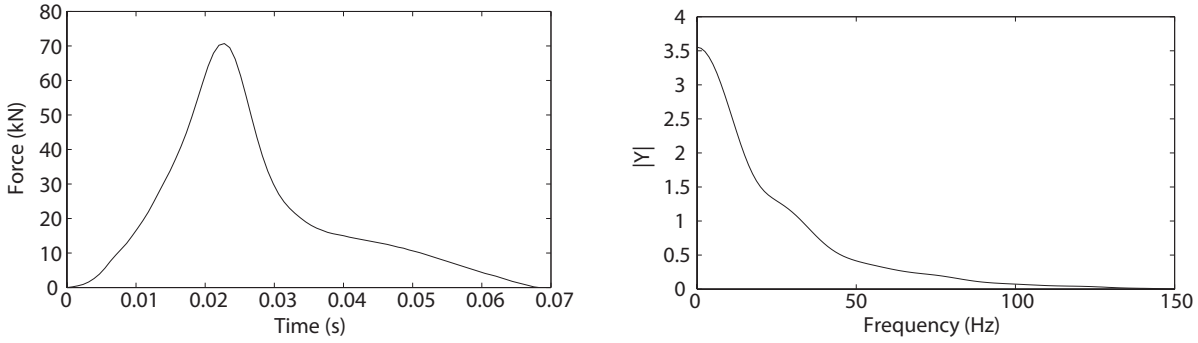

(a) (b)

Figure 3.1: Example of a FWD load that was used for measurements on a road nearby the MAX IV site, the load spectrum being shown both in the time domain (a) and in the frequency domain (b).

3.1.1 Material model

Ground materials such as soil and bedrock are not homogeneous materials because of the variations in granularity and in other material properties such as the depth of the material. In the case of wave propagation through them, local variations in the material of which they consist can be neglected, however, if these are small in comparison with the wavelengths involved. This can be illustrated by the following example, that of the quite slow wave speed of Rayleigh waves (which is the wave type having the slowest wave speed) in clay tills, such as those present at the MAX IV site, a speed of around 200 m/s. This means that the Rayleigh waves here, which have a frequency of 50 Hz, have a wavelength of 4 m. In stiffer clay tills and in bedrock, the wavelengths are still longer. Since local variations are thus negligible, a homogeneous material model is applicable here.

In many areas of civil engineering, soil is not considered to be a linear elastic material. Also, in soil dynamics, such as in connection with earthquakes, strains can be of such magnitude that nonlinearities cannot be neglected. In the case of human-made ground-borne vibrations, however, strains are usually at a level such that an assumption of linear elasticity applies. Damping, since it generally plays an important role in terms of dynamic responses that occur, is thus usually applied to the linear elastic material under such conditions.

In linear elastic materials, there are two types of waves that occur in response to dynamic loading, those being body and surface waves, respectively. Body waves are primarily P- and S-waves. P-waves are body waves that travel throughout the volume of the material in question and have the highest wave speed of the wave types involved, their thus being referred to as primary waves. There is a duality of the letter P here, P-wave motion representing changes in pressure (compression). The duality can also be applied to another type of body waves, that of S-waves, these being secondary waves involving particle motion in shearing. Like P-waves, they travel within the volume at hand, although at a wave speed that is only about half that of the former. S-waves appear in an elastic medium when it is subjected to periodic shear. The elastic deformation involved (changes in shape without a change in volume) occurs perpendicular to the direction of motion of

the wave. Surface waves travel along a free surface and are primarily Rayleigh waves and Love waves. Love waves (Q-waves) occurs perpendicular to the direction of propagation (transverse direction) in the case of a softer surface material covering a stiffer one. Since vertical displacement amplitudes are of general interest in the thesis, Love waves are not further described. Rayleigh waves travel close to the ground surface and represent a mixture of changes in both pressure and shear. The particles, that are subjected to a Rayleigh wave, moves in elliptical paths. Rayleigh waves have the slowest wave speed, compared to P- and S-waves. The relationships between the three different wave types (Rayleigh, P- and S-waves) in terms of wave speed are taken up in a later subsection.

3.1.2 Wave speeds

The wave speed for the pressure waves (P) and shear waves (S) in a linearly elastic homogeneous isotropic medium is given by

$$c_P = \sqrt{\frac{\lambda_L + 2\mu}{\rho}}; \qquad c_S = \sqrt{\frac{\mu}{\rho}} \tag{3.1}$$

where λ_L and μ are known as the first and second Lamé constant, respectively, and ρ is the mass density [8]. The Lamé constants are related to the engineering constants as

$$\lambda_L = \frac{\nu E}{(1+\nu)(1-\nu)}; \qquad \mu = \frac{E}{2(1+\nu)} \tag{3.2}$$

where ν is Poisson's ratio and E is the elastic modulus. The second Lamé constant, μ, is identified as the shear modulus, which is often referred to as G.

The wave speed of S-waves, c_S, is slower than that of the P-waves, c_P, the relationship between the two depending upon Poisson's ratio; see Table 3.1. The difference in wave speed between the two wave types increases with an increase in Poisson's ratio.

Table 3.1: Shear wave speed in relation to pressure wave speed. $\alpha = c_S/c_P$.

ν	α
0.20	0.61
0.30	0.53
0.40	0.41
0.49	0.14

P- and S-waves are derived with the assumption of an infinite medium being involved. In a finite medium, i.e. one with boundaries, Rayleigh waves also occur near to the boundaries, showing an elliptical motion. Rayleigh waves are slightly slower in speed than shear waves are, the wave speed relationship between the two depending upon Poisson's ratio; see Table 3.2. The difference in wave speed increases with an increase in Poisson's ratio. The wave speed of Rayleigh waves, c_R, can be determined on the basis of

$$V^6 - 8V^4 - (16\alpha^2 - 24)V^2 - 16(1 - \alpha^2) = 0. \tag{3.3}$$

where $V = c_R/c_S$ and α can be found in Table 3.1 [8].

Table 3.2: Rayleigh wave speed in relation to shear wave speed. $V = c_R/c_S$.

ν	V
0.20	0.91
0.30	0.93
0.40	0.94
0.49	0.95

The wavelength is the distance over which the shape of the wave repeats itself, the relationship between the wave speed, c, and the wavelength, λ_w being given by

$$\lambda_w = 2\pi \frac{c}{\omega} \tag{3.4}$$

where ω is the angular frequency.

3.2 Structural dynamics

For more information, and in more detail, about structural dynamics see, for example, [9, 10]. The easiest way to describe a dynamic system is by use of a single-degree of freedom (SDOF) model. An SDOF model involves only one degree of freedom (DOF), meaning that only one DOF is needed in order to describe the exact position of a given object (mass). The system shown in Figure 3.2 consists of a mass, m, a damper, c, and a spring, k. The load f is time-dependent. The damper and the spring are regarded as mass-less. The force equilibrium involved and Newton's second law gives

$$f - c\dot{u} - ku = m\ddot{u} \tag{3.5}$$

which if rewritten gives the equation of motion of a SDOF system

$$m\ddot{u} + c\dot{u} + ku = f. \tag{3.6}$$

In order to be able to describe the motion of a more complex structure, a multi-degree of freedom (MDOF) system is needed. The greater number of DOFs that are used to describe the system, in general, the more accurate the results achieved are. The response of a system under harmonic loading is common in structural dynamics, the

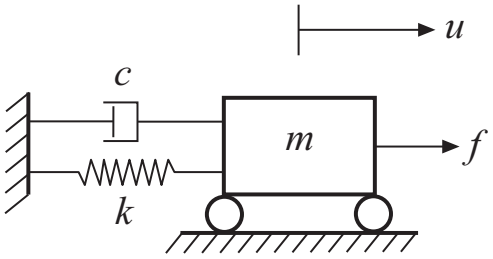

Figure 3.2: Mass-spring-damper system, involving a friction-free surface.

to harmonic loading provides insight into how the system responds to other types of excitations as well [10].

The equation of motion of a body, small deformations being assumed, can be described by the differential equation

$$\tilde{\boldsymbol{\nabla}}^T \boldsymbol{\sigma} + \mathbf{b} = \rho \frac{\partial^2 \mathbf{u}}{\partial t^2} \tag{3.7}$$

in which $\tilde{\boldsymbol{\nabla}}$ is a differential operator matrix, $\boldsymbol{\sigma}$ the stress vector, $\mathbf{b}$ the body force vector, ρ the mass density, $\mathbf{u}$ the displacement vector and t is time [11, 12]. The equation of motion of a dynamic problem, as derived from Eq. (3.7), can be written as

$$\mathbf{M}\ddot{\mathbf{u}} + \mathbf{C}\dot{\mathbf{u}} + \mathbf{K}\mathbf{u} = \mathbf{f} \tag{3.8}$$

where $\mathbf{M}$ is the mass matrix, $\mathbf{C}$ the damping matrix, $\mathbf{K}$ the stiffness matrix, $\mathbf{f}$ the load vector and $\mathbf{u}$ the nodal displacement vector. In harmonic loading, steady-state vibration occurs. The load and the corresponding displacements can be expressed as the complex harmonic functions

$$\mathbf{f} = \hat{\mathbf{f}} e^{i\omega t} \qquad\qquad \mathbf{u} = \hat{\mathbf{u}} e^{i\omega t} \tag{3.9}$$

where $\hat{\mathbf{f}}$ and $\hat{\mathbf{u}}$ denote the complex load amplitude and the displacement amplitude, respectively, i is the complex number involved and ω is the angular frequency. Inserting Eq. (3.9) into Eq. (3.8) results in the following equation of motion in the frequency domain

$$\mathbf{D}(\omega)\hat{\mathbf{u}} = \hat{\mathbf{f}} \tag{3.10}$$

where $\mathbf{D}$ is the frequency-dependent dynamic stiffness matrix, which can be expressed as

$$\mathbf{D}(\omega) = -\omega^2 \mathbf{M} + i\omega \mathbf{C} + \mathbf{K}. \tag{3.11}$$

3.2.1 Eigenfrequencies and eigenmodes

A structure has an unlimited number of natural frequencies. In an FE model, a structure is divided into finite elements having corresponding DOFs. In such a model the number of natural frequencies (eigenfrequencies) is equal to the number of DOFs. Hereafter, in discussing natural frequencies that are calculated, these will be referred to as eigenfrequencies rather than as natural frequencies.

If a structure is excited by a load with frequency close to a natural frequency, the amplitude of the vibrations produced increases significantly, a phenomenon referred to as resonance. Although if no damping were present in the structure the amplitude would ultimately become infinite, however, damping is always present in any given structure (a matter dealt with in the following section). The displacement amplitude of a steady-state response to an harmonic force of an undamped SDOF system can be written as [10]

$$u(\omega) = \frac{f}{k} \frac{1}{1 - (\omega/\omega_n)^2} \tag{3.12}$$

where ω_n is the angular eigenfrequency of the system. If the exciting frequency, ω, was equal to the eigenfrequency, ω_n, the response amplitude, u, would certainly be infinite. Since damping is always present, however, the response can never be infinite.

where ω_n is the angular eigenfrequency of the system. If the exciting frequency, ω, was equal to the eigenfrequency, ω_n, the response amplitude, u, would certainly be infinite. Since damping is always present, however, the response can never be infinite.

For any given eigenfrequency there is a corresponding deformation shape of the structure, referred to as an eigenmode of the structure. In examining how the eigenfrequencies and the corresponding eigenmodes can be determined, an undamped system will be considered. The equation of motion of such a system in the case of **f**=**0** is

$$\mathbf{M\ddot{u}} + \mathbf{Ku} = \mathbf{0}. \tag{3.13}$$

The solution $\mathbf{u}$(t) needs then to satisfy the initial conditions at t=0,

$$\mathbf{u} = \mathbf{u}(0) \qquad\qquad \dot{\mathbf{u}} = \dot{\mathbf{u}}(0). \tag{3.14}$$

The free vibration of an undamped system, in a given eigenmode, can be written as

$$\mathbf{u}(t) = q_n(t)\phi_n \tag{3.15}$$

where $q_n(t)$ is time-dependent and can be described by the harmonic function

$$q_n(t) = A_n cos\omega_n t + B_n sin\omega_n t \tag{3.16}$$

and ϕ_n, which represents the eigenmodes, does not vary over time.

If $q_n(t)$=0, there is no motion of the system, since it implies that $\mathbf{u}$(t)=**0**. Under such conditions, both ϕ_n and ω_n need to satisfy the eigenvalue problem

$$(-\omega_n^2\mathbf{M} + \mathbf{K})\phi_n = \mathbf{0}. \tag{3.17}$$

In line with the previous argument, if ϕ_n=0, there is no motion of the system. The solution then results in the eigenfrequencies $\omega_1, ..., \omega_n$ where n is the number of dofs. When the eigenfrequencies are known the eigenmodes ϕ_n can be calculated by solving the eigenvalue problem, as given in Eq. (3.17). The eigenfrequencies are a property of the structure. For an undamped system, the eigenfrequencies depend upon the value and the distribution of the mass, as well as, of the stiffness of the structure.

3.2.2 Damping

Damping is an effect that tends to reduce the level of vibration in a structure, its always being present and its arising from such sources as those of internal material damping and of friction that occurs in cracks and joints. It can have an appreciable effect on the response of a structure exposed to a dynamic force. In order for damping to be included in calculations, it needs to be determined on the basis of measurement data obtained for similar structures, since the damping properties of a given material cannot be calculated directly.

For introducing rate-independent linear damping into a system, a loss factor that takes into account of the attenuation of the propagating waves that occurs in steady-state analyses can be employed. This loss factor can be defined as

$$\eta = \frac{1}{2\pi}\frac{E_D}{E_{So}} \tag{3.18}$$

where in a steady state the energy dissipated in the form of a viscous damping of a given cycle of harmonic vibrations is denoted as E_D and the strain energy as E_{So} [10]. E_D can be written as

$$E_D = \pi c \omega u_0^2 \tag{3.19}$$

where c is the damping constant, u_o is the amplitude of the motion involved and

$$E_{S_0} = k u_0^2/2. \tag{3.20}$$

Inserting Eq. (3.19) and Eq. (3.20) into Eq. (3.29) gives the loss factor

$$\eta = \frac{\omega c}{k}. \tag{3.21}$$

In generalising this to a MDOF system, Eq. (3.21) can be written as

$$\mathbf{K}\eta = \omega \mathbf{C}. \tag{3.22}$$

Inserting Eq. (3.22) into Eq. (3.11) results in

$$\mathbf{D}(\omega) = -\omega^2 \mathbf{M} + (1 + i\eta)\mathbf{K}. \tag{3.23}$$

The imaginary part of the stiffness matrix is referred to as the structural damping matrix [9].

Rayleigh damping, which can be used in transient and steady-state analyses, is a procedure for determining the classical damping matrix by use of damping ratios. Classical damping is an appropriate idealisation if the mass and the stiffness are distributed evenly throughout the structure. It consists of two parts, the one being the presupposition of mass-proportionality and the other the presupposition stiffness-proportionality, in accordance with Eq. (3.24). Rayleigh damping is affected by the mass at the lower frequencies and by the stiffness at the higher frequencies. Although this has no physical basis, it has been shown to provide a good approximation [10].

$$\mathbf{C} = a_0 \mathbf{M} + a_1 \mathbf{K} \tag{3.24}$$

The damping ratio for the nth mode is

$$\zeta_n = \frac{a_0}{2}\frac{1}{\omega_n} + \frac{a_1}{2}\omega_n. \tag{3.25}$$

In Rayleigh damping, the damping ratio, ζ, is used to describe the effects of damping. The damping ratio is dimensionless and is the ratio of the damping constant, c, to the critical damping coefficient, c_{cr}, according to Eq. (3.26),

$$\zeta = \frac{c}{c_{cr}} \tag{3.26}$$

where c_{cr} is referred to as $c_{cr} = 2m\omega_n$.

For buildings, the damping ratio is normally less than 1, which means that the system is underdamped. If the damping ratio is equal to 1 the system is critically damped,

whereas for damping ratios greater than 1 the system is overdamped. If the damping ratios ζ_i and ζ_j, for the ith and jth modes, respectively, can be assumed to have the same value, the coefficients a_0 and a_1 can be written as

$$a_0 = \zeta \frac{2\omega_i \omega_j}{\omega_i + \omega_j} \quad \text{and} \quad a_1 = \zeta \frac{2}{\omega_i + \omega_j} \tag{3.27}$$

where ω_i and ω_j determine the frequency range in which the damping ratio is valid.

The relationship between structural damping and Rayleigh damping can be expressed in steady-state analyses as

$$\eta = \frac{1}{2\pi} \frac{E_D}{E_S o} = 2\xi \frac{\omega}{\omega_n} \tag{3.28}$$

and, when the exciting frequency is equal to the eigenfrequency, it can be expressed as

$$\eta = 2\xi. \tag{3.29}$$

As mentioned in the previous section, if the exciting frequency of an undamped system was to be equal to one of the systems eigenfrequencies, the response amplitude, Eq. (3.32), would be infinite. Since damping is always present, however, the response amplitude can never be infinite. When damping is considered in terms of a loss factor, Eq. 3.32 can be written as

$$u(\omega) = \frac{f}{k} \frac{1}{\sqrt{[1 - (\omega/\omega_n)^2]^2 + \eta^2}}. \tag{3.30}$$

The additional term containing η contributes to preventing the occurrence of an infinite response amplitude.

In the previous section it was noted that in an undamped system the eigenfrequencies depend upon both on the mass and the stiffness of the structure in question. The eigenfrequencies of a damped system also depend upon the damping properties of the material, for example the damping ratio ζ, in accordance with Eq. (3.31), [10].

$$\omega_D = \omega_n \sqrt{1 - \zeta^2}. \tag{3.31}$$

3.3 Fluid-structure interaction

Fluid-structure interaction (FSI) is the interaction between a solid body (structure) and a fluid. It is used when the structure and the fluid domain interact with one another, so that the fluid affects the behaviour of the solid body and vice versa. For further reading concerned with FSI, see for example [11, 12, 13].

The indices s and f will be used here to denote the properties of the structural and the fluid domains, respectively. Two governing equations can be employed for describing an acoustic fluid, which is assumed to be inviscid, irrotational and compressible and to undergo small pressure changes. The equation of motion, when the volumetric drag is neglected, can be written as

$$\rho_0 \frac{\partial^2 \mathbf{u}_f}{\partial t^2} + \boldsymbol{\nabla} p_d = 0 \tag{3.32}$$

where ρ_0 is the static density, $\boldsymbol{\nabla}$ is the gradient of a given variable and p_d is the dynamic pressure, the density being assumed to have only a negligible variation in space. In the absence of an added fluid mass inflow, the constitutive equation can be written as

$$p_d = -c_0^2 \rho_0 \boldsymbol{\nabla} \mathbf{u}_f \tag{3.33}$$

the speed of sound, c_0, being related to the density on the basis of the bulk modulus, K, where

$$c = \sqrt{\frac{K}{\rho}}. \tag{3.34}$$

With use of Eqs. (3.32, 3.33), the wave equation for the acoustic fluid, in which the pressure serves as the field variable, can be written as

$$\frac{\partial^2 p_d}{\partial t^2} - c^2 \boldsymbol{\nabla}^2 p_d = 0. \tag{3.35}$$

The pressure can be expressed as the complex harmonic function

$$p_d = \hat{p}_d e^{i\omega t} \tag{3.36}$$

where $\hat{p}$ denotes the complex pressure amplitude. Inserting Eq. (3.36) into Eq. (3.35) results in the wave equation for the frequency domain

$$\boldsymbol{\nabla}^2 \hat{p}_d + \frac{\omega^2}{c^2} \hat{p}_d = 0. \tag{3.37}$$

Eq. (3.37) can be formulated in terms of the FE method, the pressure serving as the approximated nodal field variable, as

$$\mathbf{M}_f \ddot{\mathbf{p}}_f + \mathbf{K}_f \mathbf{p}_f = \mathbf{f}_{f,p} \tag{3.38}$$

where $\mathbf{M}_f$ and $\mathbf{K}_f$ are matrices, $\mathbf{p}_f$ is the pressure vector and $\mathbf{f}_{f,p}$ is the boundary vector.

3.3.1 Fluid-structure coupling

The coupling of the structure and the fluid at their common boundary, S, is made through the static and the kinematic boundary conditions. The force vector $\mathbf{f}$ in Eq. (3.8) can be divided into three parts,

$$\mathbf{f} = \mathbf{f}_b + \mathbf{f}_l + \mathbf{f}_{s,p} \tag{3.39}$$

where $\mathbf{f}_b$ is the body force vector, $\mathbf{f}_l$ the boundary force vector and $\mathbf{f}_{s,p}$ corresponds to the acoustic fluid pressure that acts on the structure at S.

Continuity of the fluid displacements and the structural displacements is assumed in the normal direction to their common boundary S. Introducing a normal vector, $\mathbf{n}$, allows the kinematic boundary condition to be formulated as

$$\mathbf{u}_s \cdot \mathbf{n}|_S = \mathbf{u}_f \cdot \mathbf{n}|_S. \tag{3.40}$$

Due to the continuity in pressure at S, the static boundary condition for the coupling can be formulated as

$$\sigma_{s,n}|_S = -p_f \tag{3.41}$$

where $\sigma_{s,n}$ is the stresses at S in the normal direction and p_f is the acoustic fluid pressure.

3.4 Finite element method

Differential equations are often used for describing various physical problems. Sometimes, numerical methods are required to solve differential equations that are too complicated to be solved analytically. The FE method is a numerical method used in a large number of engineering disciplines, and related ones such as those of physics and mathematics for solving ordinary differential equations with arbitrary geometries and materials. Development of the FE method took off in the early 1960s and it is currently one of the most effective methods available within the area. In order to solve differential equations with use of the FE method, the body involved is divided into small elements, termed finite elements. Instead of approximating region in question as a whole through use of higher-order functions, simpler functions such as linear or quadratic polynomials can be used for each element. An FE solution requires that the boundary conditions for all the boundaries involved are known, i.e. the problem is a boundary-valued one. Since there are often tens of thousands (or even millions) of finite elements in the element mesh, the system of equations cannot be solved without computer calculations being carried out. The finer the mesh employed is (i.e. the larger the number of dofs is), in general, the more accurate the solution provided becomes. Extensive work on the FE method is presented in, for example, [11, 12].

3.4.1 Linear elasticity

In this subsection, the FE method will be described through use of a dynamic equilibrium situation for a linear elastic continuum body. Its differential equation is given as

$$\tilde{\boldsymbol{\nabla}}^{\boldsymbol{T}}\boldsymbol{\sigma} + \mathbf{b} = \rho\frac{\partial^2\mathbf{u}}{\partial t^2} \tag{3.42}$$

where $\tilde{\nabla}$ is a matrix differential operator, σ is a vector composed of all the stress components involved and $\mathbf{b}$ is a body force vector containing the body forces present per unit volume, such that

$$\tilde{\boldsymbol{\nabla}}^{\boldsymbol{T}} = \begin{bmatrix} \frac{\partial}{\partial x} & 0 & 0 & \frac{\partial}{\partial y} & \frac{\partial}{\partial z} & 0 \\ 0 & \frac{\partial}{\partial y} & 0 & \frac{\partial}{\partial x} & 0 & \frac{\partial}{\partial z} \\ 0 & 0 & \frac{\partial}{\partial z} & 0 & \frac{\partial}{\partial x} & \frac{\partial}{\partial y} \end{bmatrix}; \quad \boldsymbol{\sigma} = \begin{bmatrix} \sigma_{xx} \\ \sigma_{yy} \\ \sigma_{zz} \\ \sigma_{xy} \\ \sigma_{xz} \\ \sigma_{yz} \end{bmatrix}; \quad \mathbf{b} = \begin{bmatrix} b_x \\ b_y \\ b_z \end{bmatrix}; \quad \mathbf{u} = \begin{bmatrix} u_x \\ u_y \\ u_z \end{bmatrix}. \tag{3.43}$$

Matrix multiplication of Eq. (3.42) gives

$$\begin{aligned}
\frac{\partial \sigma_{xx}}{\partial x} + \frac{\partial \sigma_{xy}}{\partial y} + \frac{\partial \sigma_{xz}}{\partial z} + b_x &= \rho \frac{\partial^2 u_x}{\partial t^2} \\
\frac{\partial \sigma_{yx}}{\partial x} + \frac{\partial \sigma_{yy}}{\partial y} + \frac{\partial \sigma_{yz}}{\partial z} + b_y &= \rho \frac{\partial^2 u_y}{\partial t^2} \\
\frac{\partial \sigma_{zx}}{\partial x} + \frac{\partial \sigma_{zy}}{\partial y} + \frac{\partial \sigma_{zz}}{\partial z} + b_z &= \rho \frac{\partial^2 u_z}{\partial t^2}.
\end{aligned} \tag{3.44}$$

Whereas the body force vector, $\mathbf{b}$, acts on the body per unit volume, the traction vector acts on the surface of the body, as a force per unit area. Being present on the surface, the traction vector needs to fulfil the boundary condition

$$\begin{aligned}
t_x &= \sigma_{xx} n_x + \sigma_{xy} n_y + \sigma_{xz} n_z \\
t_y &= \sigma_{xy} n_x + \sigma_{yy} n_y + \sigma_{yz} n_z \\
t_z &= \sigma_{xz} n_x + \sigma_{yz} n_y + \sigma_{zz} n_z
\end{aligned} \tag{3.45}$$

where the vector components n_x, n_y, and n_z make up the unit normal vector, $\mathbf{n}$.

In order to derive the weak formulation, the arbitrary vector $\mathbf{v}$ is introduced

$$\mathbf{v} = \begin{bmatrix} v_x \\ v_y \\ v_z \end{bmatrix}. \tag{3.46}$$

Multiplication of Eq. (3.44) with Eq. (3.46) and integrating the expressions over the volume, V,

$$\int_V \mathbf{v}^T (\tilde{\boldsymbol{\nabla}}^{\boldsymbol{T}} \boldsymbol{\sigma} + \mathbf{b} - \rho \frac{\partial^2 \mathbf{u}}{\partial t^2}) \mathrm{d}V = 0 \tag{3.47}$$

this being followed by a integration by parts using the Green-Gauss theorem (through which the components of the traction vector emerge) on the first term in Eq. (3.47)

$$\int_V \mathbf{v}^T \tilde{\boldsymbol{\nabla}}^{\boldsymbol{T}} \boldsymbol{\sigma} \mathrm{d}V = \int_S \mathbf{v}^T \mathbf{t} \mathrm{d}S - \int_V \left(\tilde{\boldsymbol{\nabla}} \mathbf{v} \right)^T \boldsymbol{\sigma} \mathrm{d}V \tag{3.48}$$

and finally by the adding together of the terms, this resulting in the weak formulation

$$\int_V \mathbf{v}^T \rho \frac{\partial^2 \mathbf{u}}{\partial t^2} \mathrm{d}V + \int_V \left(\tilde{\boldsymbol{\nabla}} \mathbf{v} \right)^T \boldsymbol{\sigma} \mathrm{d}V = \int_S \mathbf{v}^T \mathbf{t} \mathrm{d}S + \int_V \mathbf{v}^T \mathbf{b} \mathrm{d}V. \tag{3.49}$$

In order to utilise this in the FE formulation, the displacements vector, $\mathbf{u}$, is approximated by

$$\mathbf{u} = \mathbf{N}\mathbf{a} \tag{3.50}$$

where $\mathbf{N}$ contains the global shape functions and $\mathbf{a}$ the displacements. Use of the Galerkin method implies that

$$\mathbf{v} = \mathbf{N}\mathbf{c} \tag{3.51}$$

where $\mathbf{c}$ is arbitrary. Accordingly,

$$\tilde{\nabla}\mathbf{u} = \boldsymbol{\varepsilon} = \mathbf{B}\mathbf{a} \tag{3.52}$$

and

$$\tilde{\nabla}\mathbf{v} = \mathbf{B}\mathbf{c} \tag{3.53}$$

where $\mathbf{B} = \tilde{\nabla}\mathbf{N}$. Inserting Eq. (3.51) and Eq. (3.53) into the weak formulation shown in Eq. (3.49) allows $\mathbf{c}$ to be extracted and eliminated. Introducing linear elasticity material behaviour through use of the constitutive matrix $\mathbf{D}$ results in

$$\boldsymbol{\sigma} = \mathbf{D}\boldsymbol{\varepsilon}. \tag{3.54}$$

Through use of the kinematic relationship for elastic strains, Eq. (3.52), Eq. (3.54) can be written as

$$\boldsymbol{\sigma} = \mathbf{D}\mathbf{B}\mathbf{a}. \tag{3.55}$$

The FE formulation for a linear elastic case can then be rewritten as

$$\int_V \mathbf{N}^T \rho \mathbf{N} \mathrm{d}V \ddot{\mathbf{a}} + \int_V \mathbf{B}^T \mathbf{D}\mathbf{B} \mathrm{d}V \mathbf{a} = \int_S \mathbf{N}^T \mathbf{t} \mathrm{d}S + \int_V \mathbf{N}^T \mathbf{b} \mathrm{d}V. \tag{3.56}$$

The boundary conditions involved can be stated either as the essential boundary condition (prescribed displacements, $\mathbf{u}$) or as the natural boundary condition (prescribed traction vector, $\mathbf{t}$).

To obtain a formulation of a more compact form, the matrix and vectors that follow are established,

$$\begin{aligned} \mathbf{M} &= \int_V \mathbf{N}^T \rho \mathbf{N} \mathrm{d}V; \qquad & \mathbf{K} &= \int_V \mathbf{B}^T \mathbf{D}\mathbf{B} \mathrm{d}V \\ \mathbf{f}_l &= \int_S \mathbf{N}^T \mathbf{t} \mathrm{d}S; \qquad & \mathbf{f}_b &= \int_V \mathbf{N}^T \mathbf{b} \mathrm{d}V \end{aligned} \tag{3.57}$$

so that

$$\mathbf{M}\ddot{\mathbf{a}} + \mathbf{K}\mathbf{a} = \mathbf{f}_l + \mathbf{f}_b \tag{3.58}$$

where $\mathbf{M}$ is the mass matrix, $\mathbf{K}$ the stiffness matrix, $\mathbf{f}_l$ the boundary force vector and $\mathbf{f}_b$ the body force vector. Further shortening can be achieved by having only a single force vector

$$\mathbf{f} = \mathbf{f}_l + \mathbf{f}_b \tag{3.59}$$

which results in a short FE formulation of a dynamic situation

$$\mathbf{M}\ddot{\mathbf{a}} + \mathbf{K}\mathbf{a} = \mathbf{f}. \tag{3.60}$$

3.4.2 Isoparametric elements

Use of isoparametric elements allows the sides of the quadrilateral elements to be non-parallel to the coordinate axes and still behave in a compatible manner. This is necessary for the modelling of structures having an arbitrary geometry.

Consider a cubic domain bounded by a $\xi\eta\zeta$-coordinate system (parent domain) in which $\xi = \pm 1$, $\eta = \pm 1$ and $\zeta = \pm 1$. The transformation through which the parent domain is transformed into another and more complicated region is called mapping. Mapping transforms the parental domain here into a global Cartesian xyz-coordinate system through

$$x = x(\xi, \eta, \zeta); \qquad y = y(\xi, \eta, \zeta); \qquad z = z(\xi, \eta, \zeta). \tag{3.61}$$

This relationship is unambiguous, since for every point given by $\xi\eta\zeta$-coordinates in the parent domain there exists a unique point given by xyz-coordinates in the global domain. Differentiating Eq. (3.61) and using the chain rule, results in an expression that allows transformation between two domains to be carried out,

$$\begin{bmatrix} dx \\ dy \\ dz \end{bmatrix} = \begin{bmatrix} \frac{\partial x}{\partial \xi} & \frac{\partial x}{\partial \eta} & \frac{\partial x}{\partial \zeta} \\ \frac{\partial y}{\partial \xi} & \frac{\partial y}{\partial \eta} & \frac{\partial y}{\partial \zeta} \\ \frac{\partial z}{\partial \xi} & \frac{\partial z}{\partial \eta} & \frac{\partial z}{\partial \zeta} \end{bmatrix} \begin{bmatrix} d\xi \\ d\eta \\ d\zeta \end{bmatrix} \tag{3.62}$$

where the Jacobian matrix $\mathbf{J}$ can be written as

$$\mathbf{J} = \begin{bmatrix} \frac{\partial x}{\partial \xi} & \frac{\partial x}{\partial \eta} & \frac{\partial x}{\partial \zeta} \\ \frac{\partial y}{\partial \xi} & \frac{\partial y}{\partial \eta} & \frac{\partial y}{\partial \zeta} \\ \frac{\partial z}{\partial \xi} & \frac{\partial z}{\partial \eta} & \frac{\partial z}{\partial \zeta} \end{bmatrix} \tag{3.63}$$

If the values in the parental domain are the ones to be determined, Eq. (3.62) can be written as

$$\begin{bmatrix} d\xi \\ d\eta \\ d\zeta \end{bmatrix} = \mathbf{J}^{-1} \begin{bmatrix} dx \\ dy \\ dz \end{bmatrix} \tag{3.64}$$

which obviously requires $\det \mathbf{J} \neq 0$. If an element behaves in a conforming, i.e. compatible manner in the parent domain, its isoparametric version also behaves in a conforming way and no mismatch between adjacent elements exists. The completeness criterion is satisfied if and only if

$$\sum_{i=1}^{n} \mathbf{N}_i^e = 1. \tag{3.65}$$

If the compatibility and completeness requirements are fulfilled individually, then the element fulfils the convergence criterion as well. Mapping an element requires that the vertex-nodes on the parent domain also be located on the boundary following the transformation.

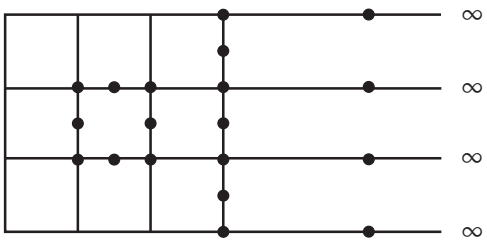

Figure 3.3: Example of a mesh involving nine finite and three infinite elements under plane strain conditions using quadric approximation. The element nodes are shown for one finite element and for the three infinite elements.

3.4.3 Infinite elements

Infinite elements, which are intended to represent a non-reflecting boundary, are convenient to use when the region of interest is small as compared with the surrounding region. Finite elements can be used for the region of interest and infinite elements for the far-field region. In Figure 3.3, an example of a mesh involving both finite and infinite elements is shown. The material responses in the infinite elements are assumed to be isotropic and the solution involved being linear. Infinite elements provide non-reflecting boundaries through their suppressing of the damping and of the stiffness matrix of the elements, the elements providing no contribution to the eigenmodes. The far-field nodes in the infinite elements are not displaced in the results obtained. The infinite elements are usually not completely non-reflecting but in most engineering problems the reflections they show are insignificant. Due to the suppressing of the stiffness matrix in the infinite elements, rigid body motions can occur but they are usually of no significance.

3.4.4 Commercial finite element software

In the appended Paper A the FE software package *Abaqus*, [14], was used for the calculations, and in the appended Paper B both *Abaqus* and the FE software package *HyperWorks*, [15], were used for the calculations.

Dassault Systemes's FE software package *Abaqus 6.11* was used for the FE calculations both in Paper A and in parts of Paper B. *Abaqus* is divided into three different parts, *Abaqus/CAE*, *Abaqus/Standard* and *Abaqus/Explicit*. *Abaqus/CAE* is a user interface employed for modelling and meshing a structure and for visualising the results. *Abaqus/Standard* is an implicit solver for various dynamic finite element problems such as low-speed or steady-state analyses. It is also used for static problems. *Abaqus/Explicit*, which makes use of an explicit solver, is more appropriate for high-speed, nonlinear and transient response analyses. *Abaqus* in its different parts are used by both consultants and researchers in several fields such as those of automotive, aerospace and civil engineering. For the FE calculations in Paper A and in the second part of Paper B, *Abaqus/CAE* was used for pre- and post-processing and *Abaqus/Standard* for the analyses. In Paper A, *Abaqus/Standard* was run on a PC. The FE calculations in Paper B, in contrast, were run on the high performance cluster *Alarik* at the computing centre *Lunarc* at Lund University.

Altair's FE software package *HyperWorks 11.0* was used for the parametric FE analyses in Paper B. The pre-processor, in which the model parameters (concerning the geometry, materials, loads, mesh, etc. employed) were defined, is termed *HyperMesh*. *HyperMesh* contains a tool termed HyperMorph, which was used here to model the different shapes in the shaped landscape. The shapes were obtained by mapping a set of nodes, defined by a domain, onto a line (in the 2D analyses) or a surface (in the 3D analyses) that was drawn independently of the mesh. The process does not change the number of elements involved, but only stretches or compresses them. The solver used was *RADIOSS* Bulk Data Format. For the analyses performed in the frequency domain, the solver was implemented in *HyperStudy*, which is a design and optimisation software. The post-processing for visualisation purposes was carried out in *HyperView*. For the 2D parametric studies, *RADIOSS* was run on a PC. For the 3D parametric studies, in contrast, the calculations were run on the high performance cluster *Platon* at the computing center *Lunarc*.

3.5 Evaluation

3.5.1 RMS value

In evaluating the effectiveness of a wave obstacle in the papers that are appended, a root mean square (RMS) value can be used as a measure of vibration magnitude.

The RMS value of time-dependent displacements (time domain) can be determined as

$$u_{RMS} = \sqrt{\frac{1}{\Delta t}\int_{t_0}^{t_0+\Delta t} u^2(t)dt} \tag{3.66}$$

where u_{RMS} is the RMS value of the displacements and t is the time. According to Parseval's theorem, the RMS value of a continuous frequency response function (frequency domain) can be written in the same manner as Eq. (3.66), in the form

$$u_{RMS} = \sqrt{\frac{1}{\Delta f}\int_{f_0}^{f_0+\Delta f} u^2(f)df} \tag{3.67}$$

where f is the frequency.

The RMS value used to evaluate the displacements obtained from the steady-state analyses in the appended papers was determined by

$$u_{RMS} = \frac{1}{n}\sqrt{(u_1^2 + u_2^2 + ... + u_n^2)} \tag{3.68}$$

where u_i is the magnitude of the displacement at each frequency and n is the number of frequencies in the interval.

3.5.2 Measure of reduction

Distributed evaluation points were used to calculate an average displacement reduction factor; see Eq. (3.70). This was used as a measure of the effectiveness of the wave obstacle. The displacement reduction factor, U_{red}, pertains to the relationship of the vertical

vibrational amplitude after a wave obstacle has been introduced (post-obstacle), U_{post}, to the amplitude prior to its being introduced (pre-obstacle), U_{pre}, in accordance with Eq. (3.69). U_{pre} and U_{post} were determined on the basis of the complex displacement magnitudes obtained for the different frequencies, these being calculated as RMS values at the evaluation points, in accordance with Eq. (3.68).

$$U_{red} = \frac{U_{pre} - U_{post}}{U_{pre}}. \tag{3.69}$$

$$\bar{U}_{red} = \frac{1}{n} \sum_{i=1}^{n} U_{red,i} \tag{3.70}$$

where n is the number of evaluation points.

4 Ground modifications

A number of different modifications of the structures involved and of the ground can be carried out in order to reduce the vibrations in a building that are induced by incident ground vibrations. Persson [1] found, for a particular building that was investigated, that when harmonic and transient internal loads were applied, modifications of the soil had a greater effect on the levels of vibration that occurred than structural modifications did. In Persson and Persson [3] it was found that the parameters of the soil also had the major effect when external loads were involved.

One approach to modifying the ground parameters is to stabilise the soil beneath a concrete slab, through increasing the stiffness of the soil, so as to change the geotechnical properties of the foundation. The procedure of mixing various types of binders with soil, developed both in Sweden and in Japan in the 1970s, is a frequently used method for the improvement of soft soils in connection with road and railway construction and also when creating the foundations for buildings. There are several different types of binders that can be used for this purpose, either singly or in conjunction with one another, such as cement, lime, blast furnace slag and fly ash, the first two being those used most frequently. The fundamental aim is to increase the elastic modulus of the soil through adding an adequate amount of binder (the elastic modulus of the stabilised soil depends then on the amount and types of binder employed). For example, a 4 m thick layer, in general, of soil located underneath the concrete slab of the ring-shaped building at MAX IV was stabilised in this way.

Another approach that can be taken is to reflect incident ground waves by placing a suitable trench in the ground between the wave source and area where the level of vibration are to be reduced. Shaping the landscape to create an irregular topography of the ground surface involving hills and valleys scatters the incident surface waves so as to be able to reduce vibration levels. This method and the other one for reducing the level of the incident ground vibrations that occur, in the area of interest, are investigated in each of the two papers that are appended and are also described in detail in the subsections that follow.

4.1 Trenches

Most of the vibration energy that originates from excitation of the ground surface is carried by Rayleigh surface waves that propagate close to the ground surface. Since these waves attenuate with horizontal distance to the source and with depth in the ground, it is

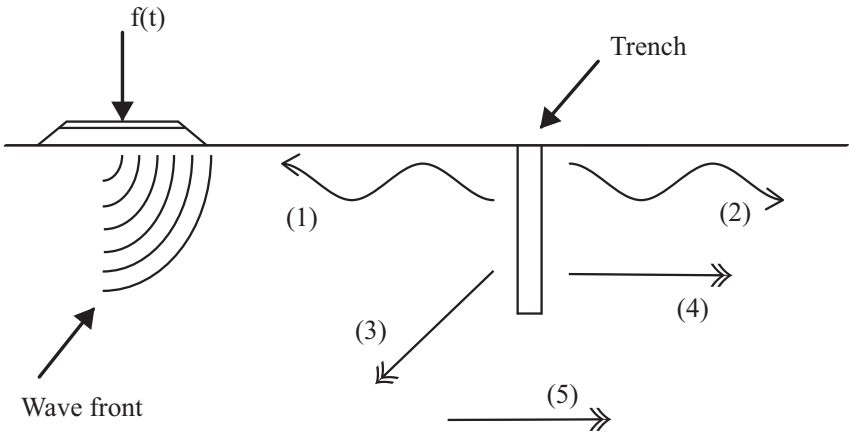

Figure 4.1: Different waves stemming from waves incident to a trench.

possible to reduce the level of the ground vibrations that occur by placing a suitable wave barrier in the ground between the wave source and the facility that is to be protected.

Installing a trench in the ground as a wave barrier between a vibration source and an area where the vibrations are to be reduced, such as a facility, creates a discontinuity for the propagating waves. Waves that are incident to the trench give rise to different types of waves. These can be divided into five separate groups (cf. Figure 4.1): (1) Rayleigh waves reflected back by the trench, (2) Rayleigh waves transmitted through the trench, (3) body waves from the trench propagating downwards and back towards the wave source, (4) body waves from the trench propagating away from the wave source and (5) waves propagating through the soil and bedrock under the trench. Ground vibrations after the trench has been passed are caused by transmitted Rayleigh waves (2), by body waves propagating to the right of the trench (4) and by waves propagating in the soil and bedrock under the trench (5).

The effects of using a trench as a wave obstacle are investigated in appended Paper A – *Numerical investigation of reduction in traffic-induced vibrations by the use of trenches.*

4.2 Landscape shaping

Constructing a shaped landscape as a wave obstacle located between a vibration source and the facility that is to be protected creates a discontinuity of the propagating surface waves though irregular topography this landscape possesses. Waves that are incident to the shaped landscape show different types of behaviours associated with changes in the direction of the propagating waves. The waves are subjected to both reflection and diffraction at the irregular ground surface of the shaped landscape, each of these two phenomena scattering the wave front and thus reducing the level of vibration at the facility.

At large construction sites, considerable amounts of soil are excavated in order to level the ground surface. This is necessary since, generally speaking, the surface needs to be horizontal before the construction of a building begins, the loose topsoil needing to be

removed. The large amounts of excavated soil produced often need to be transported away from the construction site, a matter which can be costly for the construction project. If instead these soil masses can serve a useful purpose at the construction site, they can be retained and be used to construct a shaped landscape with hills and valleys or whatever characterise it; see Figure 1.1. A shaped landscape can serve to reduce traffic-induced ground vibrations incident to a facility and can also be regarded as representing an aesthetically desirable solution.

The effects of using a shaped landscape as a wave obstacle are investigated in appended Paper B – *Reduction in ground vibrations by using shaped landscapes.*

5 Discussion

The continual increases in population that occur require that more dwellings and other facilities, such as office buildings and sport stadiums, to be built. This result in that houses needing to be built in unbuilt spaces within cities and in areas close to such vibration sources as motorways, railways and temporary construction sites. There is thus a need of having efficient methods available for reducing ground vibrations when the building up of more densely populated areas is to be planned.

5.1 Conclusions

Both types of ground modifications that was investigated were shown to achieve an appreciable reduction in the level of vibrations. Both the use of a trench filled with a solid material and the use of a shaped landscape were found to achieved a reduction in the level of vibrations of approximately 35 %. It is clearly difficult to construct a completely open trench (containing only air), i.e. without water infiltrating into it. Since the water level in a trench varies over the course of a year and is also dependent upon the groundwater level and the hydraulic conductivity of the soil, it is difficult to draw precise conclusions regarding a water-infiltrated trench. Due to achievement of a reduction in the level of vibrations of some 35 %, however, both the installation of a trench and the construction a shaped landscape can be regarded as effective methods for reducing incident traffic-induced ground vibrations. Both these types of methods can thus be regarded as be suitable for making it possible to construct buildings close to vibration sources in this respect.

The effectiveness of a trench and of a shaped landscape in reducing ground vibrations was found to be dependent upon the geotechnical conditions present at the construction site. For example, a trench filled with a solid material having a low elastic modulus (e.g. E=1 MPa) was found to be less effective in a very soft soil (e.g. E=50 MPa) than one in a very stiff soil (e.g. E=1500 MPa). Also regarding a shaped landscape, small irregularities in the surface (in the form of small hills and valleys) were found to be less effective in reducing vibrations in the case of a particular stiff soil due to the long wavelengths present there). It can thus be concluded that it is important to conduct measurements at the sites that are involved so as to be able to evaluate adequately the material parameters that are needed for the FE calculations to provide results of sufficient accuracy.

5.2 Proposals for future work

The method presented in section 2.4.1 to obtain a traffic load from a calculated FRF is not only valid for studying vibrations induced by traffic on motorways. It can also be used to obtain other traffic loads by scaling the FRF with frequency spectrums of other types of loads, originated from, for example trams and trains. If a frequency spectrum is not possible to obtain from measurements at the specific construction site, it should at least be based on measurements at sites with similar geotechnical conditions.

One of the general conclusions regarding shaped landscape is that the use of only valleys amplified the level of vibration in the area where it was expected to result in a reduction. The effects of having water in valleys, as an effect of water-infiltration or by precipitation, have not been studied yet and may influence the effectiveness of the shaped landscape as the diffraction and reflection of the wave front caused by the shaped landscape will change compared to having valleys without water. A shaped landscape with only water-filled valleys (i.e. a landscape with ponds) will not affect the architecture of the surrounding landscape to the same extent as a shaped landscape with empty valleys would do. Water-infiltrated valleys can, thus, be architecturally desirable.

The combined effect of having a trench and a shaped landscape could be studied as well. Since the geometry of the FE model is changed when a wave obstacle is involved, it is not possible to obtain the combined effect of them by superimposing the degree of reduction achieved for the wave obstacles. All wave obstacles must, thus, be involved in an analysis. To obtain more efficient numerical models, the boundary element method may be employed in combination with the FE method. By doing so, the computational time can be reduced significantly. This is primarily valuable for large 3D FE models since 2D models are usually relatively time-effective.

Bibliography

[1] Persson P. Analysis of Vibrations in High-Tech Facility, Report TVSM-5164, Division of Structural Mechanics, Lund University, 2010.

[2] Persson P., Persson K., Analysis of Dynamic Soil-Structure Interaction at High-Tech Facility, Proceedings of NSCM-23: the 23rd Nordic Seminar on Computational Mechanics, Stockholm, 2010.

[3] Persson P., Persson K., Sandberg G., Reduction of traffic-induced vibrations at high-tech facility using trenches, Proceedings of NSCM-24: the 24rd Nordic Seminar on Computational Mechanics, Helsinki, 2011.

[4] MAX IV, Detailed design report in the MAX IV facility, 2010.

[5] TYRÉNS, Geotechnical investigation report, Reference number 225686G, Helsingborg 2010-12-10.

[6] Richart FE., Hall Jr. JR., Woods R. D. Vibrations of soils and foundations, Prentice Hall, Englewood Cliffs, 1970.

[7] Andersen L. Lecture notes: Linear elastodynamic analysis, Aalborg University, 2006.

[8] Das BM., Ramana GV. Principles of soil dynamics, Cengage Learning, Stamford, 2011.

[9] Craig Jr RR. Structural dynamics, John Wiley & Sons, New York, 1981.

[10] Chopra AK. Dynamics of structures, Prentice Hall, Upper Saddle River, 1995.

[11] Zienkiewicz OC., Taylor RL. The finite element method, volume 1 and 2, MacGraw-Hill, London, 1994.

[12] Bathe KJ. Finite element procedures, Prentice Hall, New York, 2006.

[13] Sandberg G. Finite element modelling of fluid-structure interaction. Lund University, Division of Structural Mechanics, TVSM-1002, 1986.

[14] Dassault Systemes, Abaqus 6.11 Documentation, USA, 2011.

[15] Altair Engineering, Hyperworks 11.0.

[16] SGU - Geological Survey of Sweden, MAX IV - Kartering av kärnborrningarna GS1 och GS2, Reference number 08-852/2010, Lund 2010-12-02.

[17] Axelsson K. Introduktion till geotekniken, Uppsala Universitet, 2005.

[18] Sällfors G. Lecture notes: Grundläggningsteknik, Lunds Universitet, 2008.

[19] PEAB, Rapport avseende vibrationer från lokalvägar till Max IV, 2012-04-19.

Part II

Appended publications

Summary of appended papers

Paper A – Numerical simulations for studies of reduction in traffic-induced vibrations by the use of trenches

Reduction in traffic-induced ground vibrations by use of trenches is investigated here in a parametric study. The effects of geometric parameters on various open trench material parameters in filled trenches and of infiltrated water in open trenches were examined. A finite element method involving use of both finite and infinite elements in the frequency domain was employed. In investigating the effects of the infiltrated water, account was taken of fluid-structure interaction. The finite element model, in which plane strain conditions were assumed, was applied to a road, the bedrock, two layers of soil and a trench. The depth of the trench and the elastic modulus of the solid material that was inserted were found to be the most important parameters to consider. The results concerning the infiltration of water into an open trench indicated the presence of water there to increase the vibration levels.

Contributions by P. Persson

P. Persson contributed to the work by being the main author of the paper and writing it, as well planning several of the research tasks. He developed the finite element models employed, performed the calculations and drew conclusions that were presented.

Paper B – Reduction in ground vibrations by using shaped landscapes

Reduction in traffic-induced ground vibrations by use of shaped landscapes is investigated here by shaping the landscape surrounding a high-tech facility and using the landscape thus produced as a wave obstacle. The effects of the geometric parameters of a shaped landscape were examined in parametric studies. An architectural landscape design was also investigated in terms of its effectiveness in reducing traffic-induced ground vibrations. A finite element method involving use of both finite and infinite elements in the frequency domain was employed. The finite element models employed concern a layer of soil and the underlying bedrock. It was found that anywhere from an appreciable reduction to

an appreciable amplification of the vibrations produced can occur, depending upon the geometric parameters of the shaped landscape involved.

Contributions by P. Persson

P. Persson contributed to the work by being the main author of the paper and writing it, as well as developing research tasks. He created finite element models, performed calculations and drew conclusions that were presented.

Paper A

Numerical simulations for studies of reduction in traffic-induced vibrations by the use of trenches

Peter Persson, Kent Persson and Göran Sandberg

Division of Structural Mechanics
Lund University
Sweden

Submitted for publication

Numerical simulations for studies of reduction in traffic-induced vibrations by the use of trenches

Peter Persson, Kent Persson, Göran Sandberg
Department of Construction Sciences, Lund University, Sweden
Submitted for publication

Abstract

A numerical strategy for investigation of reduction in traffic-induced ground vibrations by the use of trenches is developed. The effects of geometric parameters on various open trenches, of material parameters in filled trenches and of infiltrated water into open trenches were examined by the use of the numerical procedure in a parametric study. The finite element method involving use of both finite and infinite elements in the frequency domain was employed. In investigating the effects of the infiltrated water, account was taken of fluid-structure interaction. A finite element model, in which plane strain conditions were assumed, was applied to a road, the bedrock, two layers of soil and a trench. The depth of the trench and the elastic modulus of the solid material inserted were found to be the most important parameters to consider. The results concerning the infiltration of water into an open trench indicated that the presence of water increases the vibration levels.

Keywords: Vibration reduction; trench; finite element method; fluid-structure interaction; traffic-induced vibrations; wave propagation

1 Introduction

Occasionally, very strict vibrational requirements are specified for vibration-sensitive equipment used in high-tech facilities, such as radar towers and synchrotron facilities. High-tech facilities are often located in the vicinity of vibration sources of significant amplitude, radar towers often being found near rocket-launching facilities, for example, and synchrotrons near heavily trafficked roads, the latter for logistic reasons. Traffic-induced ground vibrations can propagate to facilities nearby and lead to the vibration requirements for sensitive equipment being exceeded. It can be desirable in such cases to reduce the ground vibrations by use of wave barriers. The traffic-induced vibrations can be reduced by various means, such as by placing a trench between the road and the facility [1, 2].

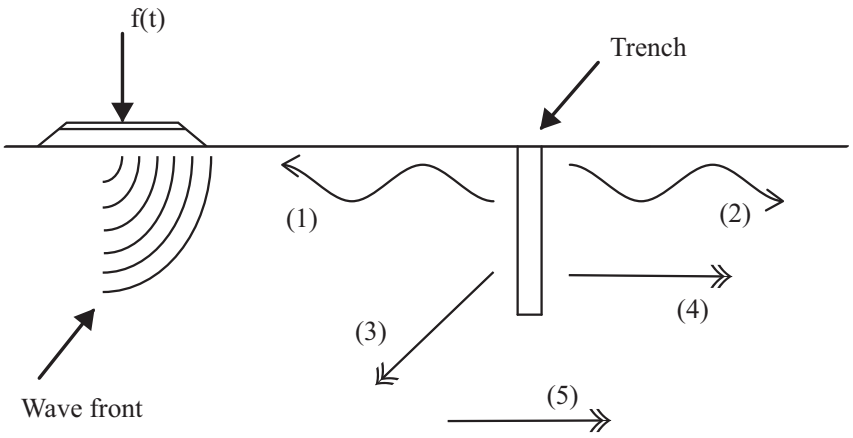

Figure 1: Different waves stemming from waves incident to a trench.

Installing a trench in the ground as a wave barrier between a vibration source and a facility creates a discontinuity for the propagating waves. Waves that are incident to the trench give rise to different types of waves. These can be divided into five separate groups (cf. Figure 1): (1) Rayleigh waves reflected back by the trench, (2) Rayleigh waves transmitted through the trench, (3) body waves from the trench propagating downwards and back, (4) body waves from the trench propagating forward and (5) waves propagating through the soil and the bedrock, under the trench. Ground vibrations after the trench has been passed are caused by (2), (4) and (5).

In the paper, results concerning reductions in traffic-induced vibration at the MAX IV synchrotron facility serve as numerical examples of the effect of using trenches as wave barriers. Figure 2 presents an architectural sketch of the facility as planned. MAX IV will be built approximately 100 m from a motorway. In the MAX IV facility a beam of electrons is to be controlled by a large number of magnets that are distributed along the ring-shaped structure and along beam lines that lead beams of electrons that are produced to measurement stations. Since the quality of the measurements obtained is dependent upon the levels of vibration of the magnets, very strict requirements are specified regarding the vibration levels. The vibration requirements for MAX IV regarding vertical displacements of the magnets are especially strict, its being required that these be less than 20-30 nm in RMS per second within a frequency span of 5-100 Hz.

1.1 Literature review

Several investigations of the effectiveness of trenches in terms of reduction in ground vibrations have been carried out, such as field tests and numerical simulations by means of both the boundary element (BE) method and the finite element (FE) method, as well as a combination of the two (FE-BE).

Since field tests are expensive to conduct they are not suitable to perform as series of tests, despite their providing highly relevant information regarding the site. A potential problem with the FE method is the boundaries that act like reflectors for the propagating waves. The boundaries can be places very far away from the region of interest

Figure 2: The MAX IV facility as it is expected to appear, as rendering in a drawing by the architect bureaus FOJAB and Snøhetta.

or using non-reflecting (infinite) elements at the boundaries. The infinite elements are not completely non-reflecting, therefore, the boundaries must still be the placed quite far from the region of interest. For two-dimensional (2D) FE models using infinite elements, the computational cost will still be reasonable. With use of the BE method, completely non-reflecting boundaries are provided, however, structures such as a road and a trench cannot be modelled by the BE method, whereas the FE method is needed. With use of the FE method, visualisation of the results of the whole numerical model are automatically performed, which is not the case for the BE method. Combinations of the two methods are clearly of interest for large numerical models, such as three-dimensional (3D) models involving soil and structures.

Woods [3] performed extensive scaled field tests to study the effectiveness of open trenches as wave barriers, both close to the vibration source and at a considerable distance from it. On the basis of the experimental findings obtained, Woods presented certain guidelines concerning the dimensions of an open trench that are needed in order to achieve a 75 % reduction in the ground displacement amplitudes that vertical excitation results in. It was concluded also that, because of its being difficult to extrapolate from results of small-scale field tests the results one could expect for full-scale field tests, numerical investigations are clearly of interest.

Studies of the effectiveness of trenches in terms of reduction in ground vibrations by means of the BE method have been carried out by, for example, Emad and Manolis [4], Beskos et al. [5], Dasgupta et al. [6], Leung et al [7, 8], Al-Hussaini et al. [9], Ahmad et al. [10], Klein et al. [11], Al-Hussaini et al. [12] and Kattis et al. [13]. The FE method is extensively used in studies of the effectiveness of trenches in terms of reduction in ground vibrations by, for example, Yang and Hung [14], Shrivastava and Kameswara [15], Hung et al. [16], Wang et al. [17] and Alzawi and El Naggar [18]. Coupled FE-BE methods for studying the effectiveness of trenches in terms of reduction in ground vibrations have

been employed by, for example, Adam and von Estorff [19], Andersen and Liingaard [20], Andersen and Nielsen [21], Andersen et al. [22], Andersen and Augustesen [23].

Some general conclusions from the numerical investigations are that open trenches provide a more effective vibration isolation than trenches filled with a solid material and that the depth of an open trench being the one parameters that has the greatest affect on the effectiveness of a trench and the width could be negligible while the distance to the vibration source needs to be considered. Further conclusions are that the effectiveness of trenches filled with solid material depends upon the material parameters of the filling material and that both open and filled trenches, as well as, sheet-pile walls and row of piles can be suitable as wave barriers. The use of a softer filling material increases the effectiveness of a filled trench and also permits larger depths to be used than in the case of an open trench, the depth of a trench is more effective than increasing its width, mass density and Poisson's ratio of the filling material were found to not affect appreciably the effectiveness of a filled trench, both a concrete lid placed on top of a trench with double sheet-pile walls and the inclination of the trench was found to not affect the effectiveness.

It is known from previous work [2, 24, 25] concerning the synchrotron facility MAX IV in Lund, Sweden, that when taking account of both internal and external sources of vibration the material parameters (concerning realistic values of them) of the soil have a strong effect on the vibration levels that occur in sensitive parts of the facility, whereas structural modifications of the facility itself have only a slight effect. It was also concluded that vibration source frequencies exceeding 25 Hz are effectively damped out in the soil so that they have only a negligible effect on the vibration levels in the facility.

1.2 Present study

None of the investigations of trenches referred to above considered the combined effects of the characteristics of the underlying bedrock and of the traffic loads to be expected, also the effects of infiltration of water into an open trench were not examined. The main objective of the study was to investigate the use of trenches as wave barriers for minimising traffic-induced vibrations. This was done by establishing numerical models, through use of the FE method as well as that of fluid-structure interaction (FSI), to account for infiltration of water, for predicting the effectiveness of using a trench. FE models making use of both finite and infinite elements, applied to the road, to the different soil layers and to the bedrock. The vibrations involved were investigated in the frequency domain by use of steady-state analyses. Open, as well as water-infiltrated and filled trenches parallel to a nearby motorway were studied, the traffic load on the motorway being employed in the analysis. The intention here was to extend knowledge of the use of trenches as wave barriers by considering both traffic loads and water-infiltration into an open trench through evaluation of reduction in the level of vibration. The general knowledge of the reduction achieved by the use of trenches needs to be extended so as to encompass traffic-induced vibrations from motorways generally, so as to be able to fulfil the increasing needs in the future of placing buildings closer to vibration sources such as motorways.

2 Numerical calculations

2.1 Structural dynamics

The open and filled trenches were investigated by steady-state analyses employing the FE method.

The equation of motion of a body, assuming small deformations, can be described by the differential equation

$$\tilde{\nabla}^T \sigma + \mathbf{b} = \rho \frac{\partial^2 \mathbf{u}}{\partial t^2} \tag{1}$$

where $\tilde{\nabla}$ is a differential operator matrix, σ is the stress vector, $\mathbf{b}$ the body force vector, ρ the mass density, $\mathbf{u}$ the displacement vector and t is time [26, 27]. The governing finite element formulation of a dynamic problem, as derived from Eq. (1), can be written as

$$\mathbf{M}\ddot{\mathbf{u}} + \mathbf{C}\dot{\mathbf{u}} + \mathbf{K}\mathbf{u} = \mathbf{f} \tag{2}$$

where $\mathbf{M}$ is the mass matrix, $\mathbf{C}$ the damping matrix, $\mathbf{K}$ the stiffness matrix, $\mathbf{f}$ the load vector and $\mathbf{u}$ the nodal displacement vector. In harmonic loading, steady-state vibration occurs. The load and the corresponding displacements can be expressed as complex harmonic functions

$$\mathbf{f} = \hat{\mathbf{f}} e^{i\omega t}; \mathbf{u} = \hat{\mathbf{u}} e^{i\omega t} \tag{3}$$

where $\hat{\mathbf{f}}$ and $\hat{\mathbf{u}}$ denote the complex load amplitude and the displacement amplitude, respectively, i is the complex number involved and ω is the angular frequency. Inserting Eq. (3) into Eq. (2) results in the following equation of motion in the frequency domain

$$\mathbf{D}(\omega)\hat{\mathbf{u}} = \hat{\mathbf{f}} \tag{4}$$

where $\mathbf{D}$ is the frequency-dependent dynamic stiffness matrix, which can be expressed as

$$\mathbf{D}(\omega) = -\omega^2 \mathbf{M} + i\omega \mathbf{C} + \mathbf{K}. \tag{5}$$

Since damping generally plays an important role in the dynamic response in soils, a rate-independent linear damping in the system was assumed. The loss factor which represents the attenuation of the propagating waves is defined as

$$\eta = \frac{1}{2\pi} \frac{E_D}{E_{So}} \tag{6}$$

where in a steady state, the energy dissipated in the form of viscous damping in a given cycle of harmonic vibration being denoted as E_D and the strain energy as E_{So} [28].

By consideration of the loss factor in the dynamic stiffness matrix results in

$$\mathbf{D}(\omega) = -\omega^2 \mathbf{M} + (1 + i\eta)\mathbf{K}. \tag{7}$$

The imaginary part of the stiffness matrix is referred to as the structural damping matrix [29].

2.2 Fluid-structure interaction

To be able to investigate the water-infiltrated trenches, FSI was considered.

The indices s and f will be used to denote the properties of the structural and the fluid domains, respectively. Two governing equations can be employed for describing an acoustic fluid, which is assumed to be inviscid, irrotational and compressible and to undergo small pressure changes. The equation of motion, the volumetric drag being neglected here, can be written as

$$\rho_0 \frac{\partial^2 \mathbf{u}_f}{\partial t^2} + \nabla p_d = 0 \tag{8}$$

where ρ_0 is the static density, ∇ is the gradient of a variable and p_d is the dynamic pressure [26, 27, 30], the density being assumed to have a negligible variation in space. With the absence of an added fluid mass inflow, the constitutive equation can be written as

$$p_d = -c_0^2 \rho_0 \nabla \mathbf{u}_f \tag{9}$$

where c_0 is the the speed of sound. With use of Eqs. (8, 9), the wave equation for the acoustic fluid, the pressure serving as the field variable, can be written as

$$\frac{\partial^2 p_d}{\partial t^2} - c^2 \nabla^2 p_d = 0. \tag{10}$$

The pressure can be expressed as a complex harmonic function

$$p_d = \hat{p}_d e^{i\omega t} \tag{11}$$

where $\hat{p}$ denotes the complex pressure amplitude. Inserting Eq. (11) into Eq. (10) results in the wave equation in the frequency domain

$$\nabla^2 \hat{p}_d + \frac{\omega^2}{c^2} \hat{p}_d = 0. \tag{12}$$

Eq. (12) can be formulated in terms of the finite element method, the pressure serving as the approximated nodal field variable, as

$$\mathbf{M}_f \ddot{\mathbf{p}}_f + \mathbf{K}_f \mathbf{p}_f = \mathbf{f}_{f,p} \tag{13}$$

where $\mathbf{M}_f$ and $\mathbf{K}_f$ are matrices, $\mathbf{p}_f$ is the pressure vector and $\mathbf{f}_{f,p}$ is the boundary vector.

Continuity in of the fluid displacements and the structural displacements is assumed in the normal direction to their common boundary S. By introducing a normal vector, $\mathbf{n}$, the kinematic boundary condition can be formulated as

$$\mathbf{u}_s \cdot \mathbf{n}|_S = \mathbf{u}_f \cdot \mathbf{n}|_S. \tag{14}$$

Due to the continuity in pressure at S, the static boundary condition for the coupling can be formulated as

$$\sigma_{s,n}|_S = -p_f \tag{15}$$

where $\sigma_{s,n}$ is the stresses at S in the normal direction and p_f is the acoustic fluid pressure.

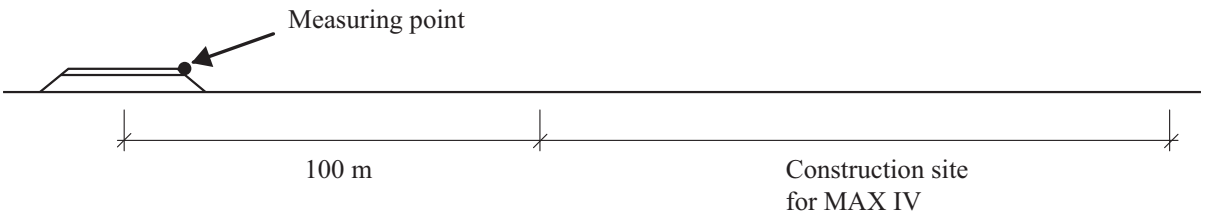

Figure 3: Schematic measurement setup.

2.3 Traffic load

A frequency spectrum of a traffic load was created from an experimental investigation of traffic-induced vibrations. For such vibrations, strains are usually at a level such that the assumption of linear elasticity is applicable. With use of a system of linear equations, the frequency content of the traffic load can be employed for scaling the calculated displacements in order to account for the traffic load, thus only a frequency response function (FRF) needs to be obtained. This being suitable for studying reduction in the level of vibration for various types of wave barriers and is not possible to employ for investigating absolute levels of vibration.

As the vibration requirements for MAX IV are especially strict within a frequency span of 5-100 Hz and that various studies of the MAX IV site concluded that vibration source frequencies exceeding 25 Hz have only a negligible effect on the amplitudes of vibrations in the facility, a frequency span of 5-25 Hz for the traffic load was considered. The frequency content of the traffic load at the motorway near MAX IV was evaluated on the basis of green-field in-situ measurements; see Figure 3 for a schematic presentation of the measurement setup. The velocity versus time was measured at the top of the slope of the road embankment of the motorway during the passage of trucks, which generated the highest velocities at the measuring point. The ten events having the highest velocity amplitudes caused by heavy trucks during the period of one hour were registered. The displacements involved were evaluated and a Fast Fourier Transform (FFT) of the displacement-time curves was performed to determine the frequency content of the response at the embankment. Since high frequencies are damped out quickly in the soil, the measurements on the embankment do not have the same frequency content as the traffic load. However, in the frequency range of interest (below 25 Hz) this difference in location was assumed to have a negligible effect because of the distances between the load (on the truck wheels) and the embankment being so short. A frequency spectrum for the traffic load was created by fitting a second-degree polynomial to the experimental data; see Figure 4. The second-degree polynomial was normalised by its largest magnitude and considered to be representative of the frequency content of the traffic load.

2.4 Evaluation

A frequency spectrum was employed for scaling the calculated displacements in order to account for the traffic load, according to the method described in subsection 2.3.

To evaluate and to compare results from various analyses performed, an RMS value can be used as a measure of the vibration magnitude. The RMS value of the displacements

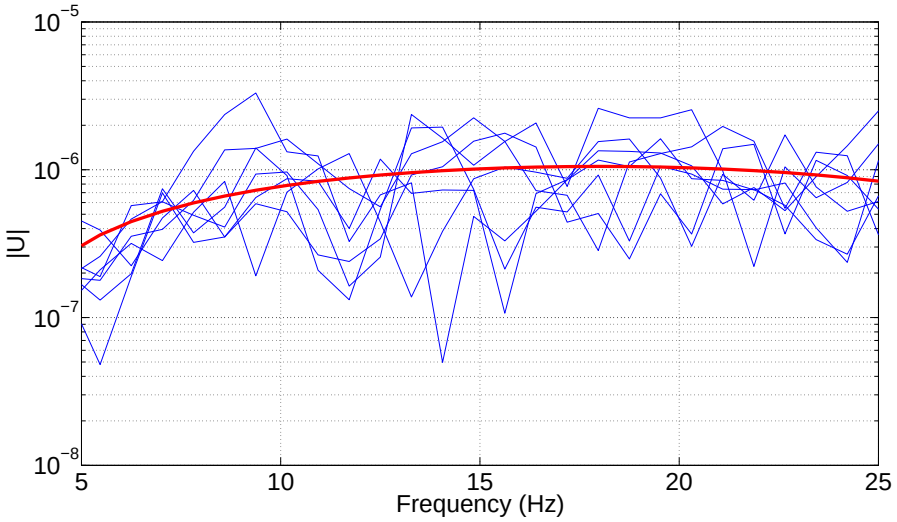

Figure 4: The magnitude spectrum of displacements, U(t), as obtained on the basis of measurements.

from the steady-state analyses was determined here by

$$u_{RMS} = \frac{1}{n}\sqrt{(u_1^2 + u_2^2 + ... + u_n^2)} \tag{16}$$

where u_{RMS} is the RMS value of the displacements, u_i is the magnitude of the displacement at each frequency and n is the number of frequencies in the interval.

To determine the effectiveness of the trench five equally spaced evaluation points were used to calculate an average displacement reduction factor; see Eq. (18). They were located at, points 100, 150, 200, 250 and 300 m from the excitation point; see Figure 5. This was used as a measure of the effectiveness of the trench as a wave barrier. The displacement reduction factor, U_{red}, pertains to the vibrational amplitude after a trench had been installed (post-trench), U_{post}, to the amplitude prior to its being installed (pre-trench), U_{pre}, in accordance with Eq. (17). U_{pre} and U_{post} were determined on the basis of the complex displacement magnitudes for the different frequencies and was calculated as the RMS values at the evaluation points, in accordance with Eq. (16).

$$U_{red} = \frac{U_{pre} - U_{post}}{U_{pre}}. \tag{17}$$

$$\bar{U}_{red} = \frac{1}{m}\sum_{i=1}^{m} U_{red,i} \tag{18}$$

where m is the number of evaluation points.

3 Finite element model and considered parameters

In the numerical example employed here, the soil at the site consisted of 16 m of two different clay tills identified as Low Baltic clay till covering the stiffer Northeast clay till

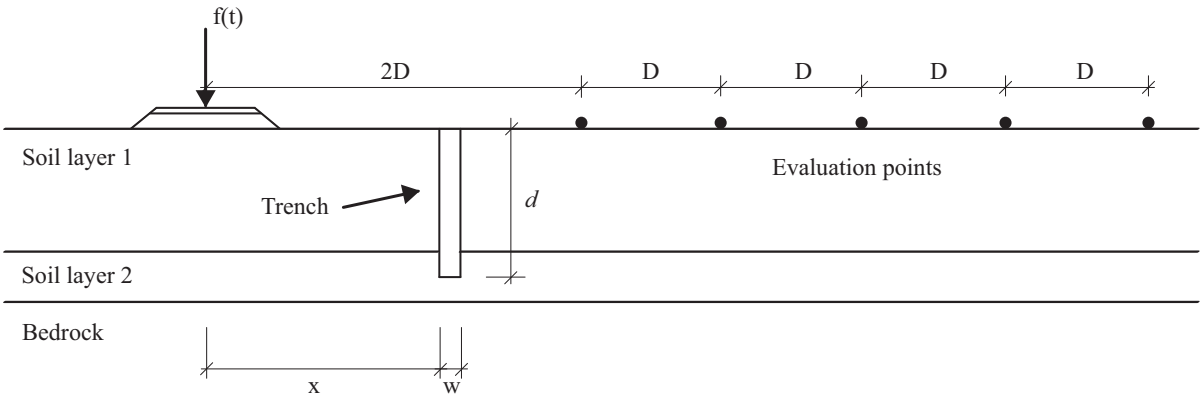

Figure 5: FE model. Distance, D=50 m

on top of bedrock consisted of sandstone and shale [32, 33]. All interfaces in the model were assumed to have full interaction, so that no relative motion between the interfaces was allowed. The geometry was that of the road, the trench, 16 m of soil and 100 m of bedrock; see Figure 5. The road was modelled as having a layer of asphalt covering a layer of unbounded granular material (UGM). A 2D FE model was developed with the use of the FE software package *Abaqus*. The trench being assumed to be regarded as long, i.e. wave phenomena that occurs at the edges are assumed to be negligible and, therefore, not affect the effectiveness of the trench as it was evaluated here. The size of the model was 116×350 m^2 (height×width). Quadrilateral 8-node plane strain elements obtained by quadratic approximation using reduced integration were employed. To simulate the far-field conditions and avoid reflecting boundaries, 5-node quadratic one-way infinite elements were employed. To ensure that the analyses provided results of adequate accuracy, an element mesh with a minimum of nine element nodes representing the shortest wavelengths were employed. The soil materials had for the most part an element size of 2x2 m^2, the bedrock having mainly an element size of 2x8 m^2; see Figure 6. The model contained approximately 3,800 elements with approximately 11,800 degrees of freedom. A harmonic point load, f(t), was applied to the modelled road, representing the traffic load from the motorway. The vibrations with the highest amplitudes, from the motorway, occur when the road is heavily trafficked, thus the traffic load can be regarded as a line load. The load from each truck is then, however, assumed to be in phase, which is assumed to have a negligible effect on the evaluation of the effectiveness. A FRF was obtained by applying a harmonic load of 1 N for frequencies from 5 to 25 Hz in steps of 0.1 Hz.

Local variations in the road materials, the soil layers and the bedrock, such as stratum and granularity, were assumed to be small as compared with the wavelengths in the frequency range of interest. Thus, the road, the soil and the bedrock were modelled as being isotropic homogeneous materials [31]. The material parameters employed here were evaluated from both geotechnical and geophysical measurements that were carried out at the MAX IV site in collaboration with the companies *PEAB*, *TYRÉNS* and *NGI*, as well as from comparison between FE simulations and those measurements, in order for agreement to be achieved; see Table 1 [33]. The loss factors include all attenuation effects

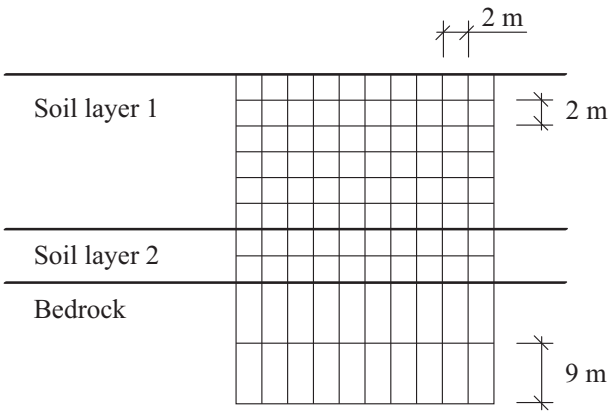

Figure 6: Schematic drawing of the FE mesh.

such as material and geometrical damping, as well as the varying topography of the soil and of the bedrock.

Table 1: Material parameters.

Property	Asphalt	UGM	Soil layer 1	Soil layer 2	Bedrock
Depth (m)	0.15	0.5	12	4	100
Elastic modulus (MPa)	5000	315	378	1136	8809
Loss factor	0.10	0.10	0.10	0.10	0.04
Mass density (kg/m^3)	2600	2300	2125	2125	2600
Poisson's ratio	0.25	0.20	0.48	0.48	0.40

The infiltrated water was modelled as an acoustic fluid and investigated by means of FSI analyses. In modelling of the water, 8-node biquadratic acoustic pressure elements were employed. The water was assumed to have a temperature of 10 °C, the static density of it, ρ_0, being set to 1000 kg/m^3 and the speed of sound, c_0, to 1450 m/s giving a bulk modulus, K, of 2.10 GPa. The pressure at the free surface of the acoustic medium was prescribed to zero, as surface gravity waves were neglected due to the very low vibration amplitudes.

4 A parametric study of open trenches

A parametric study of the open trenches was carried out first, for differing locations, widths and depths of the trench. As a base state, the trench was placed at a distance, d, of 50 m from the centre of the road, having a width, w, of 1 m and a depth, d, of 12 m (the same as the depth of the top soil layer); see Figure 5 for the notations. Each parameter was varied from the base state while the other parameters were kept constant.

In Figure 7, the vertical displacements from simulations prior and after a trench had been installed, respectively, are shown for a harmonic load at 9 Hz. The open trench has the same depth as the soil. As it can be seen in Figure 7(b), in comparison to Figure 7(a), the wave front is directed downwards into the bedrock, propagates forward through the

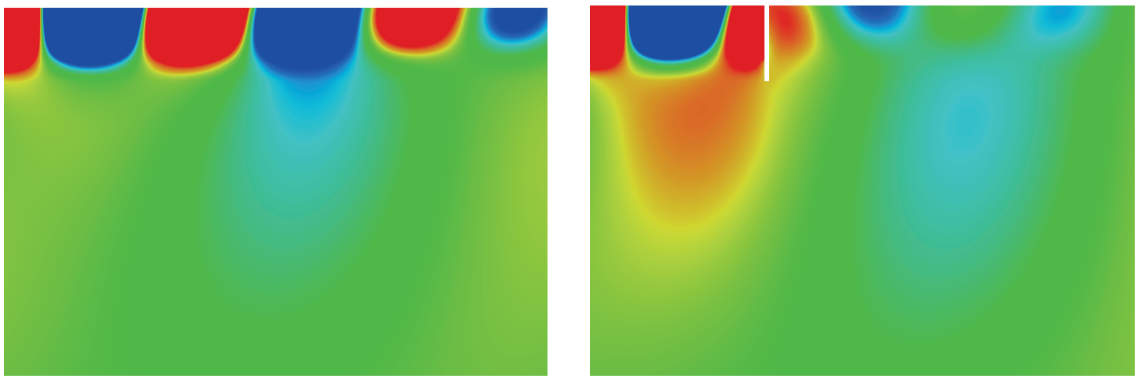

(a) (b)

Figure 7: Simulation results of vertical displacements, (a) prior the installation of a trench and (b) for an open trench with the geometry x=40 m, w=1 m, d=16 m. (The total horizontal extension of the soil and of the bedrock are not shown.)

bedrock and excites the soil layers. The vibration levels in the bedrock are increased when an open trench had been installed. It is also visible that the vibration levels at the ground surface, after the trench, are decreased in comparison to the situation prior the installation of a trench.

The reduction in the vibration level is shown in Figure 8 as a function of the depth of the trench. The depth, d, was varied between 0 and 16 m. The reduction becomes larger as the depth of the trench is increased. It is evident that in the present case the trench needs to be deeper than 4 m in order for the vibration levels at the facility to be reduced appreciably. The largest change was found to be for the increase from 6 to 10 m in depth. Between 6 and 10 m the reduction in the vibration level increases from 21 to 55 %. For a trench deeper than 10 m, the waves propagating in the bedrock appear to dominate. A reduction of between 0 and 65 % could be obtained by varying the depth of an open trench.

A trench reflects incident waves but also contributes to disturbances in the wave front, this causing refraction and diffraction of the propagating waves. The changes in speed and in the direction of the wave front due to reflection, refraction or diffraction results in interference of the waves at certain distances from the trench in particular. Thus, the most effective location, in terms of reducing vibrations, for the trench needs to be sought. A study of the effect of the location of the trench was carried out. The distance between the motorway (the excitation point) and the MAX IV building (the evaluation points), was 100 m. In consideration of this, the location of the trench was varied between a distance, x, of 10 m and a distance of 90 m from the motorway. In Figure 9 the reduction obtained in the level of vibration is shown as a function of the location of the trench. It was found that the most effective location of the trench was 40 m from the road, however, there was only a slight variation of the reduction in the level of vibration for distances between 20 and 80 m from the motorway. The worst location was at 10 m from the motorway and at 10 m from the building, respectively, i.e. close to the vibration source or close to the area that are to be protected. A reduction in the vibration level of between 50 and 63 % was obtained for the different locations of the open trench considered.

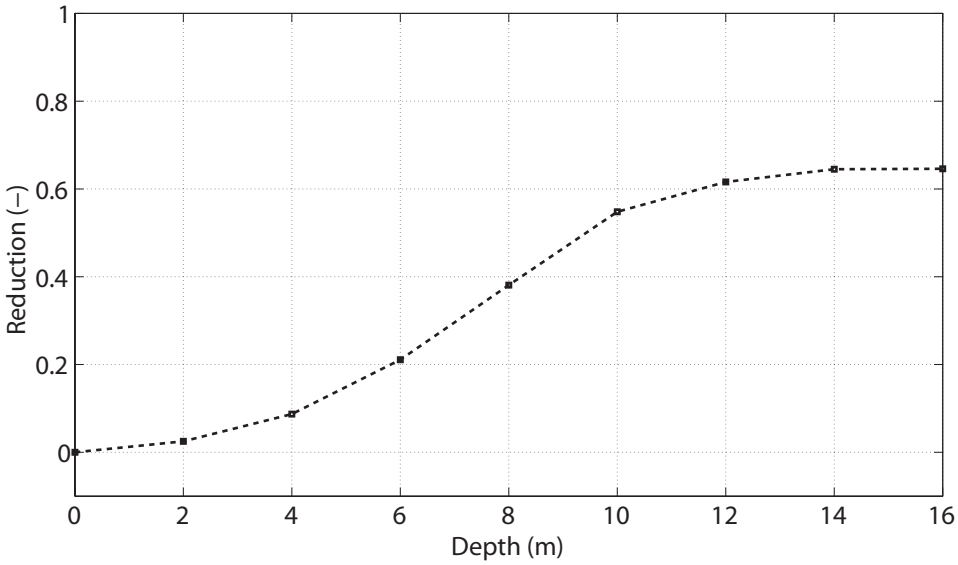

Figure 8: Average reduction in the vibration (displacement) levels versus the depth of the trench.

The width, w, was varied between 0.25 and 4 m. It was found that the width of the trench has only a very slight effect on the reduction in the vibration level achieved by an open trench. For a shallow trench, the effect of the width was not investigated, although there the width may have a stronger effect on the vibration levels than in the case of a deep trench. A reduction of between 62 and 64 % was obtained for the different widths of an open trench that were studied.

5 Parametric studies of filled trenches

In practice, it can be difficult to use open trenches as wave barriers due to the infiltration of water into them and safety aspects that needs to be considered. This motivates the use of trenches containing filling material of some sort. Use of filled trenches also allows trenches to be of greater depth because of the lack of need for lateral support at the sides. A parametric study of the material properties of the filling material was carried out. Four material parameters were varied, those of the elastic modulus, the loss factor, the mass density and Poisson's ratio. The trench was placed 50 m from the centre of the road, its having a width of 1 m and a depth of 12 m (the same depth as that of the top soil layer). It was assumed, as a base state, that the material properties of the filling material were the same as those of the excavated soil, the elastic modulus being set to 378 MPa, the loss factor to 0.10, the mass density to 2125 kg/m^3 and Poisson's ratio to 0.48. Each material parameter was varied from the base state while the others were kept constant.

The elastic modulus was varied between 1 and 50,000 MPa. In Figure 10, values of the elastic modulus lower than that of the top soil layer (the base parameter) are shown. As can be seen in the figure, up to a value of approximately 35 MPa, the elastic modulus has a marked influence on the effectiveness of the trench in reducing the degree of vibration. A reduction of from 39 to 10 % was obtained in varying the value of the elastic modulus

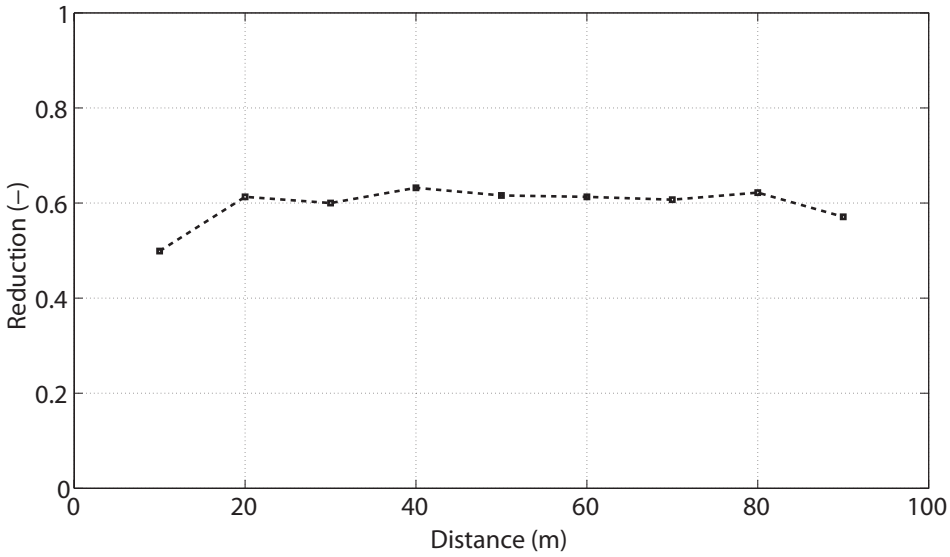

Figure 9: Average reduction in the level of vibration (displacement) versus the trench location.

from 1 to 35 MPa, Values higher than 39 % do not affect the effectiveness of the trench appreciably. As the elastic modulus approaches zero, the reduction in level of vibration approaches the same level as that for an open trench, although it may not have exactly the same level as that, since the filling material has a mass density. Varying the elastic modulus of the filling material to a value larger than that of the top soil layer has only a slight effect on the reduction in the level of vibration. A reduction of between 0 and 1 % was obtained through varying the elastic modulus for values higher than of the top soil layer.

The loss factor was varied between 0.01 and 2. As is shown in Figure 11, varying the loss factor of the filling material between values of 0.01 and 0.1 has only a slight effect of the degree of reduction achieved in the level of vibration. Regarding the loss factor, the reduction in the level of vibration became greater as the loss factor was increased.

The mass density was varied between 10 and 3000 kg/m^3. Varying the mass density of the filling material has only a slight effect on the reduction achieved in the vibration level. A reduction of between 0 and 2 % was obtained by varying the mass density.

Poisson's ratio was varied between 0.01 and 0.48. Varying Poisson's ratio of the filling material has only a slight effect on the reduction achieved in the degree of vibration. A reduction of only between 0 and 1 % could be obtained by varying Poisson's ratio.

5.1 Water-infiltrated trenches

To investigate the effects of water infiltration into an open trench, a numerical parametric study was carried out by considering FSI in the FE analyses in which the water level in an open trench was varied. The depth of the trench was set to 16 m, its being placed 50 m from the motorway and having a width of 1 m. The depth of the water in the trench was varied between 0 and 16 m (0 m corresponding to an open trench 16 m deep containing

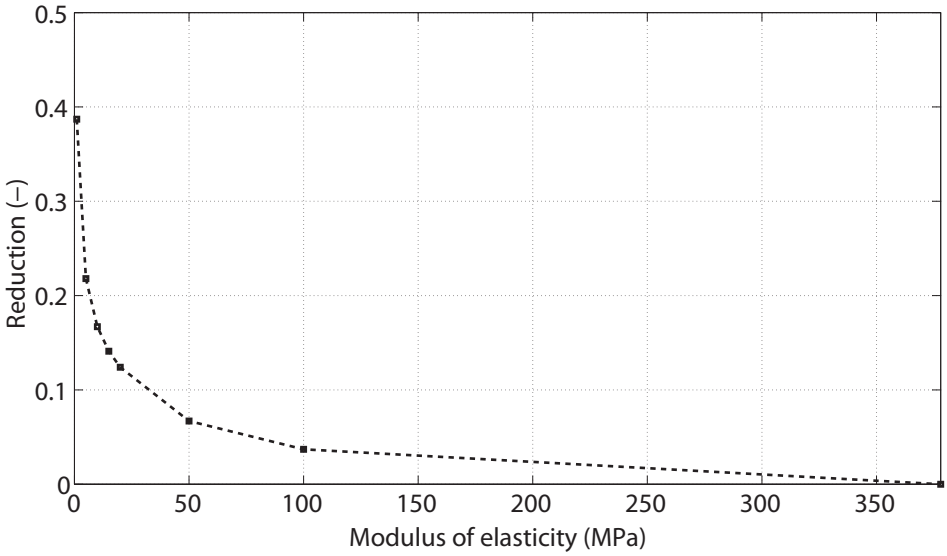

Figure 10: Average reduction in the level of vibration (displacement) versus the elastic modulus of the filling material (for values of the latter lower than that of the top soil layer).

no infiltrated water and one of the same depth completely filled with water), while the other parameters were kept constant.

Variation of the water level in the trench can be a result of, for example, heavily precipitation or of installation of water pumps that drains the trench by pumping of the infiltrated water away from it. The variation of the water level in the trench interacts with the groundwater level and can, therefore, affect the material parameters of the soil in proximity to the trench. Due to the clay tills' very low hydraulic conductivity, the changes in the ground water level were assumed to be a local phenomenon and, therefore, not affecting the relatively long wavelengths in the soil within the frequency range of interest (5-25 Hz).

As can be seen in Figure 12, the water level in the trench can affect very markedly the reduction in the level of vibration. A reduction of between 65 and 22 % was obtained for the various water levels involved. The reduction caused already by existence of the trench when it is empty decreases only very slightly up to a water level of 6 m, and decreases rapidly then up to a water level of 10 m, these higher water levels enabling more of the P-waves to travel through the trench (S-waves cannot propagate in water). The reduction in the level of vibration varies little then up to a water level of 14 m, within the water levels of 10-14 m the phenomena involved seeming to interact and to have about the same effect throughout. As the water level rises then up to 16 m, the reduction in the level of vibration rises appreciably, which can be due to that the water supporting the vertical walls of the trench.

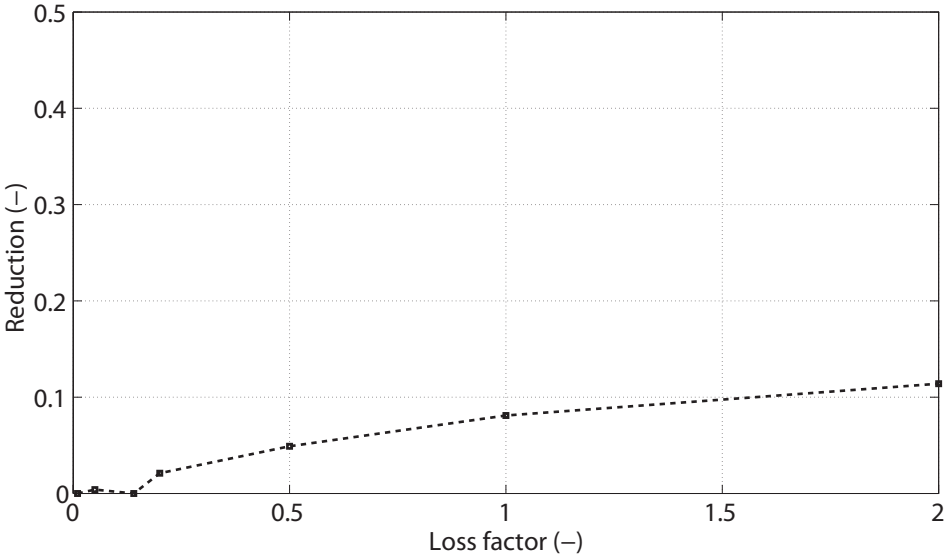

Figure 11: Average reduction in the level of vibration (displacement) versus the loss factor of the filling material.

6 Conclusions

Reduction in traffic-induced ground vibrations through use of trenches was investigated in a numerical parametric study using the FE method. The effects of geometric parameters in the case of an open trench, of material parameters in the case of a filled trench containing solid material, and of infiltrated water in an open trench at least partly filled with water were examined.

On the basis of the results obtained, the following conclusions can be drawn.

- A deeper trench provides, when the trench volume involved is constant, a greater reduction in the degree of vibration than a wider trench does. It should be pointed out that the width of the trench may be of greater importance in the case of a shallow trench than of a deeper one. Also, at certain depths the dominant Rayleigh waves are not affected, to any extent at least, by the lower part of the trench, due to their being dampened out in the vertical direction. The degree of reduction found at the greatest depths is virtually constant; see Figure 8.

- The width can be neglected in the case of an open trench, and both the mass density and Poisson's ratio can be neglected in considering the solid materials contained in a filled trench, despite the large variation of the parameters being considered.

- It is possible to determine the most effective location, in terms of reducing vibrations, for a given trench. In the present study this was found to be at a distance of 40 m from the excitation point, however, there is only a slight difference of the degree of reduction achieved in the level of vibration for distances between 20 and 80 m. The most effective location is dependent, however, on a variety of other factors too, in addition to the distance from the excitation point, in particular the

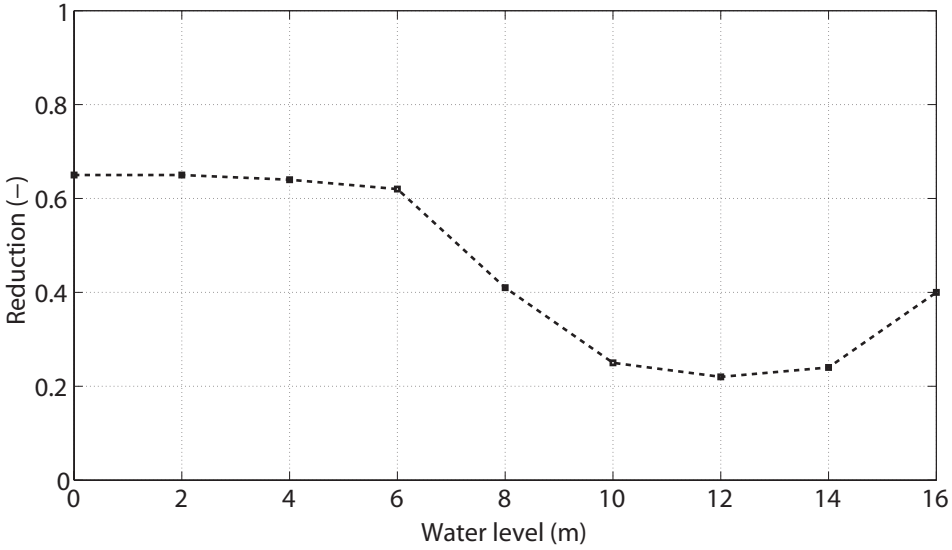

Figure 12: Average reduction in level of vibration (displacement) versus the water level in the trench.

frequency content of the load, the location of the evaluation points, and the material parameters of the soil and of the bedrock.

- The loss factor of the filling material has only a slight effect at values of less than 1. It should also be pointed out that it may be difficult to manufacture a filling material with a loss factor greater than 1. The loss factor may have a stronger effect on the reduction in the level of vibration for wide trenches than for narrow ones.

- Since the mass density of the solid filling material has little effect on the reduction in vibrations, the level of impedance ($Z = c\rho$) should not be used as a measure of the effectiveness of a filled trench. The wave speed of body waves and of Rayleigh waves depends upon both the elastic modulus and Poisson's ratio. As has been indicated, Poisson's ratio has little effect upon the effectiveness of a trench. Thus, it is quite sufficient to investigate simply the effect of the elastic modulus in order to determine adequately the effectiveness of a solid filling material in this respect. Note that it would also be sufficient to consider simply the shear modulus.

- Open trenches always provide a greater reduction in the level of vibration than filled trenches do, assuming the geometric parameters involved to be identical.

- Body waves travel through the soil and the bedrock beneath the trench before they excite the soil near the evaluation points. It is thus important to include the bedrock in the numerical models employed.

- The infiltration of water into, as well as draining of water in, an open trench can strongly affect the reduction in the level of vibration that the presence of a trench results in. The effectiveness of a trench decreases when any very appreciable amount of infiltrated water is present, since water transmits P-waves. A water level of 12 m

in a trench 16 m deep was found, for example, to decrease the reduction in the level of vibration from 65 % to 21 %.

Acknowledgments

The financial support for this work provided by the Silent Spaces project, a part of the EU program Interreg IVA, is gratefully acknowledged.

References

[1] Richart FE, Hall Jr JR, Woods RD. Vibrations of soils and foundations, Prentice Hall, Englewood Cliffs, 1970.

[2] Persson P, Persson K., Sandberg G. Reduction of traffic-induced vibrations at high-tech facility using trenches. In: Freund J, Kouhia R. editors. Proceedings of NSCM-24: the 24rd Nordic Seminar on Computational Mechanics. Helsinki, Finland: 2011.

[3] Woods RD. Screening of surface waves in soil. Journal of Soil Mechanics and Foundation Engineering (ASCE) 1968;94(4):951-79.

[4] Emad K, Manolis GD. Shallow trenches and propagation of surface waves. Journal of the Engineering Mechanics Division (ASCE) 1985;111:279-82.

[5] Beskos DE, Dasgupta G, Vardoulakis IG. Vibration isolation using open or filled trenches Part 1: 2-D homogeneous soil. Computational Mechanics 1986;1(1):43-63.

[6] Dasgupta G, Beskos DE, Vardoulakis IG. Vibration isolation using open or filled trenches Part 2: 3-D homogeneous soil. Computational Mechanics 1990;1:129-42.

[7] Leung KL, Beskos DE, Vardoulakis IG. Vibration isolation using open or filled trenches Part 3: 2-D non-homogeneous soil. Computational Mechanics 1990;1:137-48.

[8] Leung KL, Vardoulakis IG, Beskos DE, Tassoulas JL. Vibration isolation by trenches in continuously nonhomogeneous soil by the BEM. Soil Dynamics and Earthquake Engineering 1991;10(1):172-9.

[9] Al-Hussaini TM, Ahmad S. Design of wave barriers for reduction of horizontal ground vibration. Journal of Geotechnical Engineering (ASCE) 1991;117(4):616-36.

[10] Ahmad S, Al-Hussaini TM, Fishman KL. An investigation on active isolation of machine foundation by open trenches. Journal of Geotechnical Engineering (ASCE) 1996;122(6):454-64.

[11] Klein R, Antes H, Le Houédec D. Efficient 3D modelling of vibration isolation by open trenches. Computers and Structures 1997;64(1-4):809-17.

[12] Al-Hussaini TM, Ahmad S. Active isolation of machine foundations by in-filled trench barriers. Journal of Geotechnical Engineering (ASCE) 1996;122(4):288-94.

[13] Kattis SE, Polyzos D, Beskos DE. Modelling of pile wave barriers by effective trenches and their screening effectiveness. Soil Dynamics and Earthquake Engineering 1999;18(1):1-10.

[14] Yang YB, Hung HH. A parametric study of wave barriers for reduction of train-induced vibrations. International Journal for Numerical Methods in Engineering, 1997;40(20):3729-47.

[15] Shrivastava RK, Kameswara Rao NSV. Response of soil media due to impulse loads and isolation using trenches. Soil Dynamics and Earthquake Engineering 2002;22(8):695-702.

[16] Hung HH, Yang YB, Chang DW. Wave barriers for reduction of train-induced vibrations in soils. Journal of Geotechnical Geoenvironmental Engineering (ASCE) 2004;130(12):1283-91.

[17] Wang JG, Sun W, Anand S. Numerical investigation on active isolation of ground shock by soft porous layers. Journal of Sound and Vibration 2009;321:492-509.

[18] Alzawi A, El Naggar MH. Full scale experimental study on vibration scattering using open and in-filled (GeoFoam) wave barriers. Soil Dynamics and Earthquake Engineering 2011;31:306-17.

[19] Adam M, von Estorff O. Reduction of train-induced building vibrations by using open and filled trenches. Computers and Structures 2005;83(1):1124.

[20] Andersen L, Liingaard M. Vibration screening with sheet pile walls. In: Takemiva H editor. Proceedings of the 2nd international Symposium on Environmental Vibrations. Okayama, Japan: 2005. p. 429-37.

[21] Andersen L, Nielsen SRK. Reduction of ground vibration by means of barriers or soil improvement along a railway track. Soil Dynamics and Earthquake Engineering 2005;25(7-10):701-16.

[22] Andersen L, Frigaard P, Augustesen AH. Mitigation of ground vibration by double sheet-pile walls. In: Proceedings of the 8th International Congress on Advances in Civil Engineering, vol. 2. Famagusta, Cyprus: 2008. p. 247-54.

[23] Andersen L, Augustesen AH. Mitigation of traffic-induced ground vibration by inclined wave barriers - A three-dimensional numerical analysis. In: Proceedings of the 16th International Congress on Sound and Vibration. Kraków, Poland: 2009.

[24] Persson P. Analysis of vibrations in high-tech facility, Report TVSM-5164, Division of Structural Mechanics, Lund University, Lund, Sweden, 2010.

[25] Persson P, Persson K. Analysis of dynamic soil-structure interaction at high-tech facility. In: Eriksson A, Tibert G. editors. Proceedings of NSCM-23: the 23rd Nordic Seminar on Computational Mechanics. Stockholm, Sweden: 2010.

[26] Bathe KJ. Finite element procedures, Prentice Hall, New York, 2006.

[27] Zienkiewicz OC, Taylor RL. The finite element method, volume 1 and 2, MacGraw-Hill, London, 1994.

[28] Chopra AK., Dynamics of structures, Prentice Hall, Upper Saddle River, 1995.

[29] Craig Jr RR., Structural dynamics, John Wiley & Sons, New York, 1981.

[30] Sandberg G., Finite element modelling of fluid-structure interaction, Doctoral Thesis, Report TVSM-1002, Division of Structural Mechanics, Lund University, Lund, Sweden, 1986.

[31] Das BM, Ramana GV. Principles of soil dynamics, Cengage Learning, Stamford, 2011.

[32] SGU - Geological Survey of Sweden, MAX IV - Kartering av kärnborrningarna GS1 och GS2, Reference number 08-852/2010, Lund 2010-12-02.

[33] TYRÉNS, Geotechnical investigation report, Reference number 225686G, Helsingborg 2010-12-10.

Paper B

Reduction in ground vibrations by using shaped landscapes

Peter Persson, Kent Persson and Göran Sandberg

Division of Structural Mechanics
Lund University
Sweden

Submitted for publication

Reduction in ground vibrations by using shaped landscapes

Peter Persson, Kent Persson, Göran Sandberg
Department of Construction Sciences, Lund University, Sweden
Submitted for publication

Abstract

Reduction in traffic-induced ground vibrations by use of shaped landscapes is investigated here by shaping the landscape surrounding a high-tech facility, using the landscape thus produced as a wave obstacle. The effects of the geometric parameters of a shaped landscape were examined in parametric studies. An architectural landscape design was also investigated in terms of its effectiveness in reducing traffic-induced ground vibrations. A finite element method involving use of both finite and infinite elements in the frequency domain was employed. The finite element models employed involve a layer of soil and the underlying bedrock. It was found that anywhere from an appreciable reduction to an appreciable amplification of the vibrations produced can occur, depending upon the geometric parameters of the shaped landscape involved. The shaped landscape that was most effective was found to reduce the level of vibration by approximately 35 %.

Keywords: Vibration reduction; shaped landscape; wave propagation; finite element method; traffic-induced vibrations; soil dynamics; infinite elements; ground vibration; irregular topography.

1 Introduction

Occasionally, very strict vibrational requirements are specified for sensitive equipment used in high-tech facilities, such as radar towers and synchrotron facilities. Regardless of whether the sensitive equipment in itself is a significant source of vibration, or not, it is important to isolate it from external vibrations. High-tech facilities are often located in the vicinity of sources of vibrations of significant amplitude, radar towers often being found near rocket-launching facilities, for example, and synchrotrons near heavily trafficked roads, the latter for logistic reasons. The traffic-induced ground vibrations can propagate to facilities nearby and lead to the vibration requirements for sensitive equipment there being exceeded. It can be desirable under such conditions to reduce the ground vibrations by use of wave obstacles. The traffic-induced vibrations involved can be reduced by various means, such as by shaping the landscape between the road and the facility.

It is known from previous studies [1, 2, 3] concerning the synchrotron facility MAX IV in Lund, Sweden that the material parameters of the soil there have a strong effect on the vibration levels that occur in sensitive parts of the facility, whereas structural modifications of the facility itself have only a negligible effect. Most of the vibration energy produced by vibrations induced on the ground surface is transmitted by Rayleigh surface waves that propagate close to the ground surface. Since Rayleigh waves attenuate with horizontal distance as well as with depth, the ground vibrations can be reduced by constructing a suitable wave obstacle in the ground between the wave source and the facility that is to be protected. Body waves propagate as a hemispherical wave front, whereas Rayleigh waves propagate radially as a cylindrical wave front [4]. The attenuation of the body waves is thus proportional to 1/r, the attenuation of the Rayleigh waves, in contrast, being proportional to $\sqrt{1/r}$. Thus, at a relatively large distance from a vibration source the Rayleigh waves become the dominant wave form.

Constructing a shaped landscape as a wave obstacle between a vibration source and a facility creates a discontinuity for the propagating waves. Waves that are incident to the shaped landscape show different types of behaviours that are associated with changes in direction of the propagating waves. They are subjected to reflection as well as diffraction at the boundaries of the shaped landscape. These two phenomena scatter the wave front and reduce the level of vibration at the facility.

At large construction sites, large amounts of soil are excavated in order to level the ground surface. This is necessary since, generally speaking, the surface needs to be horizontal before the construction of a building begins, the loose topsoil needing to be removed. The large amounts of excavated soil produced often need to be transported away from the construction site, which can be costly for the construction project. If instead, these soil masses can serve a useful purpose at the construction site, they can be retained and be used to construct a shaped landscape with hills and valleys, for example; see Figure 1. This shaped landscape can serve to reduce traffic-induced ground vibrations incident to the facility. The architects associated with the MAX IV project have developed a design for a shaped landscape of the surroundings of the MAX IV facility, one based on ideas introduced by the Department of Construction Sciences at Lund University. Such a shaped landscape is regarded as representing an aesthetically desirable solution.

In the paper, various results concerning the reductions in vibration at the MAX IV synchrotron facility that the shaped landscape there which is planned is expected to bring about serve as numerical examples of the various principles involved. Figure 1 presents an architectural sketch of the facility as planned. MAX IV is to be built approximately 100 m from the highway E22. In the MAX IV facility, a beam of electrons is to be controlled by a large number of magnets that are distributed along the ring-shaped structure and along beam lines that lead beams of electrons to measurement stations. Since the quality of the measurements obtained is dependent upon the levels of vibration of the magnets, very strict requirements regarding the vibration levels produced have been specified. The vibration requirements for MAX IV regarding vertical displacements of the magnets are especially strict, its being required that these be less than 20-30 nm in RMS per second within a frequency span of 5-100 Hz.

Figure 1: The MAX IV facility as it is expected to appear, as rendering in a drawing by the architectural bureaus FOJAB and Snøhetta.

1.1 Literature review

Several investigations of the effects of irregular topography on ground vibrations have been carried out.

Lee and Wu [5, 6] presented a numerical solution for the two-dimensional (2D) scattering and diffraction of plane P, SV and SH waves by canyons of arbitrary shape in an elastic half space. The displacements were computed numerically using the method of weighted residuals (moment method). It was concluded that the ground vibrations were frequency dependent and were also dependent upon the orientation of the incident waves. It was found that the shape of the canyon had an effect on the displacement amplitudes at the surface of the canyon and in the nearby half space [6]. Zhou and Chen [7] investigated the effect of topography on Rayleigh waves excited by an explosive source near the surface, their employing the local indirect wave-number method. The energy and the frequency content of waves before and after passing through the topography involved were compared in order to evaluate the effect of the steepness of the topography. Reduction in the energy of the waves and loss of their high frequency content were found to occur. The authors concluded that these effects were more obvious where the topography was steeper.

Mossessian and Dravinski [8] investigated through use of an indirect boundary integral method the diffraction of plane harmonic waves by three-dimensional (3D) surface irregularities. The irregular shapes were arbitrary and were embedded in the half-space. It was found to be important to use 3D numerical models when investigating the scattering of elastic waves by surface topographies of arbitrary shape. Sánchez-Sesma and Campillo [9] investigated the topographical effects for P, SV and Rayleigh waves in an elastic half-space, through use of an indirect boundary element (BE) method, their finding that the topography can have an appreciable effect on both the amplification and the reduction in the level of vibration at or nearby the topographic features in question. Reinoso, Wro-

bel and Power [10] investigated through use of a direct BE method the 3D scattering of seismic waves from irregular topographies, due to the presence of incident P-, S- and Rayleigh waves in the time domain involved. The irregular shapes were those of both mountains and valleys. It was found that an irregularity, such as a mountain, affects by way of its geometry the level of amplification achieved. It was concluded that mountains with vertical walls generate higher amplification levels than walls of mountains with a smooth slope. Nguyen and Gatmiri [11] used a 2D direct BE method for examining the scattering of seismic waves by topographic features of different types. They found that a topographic feature modifies the seismic waves at and near to the topographic feature in question. Zhenning and Jianwen [12] investigated the scattering of incident SV waves by a canyon in a layered half-space through use of an indirect BE method. They found that the presence of a layered half-space affects both the displacement amplitudes on the ground surface and the frequency content of the displacements. They observed that the displacements obtained depended upon the type of excitation.

Bouckovalas and Papadimitriou [13] studied effects of the topography and of vertically propagating SV waves on seismic ground vibration in step-like ground slopes. The finite difference (FD) method was used in a parametric study conducted. It was found that the topography involved can lead to either an amplification or a reduction in the level of vibration at the crest of the slope or nearby. Amplification generally occurs near the crest, and reduction at the toe, of the slope. Ducellier and Aochi [14] developed an FD-FE method for modelling seismic wave propagation in a 2D elastic medium having an irregular surface topography. To study amplification effects there, numerical simulations of seismic wave propagation in a series of hills were carried out and were compared with a single-hill case. The authors found that the presence of several hills, as opposed to a single hill, can increase the amplification effects produced by the topography of the ground surface. They concluded that in evaluating topographic site effects the surrounding topography needs to be taken into account alongside the local topography.

Chongbin Zhao and Valliappan [15] used a coupled finite and infinite element method to develop a numerical model for studying wave scattering effects in the frequency domain involved. They concluded that the effect of canyon topographic and geologic conditions on ground vibrations due to P and SV earthquake waves can affect dramatically both the peak value and the frequency content of the free-field vibration occurring along the canyon surface during an earthquake. Athanasopoulos, Pelekis and Leonidou [16] investigated surface topography effects through carrying out 2D seismic response analyses based on use of the finite element (FE) method. They found that a step-like topography amplified the intensity of vibration considerably without affecting the frequency content of the vibration. They concluded that surface topography plays an important role in affecting the intensity of the ground vibration induced by seismic waves. Assimaki, Kausel, Gazetas [17] performed 2D FE analyses in the time domain for analysing topographic effects, as well as additive contributions of the soil stratigraphy, the heterogeneity of the material and the soil-structure interactions in the ground vibrations induced by an earthquake. They found the topography to have a strong effect on the seismic waves produced by ground vibrations. Gatmiri, Arson and Nguyen [18] investigated, by use of the FE method in the near-field and the BE method in the far-field, seismic effects due to irregularities of the topography at the ground surface, their carrying out parametric studies of slopes, ridges

and canyons. They concluded that ground vibration is generally amplified at the crest of ridges, at the upper corner of slopes and at the edges of canyons, but that ground vibration is reduced at the base of the different features. Gatmiri and Arson [19] investigated, by means of the FE method in the near-field and the BE method in the far-field, seismic effects due to the topography and the geotechnical characteristics of valleys. They found that horizontal displacements tended to be amplified at the edge and reduced at the centre of empty valleys, but that the horizontal displacements tended to be reduced near the edge and amplified at the centre in the case of sedimentary valleys. Duzgun and Budak [20] investigated the effects of canyon-shaped topographies on ground vibration by use of a finite and infinite element method. They found that both the topography and the geotechnical properties have an appreciable effect on the ground vibration occurring along a canyon.

Beskou and Theodorakopoulos [21] investigated various ways of modelling a road pavement, foundation soil, loads and material behaviour. Analytical and numerical methods, as well as combinations of them were considered under both plane strain and 3D conditions. It was concluded that the FE method appears to be the best numerical method with respect to efficiency, versatility and availability without compromising on accuracy.

1.2 The present study

None of the investigations referred to above considered the characteristics of the traffic loads to be expected. Also, none of them explored the usefulness of shaping the surrounding landscape so as to construct a wave obstacle with the intention of reducing incident ground vibrations so as to protect a vibration-sensitive facility. The main objective of the study was to investigate the use of shaped landscapes (man-made ground surface irregularities) as wave obstacles for minimising traffic-induced vibrations in vibration-sensitive parts of a high-tech facility such as the MAX IV one. Investigating this here was done by creating numerical models based on use of the FE method for predicting the effectiveness of using a shaped landscape as a wave obstacle. The FE models employed makes use of both finite and infinite elements, these being applied both to the soil layer and to the bedrock. The vibrations involved were investigated in the frequency domain by means of steady state analyses, the traffic load on the highway being taken into account in the analyses. The intention here was to extend knowledge of the use of shaped landscapes as wave obstacles. Some preliminary calculations were made in cooperation with the former master thesis student Jørstad [22].

The general knowledge of the reduction in vibration achieved by use of a shaped landscape needs to be extended so as to encompass traffic-induced vibrations from highways generally, to make it possible to meet the increasing needs in the future of placing buildings close to vibration sources such as highways.

2 Governing theory

2.1 Structural dynamics

The equation of motion of a body, assuming small deformations, can be described by the differential equation

$$\tilde{\nabla}^T \sigma + \mathbf{b} = \rho \frac{\partial^2 \mathbf{u}}{\partial t^2} \tag{1}$$

where $\tilde{\nabla}$ is a differential operator matrix, σ is the stress vector, $\mathbf{b}$ the body force vector, ρ the mass density, $\mathbf{u}$ the displacement vector and t is time [23, 24]. The governing finite element formulation of a dynamic problem, as derived from Eq. (1), can be written as

$$\mathbf{M}\ddot{\mathbf{u}} + \mathbf{C}\dot{\mathbf{u}} + \mathbf{K}\mathbf{u} = \mathbf{f} \tag{2}$$

where $\mathbf{M}$ is the mass matrix, $\mathbf{C}$ the damping matrix, $\mathbf{K}$ the stiffness matrix, $\mathbf{f}$ the load vector and $\mathbf{u}$ the nodal displacement vector. In harmonic loading, steady-state vibration occurs. The load and the corresponding displacements can be expressed, therefore, as complex harmonic functions

$$\mathbf{f} = \hat{\mathbf{f}} e^{i\omega t}; \mathbf{u} = \hat{\mathbf{u}} e^{i\omega t} \tag{3}$$

where $\hat{\mathbf{f}}$ and $\hat{\mathbf{u}}$ denote the complex load amplitude and the displacement amplitude, respectively, i is the complex number involved and ω is the angular frequency. Inserting Eq. (3) into Eq. (2) results in the following equation of motion in the frequency domain:

$$\mathbf{D}(\omega)\hat{\mathbf{u}} = \hat{\mathbf{f}} \tag{4}$$

where $\mathbf{D}$ is the frequency-dependent dynamic stiffness matrix, which can be expressed as

$$\mathbf{D}(\omega) = -\omega^2 \mathbf{M} + i\omega \mathbf{C} + \mathbf{K}. \tag{5}$$

Since damping generally plays an important role in the dynamic response in soils, a rate-independent linear damping in the system was assumed. The loss factor which represents the attenuation of the propagating waves is defined as

$$\eta = \frac{1}{2\pi} \frac{E_D}{E_{So}} \tag{6}$$

where in a steady state, the energy dissipated in the form of viscous damping in a given cycle of harmonic vibration being denoted as E_D and the strain energy as E_{So} [25]. E_D can be written as

$$E_D = \pi c \omega u_0^2 \tag{7}$$

where c is the damping constant, u_o is the amplitude of the motion and E_{So} can be written as

$$E_{S_0} = k u_0^2 / 2. \tag{8}$$

where k is the stiffness. Inserting Eq. (7) and Eq. (8) into Eq. (6) gives

$$\eta = \frac{\omega c}{k}. \tag{9}$$

In generalising this to multiple degrees of freedom (dofs), Eq. (9) can be written as

$$\mathbf{K}\eta = \omega\mathbf{C}. \tag{10}$$

Inserting Eq. (10) into Eq. (5) results in

$$\mathbf{D}(\omega) = -\omega^2\mathbf{M} + (1 + i\eta)\mathbf{K}. \tag{11}$$

The imaginary part of the stiffness matrix is referred to as the structural damping matrix [26].

2.2 Evaluation

The RMS value can be used as a measure of the vibration magnitude. The RMS value of the displacements obtained from the steady state analyses was determined by

$$u_{RMS} = \frac{1}{n}\sqrt{(u_1^2 + u_2^2 + ... + u_n^2)} \tag{12}$$

where u_{RMS} is the RMS value of the displacements, u_i is the magnitude of the displacement at each frequency and n is the number of frequencies in the interval.

3 Traffic load and evaluation

Several factors need to be considered in investigating traffic loads such as the speed and weight of passing vehicles, as well as irregularities of the road and inhomogeneous soil conditions [4]. Traffic-induced ground vibrations are transmitted as both body and surface waves.

The vibration requirements for MAX IV are especially strict within a frequency span of 5-100 Hz, and various studies of the MAX IV site [1, 2, 3] have concluded that vibration source frequencies exceeding 25 Hz have only a negligible effect on the amplitudes of vibrations in the facility. From the initial simulations in the present study, it was found that the limit of 25 Hz can be lowered to 20 Hz, due to the ground material parameters being slightly different here. Thus, a frequency span of 5-20 Hz for the traffic load was considered.

The frequency content of the traffic load at the highway near MAX IV was evaluated on the basis of green-field in-situ measurements; see Figure 2 for a schematic presentation

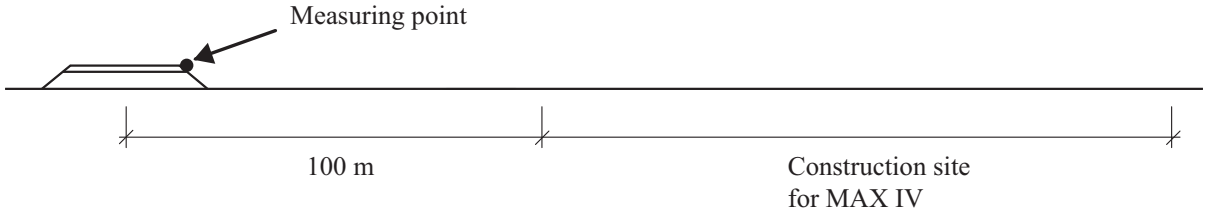

Figure 2: Schematic measurement setup.

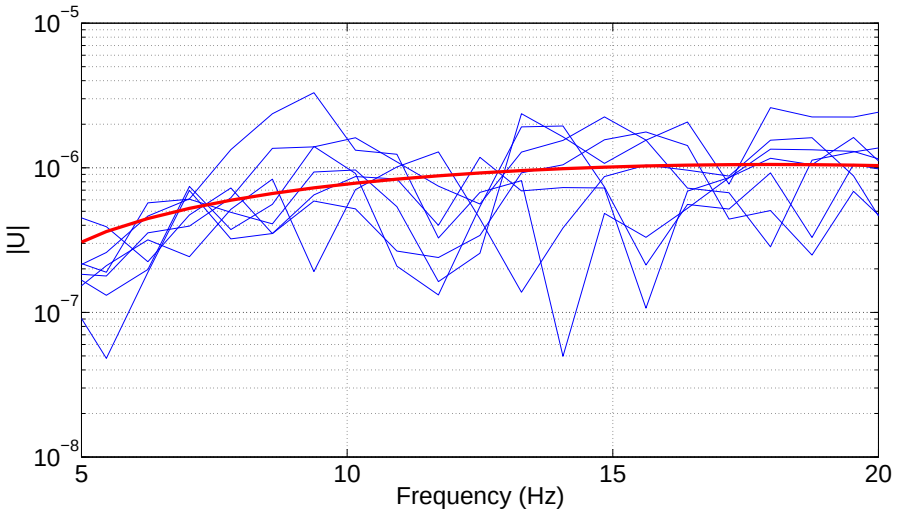

Figure 3: The magnitude spectrum of U(t), as obtained on the basis of measurements.

of the measurement setup. Velocity versus time was measured at the top of the slope of the road embankment of the highway during the passage of trucks, which generated the highest velocities at the measuring point. The ten events having the highest velocity amplitudes, caused by heavy trucks, during a one-hour period were registered. The displacements involved, U(t), were evaluated and a Fast Fourier Transform (FFT) of the displacement-time curves was performed to determine the frequency content of the response at the embankment. Since high frequencies are damped out quickly in the soil, the measurements on the embankment do not have the same frequency content as the traffic load. However, in the frequency range of interest (below 20 Hz) this difference in location was assumed to have only a negligible effect on the frequency content of the load because of the distances between the load (the truck wheels) and the embankment being so short. A second-degree polynomial was fitted to the experimental data; see Figure 3, the second-degree polynomial, normalised by its largest magnitude, being considered to be representative of the frequency content of the traffic load.

Distributed evaluation points were used to calculate an average displacement reduction factor; see Eq. (14). This was used as a measure of the effectiveness of the shaped landscape as a wave obstacle. The displacement reduction factor, U_{red}, pertains to the relationship of the vertical vibrational amplitude after a shaped landscape has been introduced (post-shaped landscape), U_{post}, to the amplitude prior to its being introduced (pre-shaped landscape), U_{pre}, in accordance with Eq. (13). U_{pre} and U_{post} were determined on the basis of the complex displacement magnitudes for the different frequencies, these being calculated as the RMS values at the evaluation points, in accordance with Eq. (12).

$$U_{red} = \frac{U_{pre} - U_{post}}{U_{pre}}. \tag{13}$$

$$\bar{U}_{red} = \frac{1}{n} \sum_{i=1}^{n} U_{red,i} \tag{14}$$

where n is the number of evaluation points.

For traffic-induced ground vibrations, stresses are usually at a level such that the assumption of linear elasticity is applicable, in the case of soil and of bedrock, $\mathbf{M}$, $\mathbf{C}$ and $\mathbf{K}$ thus being constant matrices. With use of a system of linear equations, the frequency content of the traffic load can be employed for scaling the calculated displacements in order to account for the traffic load.

4 Material parameters considered

In the numerical example employed here, that of the synchrotron facility MAX IV, the soil between the highway and the facility consisted of 14 m of a clay till and the bedrock consisted of shale, sandstone and limestone. The soil in the hills was assumed to have the same material properties as the soil prior to its being excavated.

Local variations in the soil layer and the bedrock, such as stratum and granularity, were assumed to be small as compared with the wavelengths in the frequency range of interest. Thus, the soil and the bedrock were modelled as being isotropic homogenous materials. The material parameters employed are shown in Table 1. The loss factors include material damping and geometrical attenuation effects, such as the varying topography of the soil and of the bedrock.

Table 1: Material parameters.

Property	Soil	Bedrock
Density (kg/m^3)	2125	2600
Depth (m)	14	100
Elastic modulus (MPa)	476	8809
Loss factor	0.14	0.04
Poisson's ratio	0.48	0.40

5 A two-dimensional parametric study

A 2D parametric study of shaped landscapes was carried out for differing geometric parameters of the shapes involved. The height (depth) of the hills (valleys), their width and the total number of shapes in the landscape considered were varied. The shapes and the configurations of them are described in detail in subsection 5.2 Configuration of shapes.

5.1 The finite element model

The geometry was that of 14 m of soil and 100 m of bedrock; see Figure 4. The FE model involved the use of a harmonic point load, f(t), applied to the middle of the modelled ground surface, its representing the traffic from the nearby highway; see Figure 4. The harmonic load was applied for frequencies of 5 to 20 Hz in steps of 0.5 Hz. To determine the effectiveness of a shaped landscape evaluation points were used to evaluate the displacements present where MAX IV is being built. The main evaluation point was located

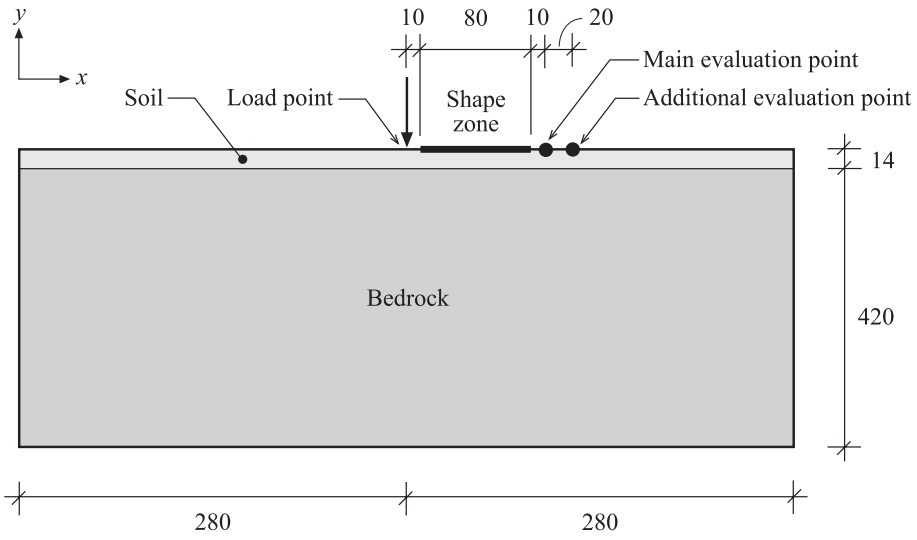

Figure 4: FE model. Dimensions, materials, location of the excitation point, evaluation points and the zone where the shapes were employed are shown. The dimensions are in units of meters.

10 m from the shaped zone (100 m from the excitation point); see Figure 4. An additional evaluation point was introduced to ensure that the response obtained at the main evaluation point was not a local phenomenon. A 2D FE model was developed with the use of the FE software package *HyperWorks 11.0*. The size of the model was 200×560 m^2 (height(z)$\times$width(x)). The distances from the region of interest to the boundaries were large, in order to avoid disturbing reflections at the boundaries. Quadrilateral 4-node plane strain elements with linear approximation were employed. To ensure that the analyses provided results of adequate accuracy, an element mesh with a minimum of seven element nodes that represented the shortest wavelengths were employed. The element size was set to 2×2 m^2 so as to be able to describe accurately the geometry of the hills and valleys in the shaped landscape, the same size being used throughout in the FE model. The model contained approximately 30,000 elements with approximately 121,000 degrees of freedom (dofs).

5.2 Configuration of shapes

The shapes were located in a zone 80 m wide, starting 10 m after the excitation point had been passed and ending 10 m before the evaluation point was reached; see Figure 4. The constant curvature of the various shapes, the maximum slope angle being one of 30 °, served as a constraint. This constraint was employed with the idea that the shapes were to be retained over an extended period of time. The number of shapes was varied across the 80 m wide zone, there being one to six shapes introduced. The shaped landscapes studied consisted of a configuration of different shapes. In Figure 5, the basic geometry that applied to each of the shapes in the configuration is shown, the dimensions of each of the shapes being shown in Table 2. Note that the height, h, could just as well be used to describe the opposite, i.e. the depth of the valleys involved.

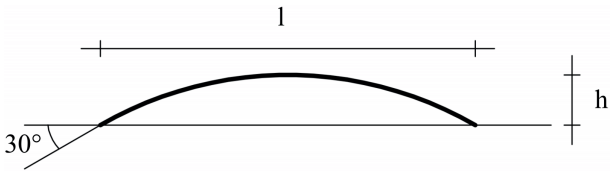

Figure 5: Geometry of one shape. The width (l), the height (h) and the maximum slope are indicated.

Table 2: Width and maximum height of each shape in a configuration.

Configuration	Width, l (m)	Height, h (m)
1 shape	80.0	10.7
2 shapes	40.0	5.36
3 shapes	26.7	3.57
4 shapes	20.0	2.89
5 shapes	16.0	2.14
6 shapes	13.3	1.79

In order to indicate whether a given shape is to be regarded as creating a hill or a valley, a notation of [X X X X] was introduced, where the number of Xs denotes the number of shapes in a given configuration, and where X was either H or V, H denoting a hill and V a valley. A geometric scale factor was used to scale the height of the shapes in a given configuration. This factor was varied between 0.25 and 1 in steps of 0.25. An extra notation, [Y], was introduced so as to be able to denote the geometric scale factor in the form [Y][X X X X], where [0.75][H V H V], for example, implies the geometric scale factor to be 0.75 applied to a configuration of four shapes that began with a hill, and was followed by a valley, then a hill and finally a valley.

For additional examples of the notation of the configurations of the different shapes, see the configurations in Figure 6.

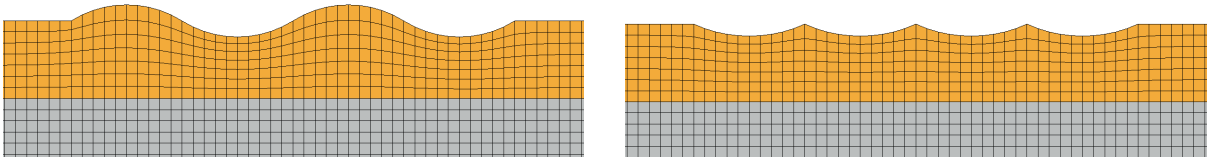

(a) (b)

Figure 6: Two examples of configurations of four shapes, the full extension of the soil and of the bedrock is not shown: (a) geometric scale factor of 1, [1][H V H V], (b) geometric scale factor of 0.75, [0.75][V V V V].

Table 3: The configurations, involving geometric scale factors (pertaining to the height) of 1, 0.75, 0.5 and 0.25.

Configuration	1 shape	2 shapes	3 shapes	4 shapes	5 shapes	6 shapes
Only hills	[H]	[H H]	[H H H]	[H H H H]	[H H H H H]	[H H H H H H]
Alternating hills and valleys		[H V]	[H V H]	[H V H V]	[H V H V H]	[H V H V H V]
Alternating hills and valleys		[V H]	[V H V]	[V H V H]	[V H V H V]	[V H V H V H]
Only valleys	[V]	[V V]	[V V V]	[V V V V]	[V V V V V]	[V V V V V V]

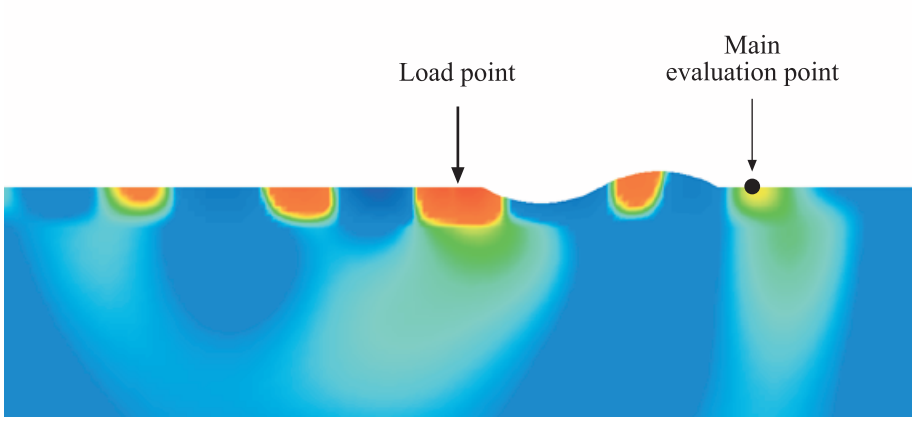

Figure 7: Simulation results for the vertical displacements found at 9.5 Hz for the configuration [1][V H].

5.3 Results

Figure 7 presents simulation results concerning the vertical displacements produced in connection with a configuration consisting of two shapes, [1][V H], at a frequency of 9.5 Hz. As is shown, the level of vibration is lower, at the main evaluation point, after the vibrations have passed through the shaped landscape than it is at the same distance on the other side of the excitation point. It can also be seen that the shaped landscape directs waves into the bedrock.

In Figure 8, the frequency response spectrum for the configurations [1][H V] and [1][V H], respectively, is shown as examples, as well as the frequency response spectrum for a flat landscape. In the figure it is shown that there is a resonance peak in the ground at around 9, 12 and 18 Hz, respectively, considering the the frequencies of interest (5-20 Hz).

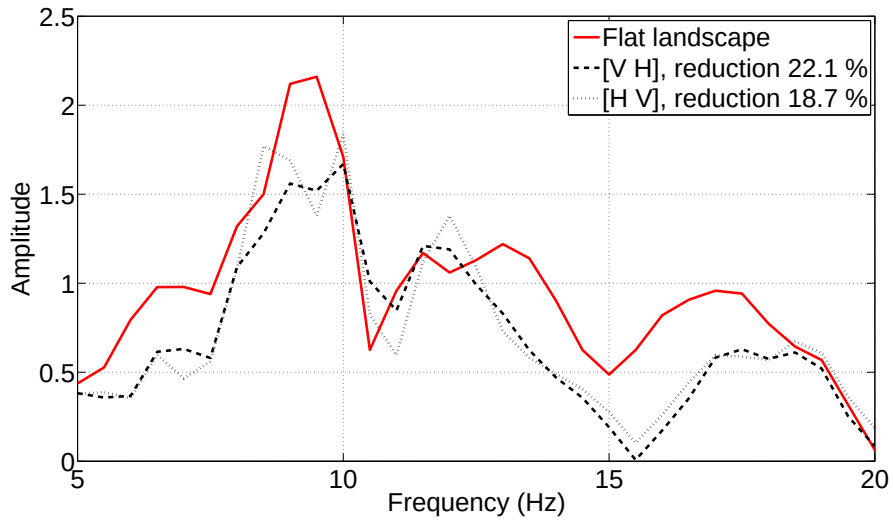

Figure 8: A frequency response spectrum, the configurations involved having a geometric scale factor of 1.

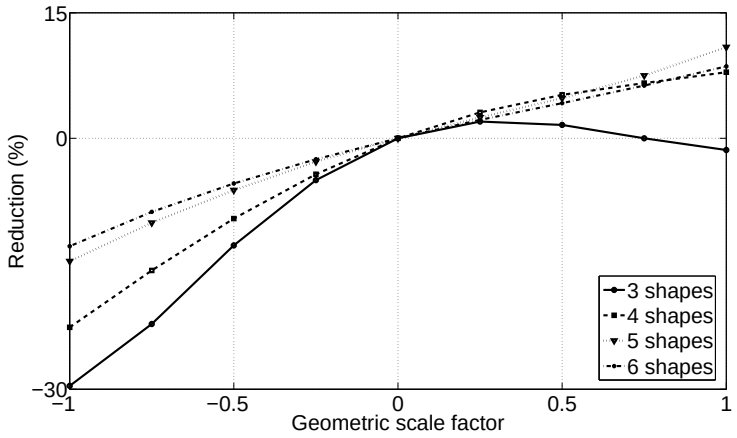

Figure 9: The degree of reduction (amplification is shown as a negative reduction) in the level of vibration in the case of only hills and only valleys, respectively (valleys are denoted by use of a negative geometric scale factor).

The degree of reduction (and amplification) in the level of vibration for different number of shapes and different geometric scale factors for only hills and only valleys, respectively, is shown in Figure 9. As can be seen, for three or more shapes, up to six at least (when there are only hills or only valleys), the behaviour shown is quite similar in each case. Valleys with a geometric scale factor of 1 (the same as hills with a geometric scale factor of -1) have the largest amplification (which is the same as the largest negative reduction) in the level of vibration. The level of amplification in the level of vibration achieved is decreased when the value of the geometric scale factor approaches zero. The degree of reduction in the level of vibration for positive values of the geometric scale factor (hills) is shown in the figure.

In Figure 10, a tendency for the degree of reduction in the level of vibration to decrease as the number of shapes increases can be noted. The plot also shows the complexity of drawing general conclusions, a matter which is especially clear in the case of three shapes (for which the difference in the level of reduction that can be seen are immense).

Figure 11 illustrates how a configuration of hills alone generally results in an appreciably larger reduction in the level of vibration than a configuration of valleys alone produce. Also, a configuration of only one shape deviates from the other numbers of shapes considered here, this illustrating the complexity of drawing general conclusions, especially in the case of three or fewer shapes.

In Table 4, the 10 most effective configurations of 2D shapes, in terms of their reduction of vibrations, are shown. The two most effective configurations consist of two shapes, a valley followed by a hill. Four of the five most effective configurations of shapes consists of two shapes, the one a hill and the other a valley, employed in an alternating manner. None of the top five configurations consisted of more than two shapes. Eight of the nine most effective configurations consisted of alternating hills and valleys (the configuration of one shape was the one that deviated). The most effective configuration, [1][V H], reduced the level of vibration by 22.1 %.

The 10 least effective configurations of 2D shapes in terms of reducing vibrations are

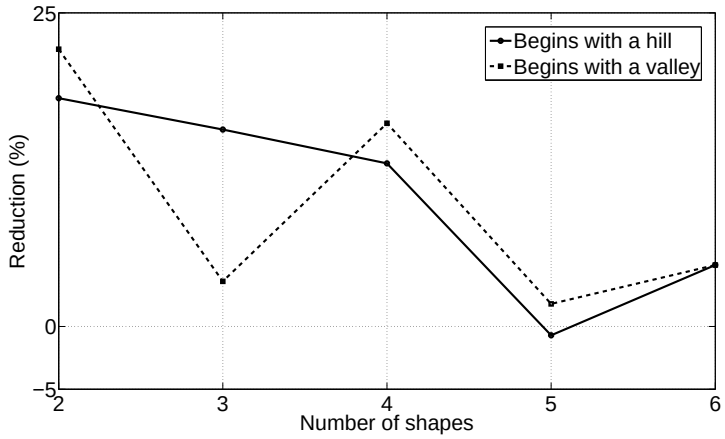

Figure 10: The degree of reduction (amplification is shown as a negative reduction) in the level of vibration in the case of alternating hills and valleys, beginning with a hill and with a valley, respectively. A geometric scale factor of 1 is employed here.

Table 4: The 10 most effective 2D configurations in terms of reducing the level of vibration (displacement).

Configuration	Reduction (%)
[1][V H]	22.1
[0.75][V H]	20.7
[0.75][V]	19.1
[1][H V]	18.7
[0.75][H V]	17.9
[1][V H V H]	16.2
[1][H V H]	15.7
[1][H V H V]	13.0
[0.75][H V H]	12.8
[1][H H H H H]	10.9

shown in Table 5. All of these configurations consists of valleys only, each of them resulting in an amplification of the vibration level. The least effective configuration for each of the different numbers of shapes involved was a configuration of valleys only.

All the configurations involving an even number of shapes (2, 4 or 6 shapes) and alternating hills and valleys that started out with a valley were just as effective or more effective than those that started out with a hill. For configurations of five or six shapes, the most effective configurations were those involving hills only, something that was not found to be the case for configurations of fewer shapes. For configurations of two or more shapes, the presence of only valleys led to an amplification of the vibration level, regardless of the geometric scale factor that was applied. Generally speaking, configurations having more valleys than hills showed an amplification in the level of vibration (though not in the case of a configuration involving only one shape). This emphasises how important it is to be careful, in designing a shaped landscape, to make the correct decision regarding

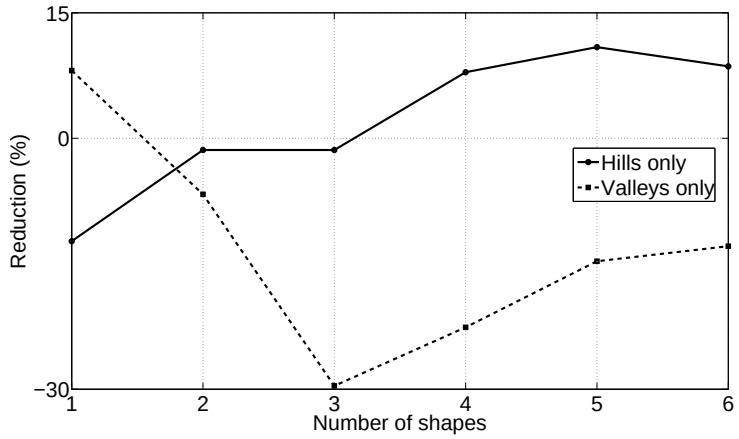

Figure 11: The degree of reduction (amplification is shown as a negative reduction) in the level of vibration for only hills and only valleys, respectively. A geometric scale factor of 1 is employed here.

Table 5: The 10 least effective configurations of 2D shapes in terms of amplifying the level of vibration (displacement). Amplification is shown as a negative reduction.

Configuration	Reduction (%)
[1][V V V]	-29.6
[1][V V V V]	-22.6
[0.75][V V V]	-22.2
[0.75][V V]	-21.3
[0.5][V V]	-19.1
[0.25][V]	-18.6
[0.75][V V V V]	-15.8
[1][V V V V V]	-14.7
[1][V V V V V V]	-12.9
[0.5][V V V]	-12.8

whether to employ a hill or a valley. In configurations containing only a valley, a reduction in the level of vibration was achieved with use of a geometric scale factor of 0.75 or more.

The level of vibration was also evaluated at an additional evaluation point that was located 10 m from the main evaluation point, i.e. 20 m from the shaped zone and 110 m from the excitation point, for each of the configurations involving use of a geometric scale factor of 1. The responses at the additional evaluation point were found to show basically the same tendencies as those at the main evaluation point.

6 A three-dimensional parametric study

A 3D parametric study of shaped landscapes for differing geometric parameters of the shapes involved was carried out. The height (depth) of the hills (valleys), their width and the numbers of shapes in the landscape were varied. Use of 3D FE models also allowed

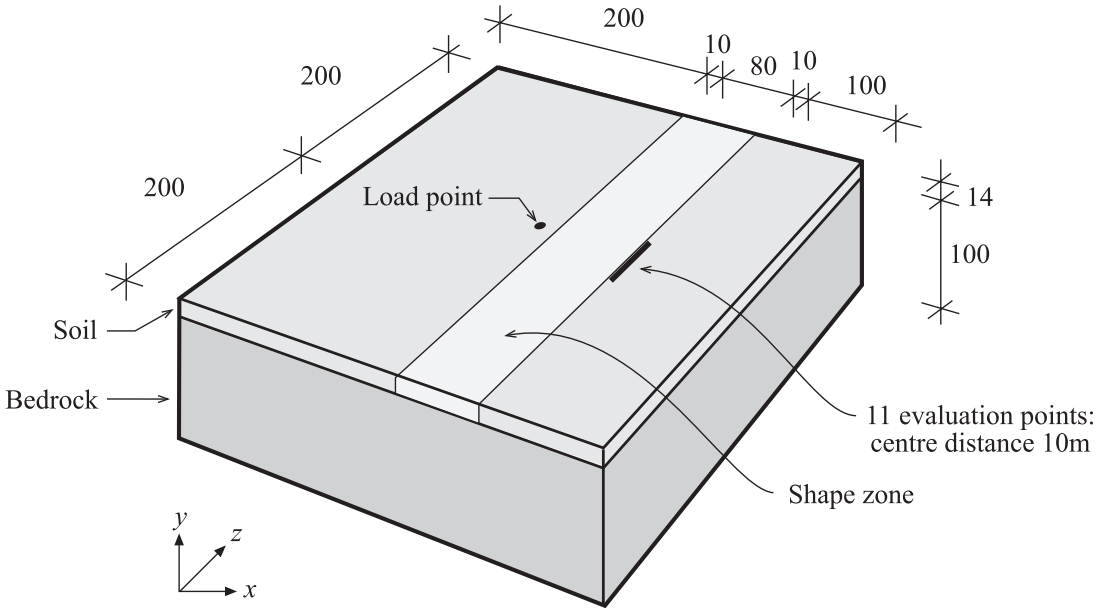

Figure 12: The FE model, showing the dimensions and the materials involved, the location of the excitation point and the locations of the evaluation points, and the zone in which the different shapes were employed. The dimensions are given in units of meters.

the traffic load to be applied as a point load rather than as a line load as it is in the case of 2D plain strain models. The shapes employed and the types of configuration of them involved are described in detail in subsection 6.2 Configuration of shapes.

6.1 The finite element model

A 3D FE model was developed with use of the FE software package *HyperWorks 11.0*. The size of the model was 400×400×114 m^3 (length(x)×width(y)×height(z)). In the z-direction, the geometry was that of 14 m of soil and 100 m of bedrock; see Figure 12. It was seen to it that the distances from the region of interest to the boundaries were large throughout, in order to avoid occurrence of disturbing reflections at the boundaries. Quadrilateral 8-node hexahedron solid elements with linear approximation were employed. To ensure that the analyses provided results of adequate accuracy, an element mesh with a minimum of seven element nodes representing the shortest wavelengths were employed. The element size was set to 2×2 m^2 in the shape zone, in order to be able to describe accurately the geometry of the hills and valleys in the shaped landscape. The model was meshed symmetrically in the horizontal (x-y) plane, the x-z-plane and the y-z-plane being the planes of symmetry. An element size of 2×2 m^2 was employed in the x-y plane, in a 120 m long zone stretching from the excitation point on through zones of increasing element size (four elements having an element length of 4 m, followed by four elements having an element length of 6 m, and finally four elements with an element length of 10 m). In the vertical (z) direction, use was made of elements 2 m in length in the soil, in the bedrock the first eight elements in the vertical direction each being 4 m in length, these being followed by six elements each 6 m in length, and then by four elements each

8 m in length. The FE mesh can be seen in Figure 13. Since the bedrock is much stiffer than the soil, which contributes to the longer wavelengths in the bedrock, the element sizes in the bedrock were larger than the element sizes in the soil. The model contained approximately 518,000 elements, its having approximately 1,100,000 dofs.

The FE model involved the use of a harmonic point load, f(t), applied to the centre of the modelled ground surface, its representing the traffic from the nearby highway; see Figure 12. The harmonic load was applied for frequencies of 5 to 20 Hz, in steps of 1/3-octave bands (5, 6.3, 8, 10, 12.5, 16 and 20 Hz, respectively).

For determining the effectiveness of a shaped landscape in 3D terms, use was made of several evaluation points in evaluating the displacements at the MAX IV site. The main evaluation point was located 10 m from the shaped zone (and 100 m from the excitation point); see Figure 12. Because of the scattering of the propagating waves when considered in 3D terms, the displacements were evaluated along a straight line; see Figure 12. A total of 11 evaluation points, with a distance of 10 m between successive ones, were placed along this line, the main evaluation point in the middle corresponding to the shortest distance to the excitation point. In comparing the results obtained here with the values obtained for the degree of reduction in the 2D analyses, use was made of the respective responses at the main evaluation points.

6.2 Configuration of shapes

In the same manner as for the configuration of 2D shapes, the shapes here were employed in a zone 80 m wide, starting 10 m after the excitation point had been passed and ending 10 m before the evaluation point was reached; see Figure 12. A constant curvature of the shapes, as well as a maximum slope angle of 30 °, served as geometric constraints here, just as for the 2D shapes. The number of shapes was varied, between the use of two and of four different shapes over the 80 m wide zone. each of the shaped landscapes studied consisting of a configuration of different shapes. The geometry of each shape in the configuration is shown in Figure 5, and the dimensions of each of the shapes in Table 2. Note that the height, h, here just as in the case of the 2D shapes, could just as well be directed in the opposite direction, i.e. for denoting the depth of a valley. The 3D shapes here followed the same name conventions as in the study of 2D shapes. In this 3D study, only a geometric scale factor of 1 was considered.

Three different types of configurations were investigated: straight shapes, rotated shapes and a chequered configuration of shapes; see Figure 13. A configuration of straight shapes corresponded, geometrically, to a configuration of 2D shapes, since the 2D shapes

Table 6: The analysed configurations of straight shapes and of rotated shapes, as well as the analysed chequered configurations of shapes.

Configuration	2 shapes	3 shapes	4 shapes
Only hills	[H H]	[H H H]	[H H H H]
Alternated hills/valleys	[H V]	[H V H]	[H V H V]
Alternated hills/valleys	[V H]	[V H V]	[V H V H]
Only valleys	[V V]	[V V V]	[V V V V]

were extended in the out-of-plane direction. In the configurations of rotated shapes, the shapes were rotated 45 ° in the horizontal (x-y) plane in relation to the straight shapes. The chequered configuration of shapes was the one that in geometric terms resembled the architectural design of the shaped landscape the most; see Figure 1.

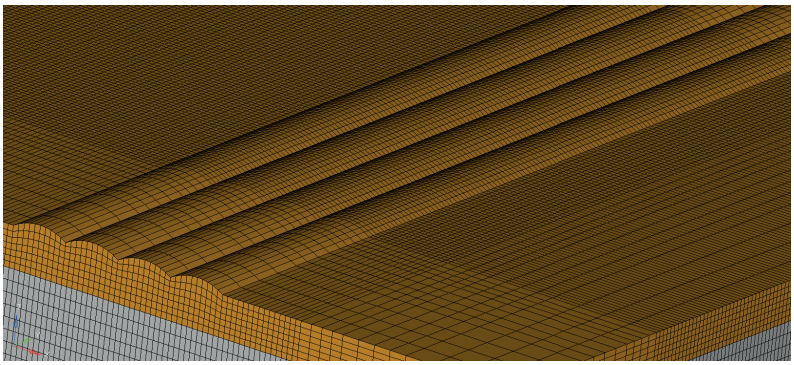

(a)

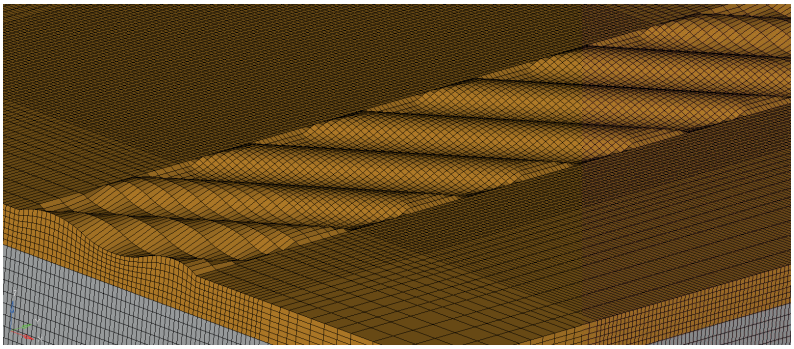

(b)

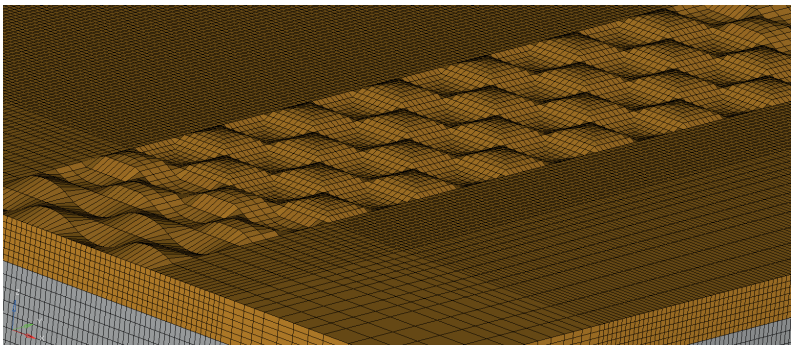

(c)

Figure 13: Examples of different configurations: (a) a configuration of four straight shapes, [H H H H], (b) a configuration of four rotated shapes, [H V H V], (c) a chequered configuration of four shapes, [H V H V].

Table 7: Reduction and amplification, respectively, in the level of vibration for different configurations of straight shapes. Amplification is shown as a negative reduction.

2 shapes	Reduction (%)	3 shapes	Reduction (%)	4 shapes	Reduction (%)
[H H]	2.4	[H H H]	-5.2	[H H H H]	-2.8
[H V]	19.6	[H V H]	10.5	[H V H V]	17.3
[V H]	20.9	[V H V]	23.8	[V H V H]	22.8
[V V]	-19.4	[V V V]	-70.0	[V V V V]	-58.4

6.3 Results

In all of the configurations, there was an appreciable reduction in the level of vibration. The results obtained are presented in three separate subsections, each dealing with a different type of configuration.

6.3.1 Configurations of straight shapes

For the simulation results, it was found that a part of the wave entered the first hill that was reached, its then being reflected along inside the hill. This was a particular reason for investigating rotated shapes, in an attempt to guide the waves. This can be seen in Figure 14a. The frequency response spectrum for configurations of alternating hills and valleys involving two, three and four shapes, respectively, is shown in Figure 14b, in which use is made of the main evaluation point. The degree to which a reduction in the level of vibration was achieved is shown in the legend of the plot. As can be seen, the degree of reduction in cases of the three types was somewhat similar, although there was a clear difference between the response for the four shapes configuration and the other two configurations, especially at 10 Hz. As can be seen, of the three types of configurations shown, it is the one with four shapes that resembles the flat landscape most closely in terms of the response spectrum.

In Figure 14c, as one can see, there is a larger reduction in the level of vibration for configurations that begin with a valley than for those that begin with a hill, the difference here depending upon the shapes involved within the range of two to four shapes, at least.

In Table 7, the degree of reduction or amplification in the level of vibration occurring for each of the different configurations of straight shapes examined is shown. As can be seen, a stronger effect on the degree of reduction achieved in the level of vibration occurring was found for configurations that began with a valley than in those that began with a hill. Configurations of valleys alone showed an appreciable amplification in the level of vibration that occurred, whereas configurations of hills alone showed only a slight effect on the level of vibration. The most effective configuration of shapes was one consisting of three shapes, with alternating hills and valleys, beginning with a valley. The reduction in the level of vibration there was found to be one of 23.8 %. Configurations of alternating hills and valleys starting out with a valley were found to be the most effective configurations, regardless of the number of shapes included in the configurations, all such configurations resulting in an appreciable reduction in the level of vibration. Configurations of valleys only were found to be the least effective, all of them resulting in an appreciable amplification in the level of vibration.

Table 8: Reduction and amplification, respectively, in the level of vibration for the configurations of rotated shapes. Amplification is shown as a negative reduction.

2 shapes	Reduction (%)	3 shapes	Reduction (%)	4 shapes	Reduction (%)
[H H]	-1.4	[H H H]	-3.3	[H H H H]	-8.9
[H V]	0.9	[H V H]	8.1	[H V H V]	17.8
[V H]	36.8	[V H V]	25.8	[V H V H]	32.3
[V V]	-10.8	[V V V]	-49.2	[V V V V]	56.3

6.3.2 Configurations of rotated shapes

In the configurations of rotated shapes the incident waves had a different incident angle than in the configurations of straight shapes. The horizontally rotated shapes here were different from the straight shapes in being non-symmetrical in the x-z-plane. This resulted in the responses at the different evaluation points varying, depending upon at which side of the main evaluation point they were located; see Figure 15a. For some configurations, reduction in the level of vibration on the one side and amplification on the opposite side were found. These differences were expected, however, since the phenomenon of the waves being guided by hills was observed already for the straight shapes. Figure 15b shows the frequency response spectrum for a configuration of alternating hills and valleys, three shapes being shown for the two different evaluation points involved. One of the evaluation points was located at the same level on the y-axis as the load point, and the other evaluation point was located 40 m from it in the direction of the y-axis. The degree of reduction or amplification in the level of vibration that was achieved is shown in the legend of the plot. One can note that at the main evaluation point (y=0) an appreciable reduction in the level of vibration was attained, whereas at the other evaluation point (y=40 m) there was an appreciable degree of amplification. The rotated shapes behaved as wave guides, meaning that the degree both of reduction and of amplification achieved in the level of vibration was very sensitive to the evaluation point selected.

Figure 15c shows there to be a significantly greater reduction in the level of vibration for configurations that begins with a valley, as shown for various of the numbers of shapes involved. As can be seen, in the case of two-shape configurations in particular, there is a much larger degree of reduction for a configuration that starts off with a valley than for one that starts off with a hill. One that started off with a valley was found to generate a very appreciable reduction in the level of vibration, whereas one that started off with a hill was found to have only a very slight effect on the degree of reduction that was achieved in the level of vibration.

The reduction and the amplification, respectively, of the level of vibration for configurations of rotated shapes are shown in Table 8. As can be seen, configurations of hills only had only a slight effect on the degree of amplification achieved in the level of vibration. The most effective configuration of shapes was found to be one of two shapes in which there were alternating hills and valleys, beginning with a valley. The reduction in the level of vibration there was found to be 36.8 %. Configurations of alternating hills and valleys starting out with a valley were found to be the most effective configurations, regardless of the number of shapes that were included in the configuration, each of the numbers

involved resulting in an appreciable reduction in the level of vibration. Configurations of valleys only were found to be the least effective configurations, all of them resulting in an appreciable amplification in the level of vibration.

6.3.3 Chequered configurations of shapes

On the basis of the simulation of results carried out, it could be seen that configurations of four shapes with alternating hills and valleys created more obvious diagonals made up of hills, into which the waves were guided, than was the case for constellations of fewer shapes, analogous to the results obtained for rotated shapes; see Figure 16a.

The frequency response spectrum for each of two chequered configurations of four shapes, the one of them with alternating hills and valleys and the other with hills alone, is shown in Figure 16b. Use is made of the main evaluation point here. The degree of reduction in the level of vibration achieved is shown in the legend of the plot. As can be seen, there are appreciable differences between the two configurations, both in the degree of reduction achieved in the level of vibration and in the response obtained. Also, the response that the configuration of hills alone produces resembles most the response to a flat landscape.

In the case of a chequered configuration, a hill (or a valley) has four neighboring valleys (or hills). This means that it is only a part of the wave front that hits a hill (or a valley) first, since on each side the wave front hits a valley (or a hill). This can explain why the reduction in the level of vibration is no greater than it is here, the results for configurations that begin with a valley being shown in Figure 16c and also in Figures 14c and 15c.

The degree of reduction and of amplification, respectively, in the level of vibration for chequered configurations of shapes are shown in Table 9. As can be seen there, configurations of valleys only result in an appreciable amplification in the level of vibration, their for this reason being found to be the configurations that are the least effective. Configurations of hills only were found to have a lesser effect on the degree of amplification achieved in the level of vibration, than configurations of valleys only had, a reduction in the level of vibration also being seen for two-shape configurations. Three- and four-shape configurations were found to be the most effective configurations in the case of alternating hills and valleys, whereas for two-shape configurations, those of hills alone were found to be the most effective ones. The most effective configuration was a three-shape one involving alternating hills and valleys, beginning with a valley. The reduction in the level of vibration there was found to be 27.2 %.

In comparing the three different types of configurations, both of hills alone and of valleys alone, with one another, marked differences in the degree of reduction achieved between configurations of hills alone, on the one hand, and valleys alone, on the other, were found, as can be seen in Figure 17.

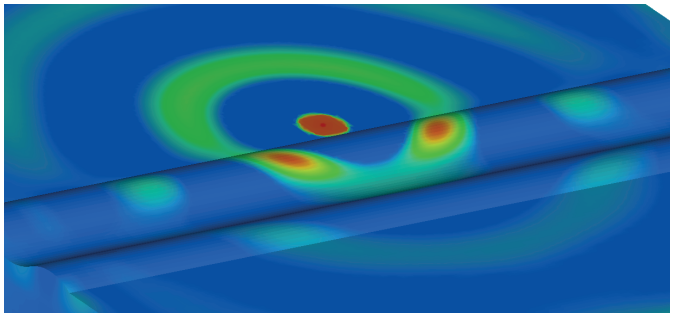

(a)

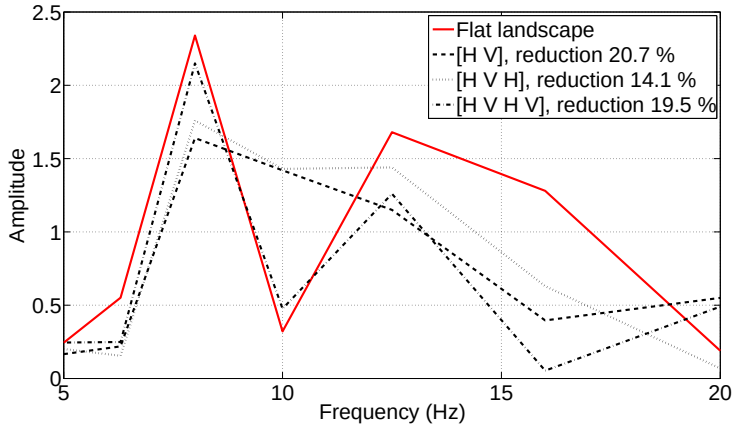

(b)

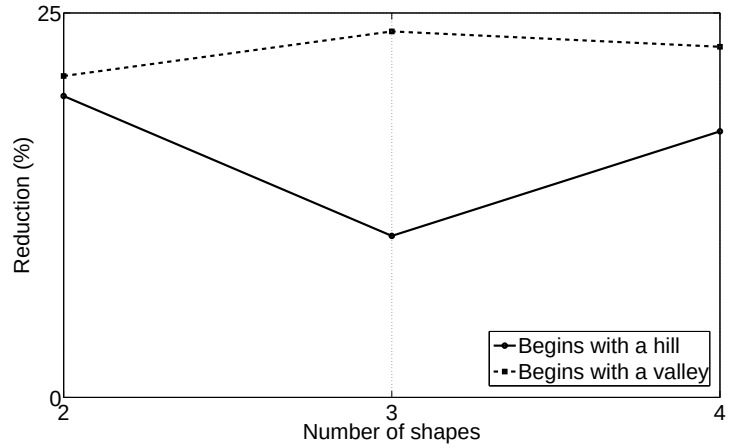

(c)

Figure 14: Different subfigures concerning the result of configurations of straight shapes: (a) Simulation results for the vertical displacements connected with a configuration of three shapes, [H V H]. (b) A frequency response spectrum for each of three different configurations, as well as the frequency response spectrum for a flat landscape. (c) The degree of reduction in the level of vibration for cases of alternating hills and valleys, beginning in the one set of cases with a hill and in the other set of cases with a valley.

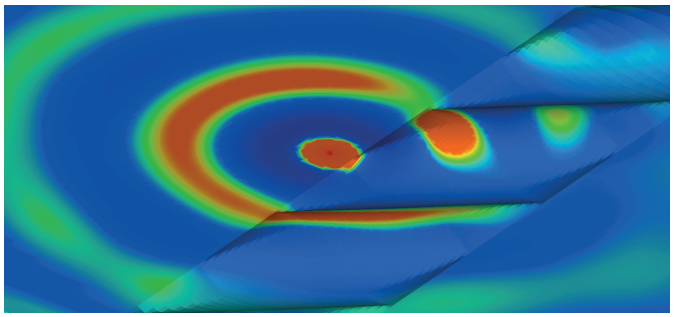

(a)

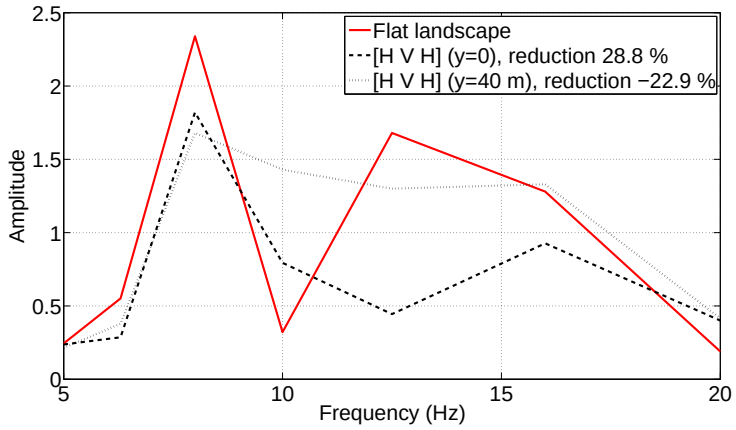

(b)

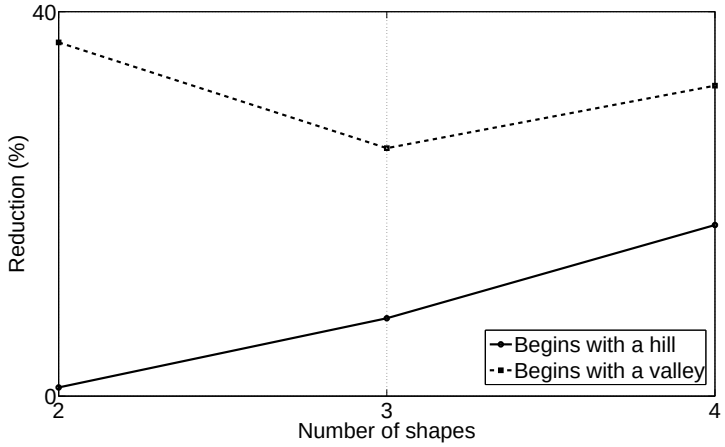

(c)

Figure 15: Different subfigures concerning the result of configurations of rotated shapes: (a) Simulation results for vertical displacements in a configuration consisting of two shapes, [H V]. (b) A frequency response spectrum for two different configurations of shapes, as well as the frequency response spectrum for a flat landscape. Amplification being shown as negative reduction. (c) The degree of reduction in the level of vibration in cases of an alternation of hills and valleys, both those beginning with a hill and those beginning with a valley.

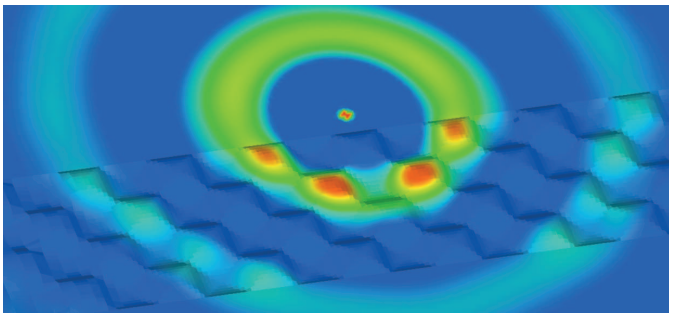

(a)

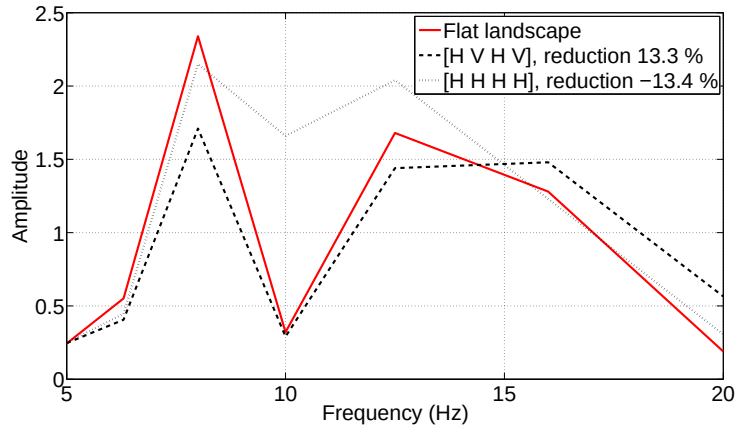

(b)

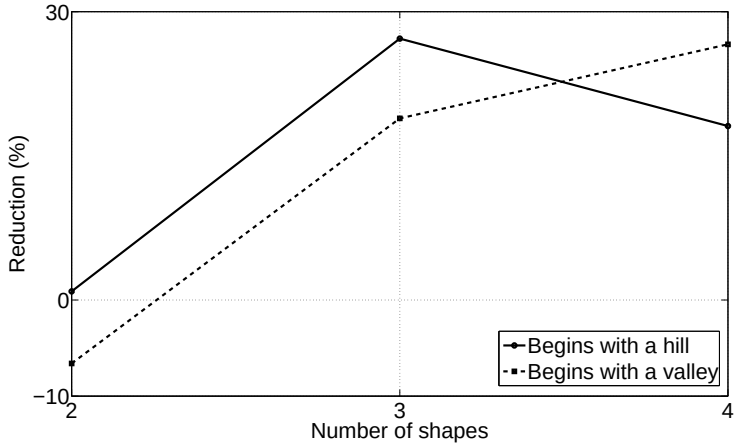

(c)

Figure 16: Different subfigures concerning the result of chequered configurations of shapes: (a) Simulation results for vertical displacements in a configuration consisting of four shapes, [H V H V]. (b) A frequency response spectrum for two different configurations of shapes, as well as the frequency response spectrum for a flat landscape. Amplification being shown as negative reduction. (c) The degree of reduction (amplification being shown here as negative reduction) in the level of vibration for cases of alternating hills and valleys, those beginning with a hill and those beginning with a valley.

Table 9: Reduction and amplification, respectively, in the level of vibration in different chequered configurations of shapes. Amplification is shown as a negative reduction.

2 shapes	Reduction (%)	3 shapes	Reduction (%)	4 shapes	Reduction (%)
[H H]	10.9	[H H H]	-8.8	[H H H H]	-10.2
[H V]	0.9	[H V H]	27.2	[H V H V]	18.1
[V H]	-6.6	[V H V]	18.9	[V H V H]	26.6
[V V]	-44.9	[V V V]	-54.7	[V V V V]	-42.0

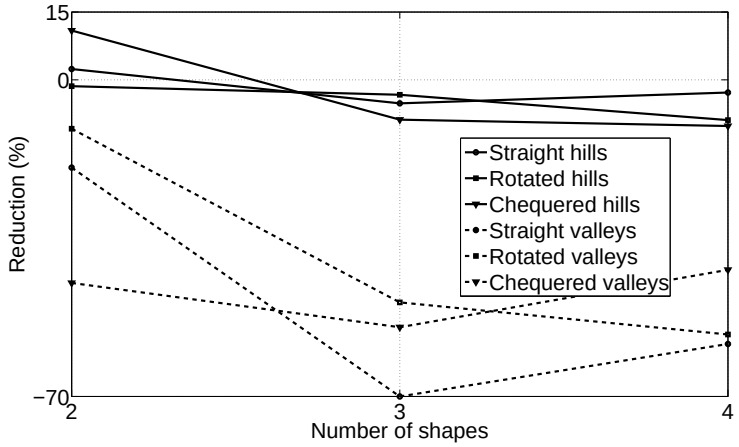

Figure 17: The degree of reduction (amplification being shown as negative reduction) in the level of vibration for different configurations of hills only and of valleys only, all three types of configurations being involved.

7 Three-dimensional architectural design

The landscape architects within the MAX IV project designed a shaped landscape around the MAX IV facility; see Figure 1. In the present investigation, the landscape design was extended to include the area between the highway and the research facility; see Figures 18 and 19. The shaped landscape, designed by the architectural bureaus FOJAB and Snøhetta, was analysed by use of finite element software.

7.1 Finite element model

The shapes contained in the architectural landscape design have a rounded and natural form, which applied as well to the shapes considered in the parametric analyses. The maximum slope angle for the shapes was one of about 30 °, similar to the shapes employed in the parametric studies. The hills had a height of up to about 5.5 m and the valleys a depth of approximately 2.5 m. Both measures concern the vertical distance to the initially flat ground surface. The maximum vertical distance between an adjacent hill and valley was approximately 6 m. The shortest width (distance in along the x-axis) of the shaped

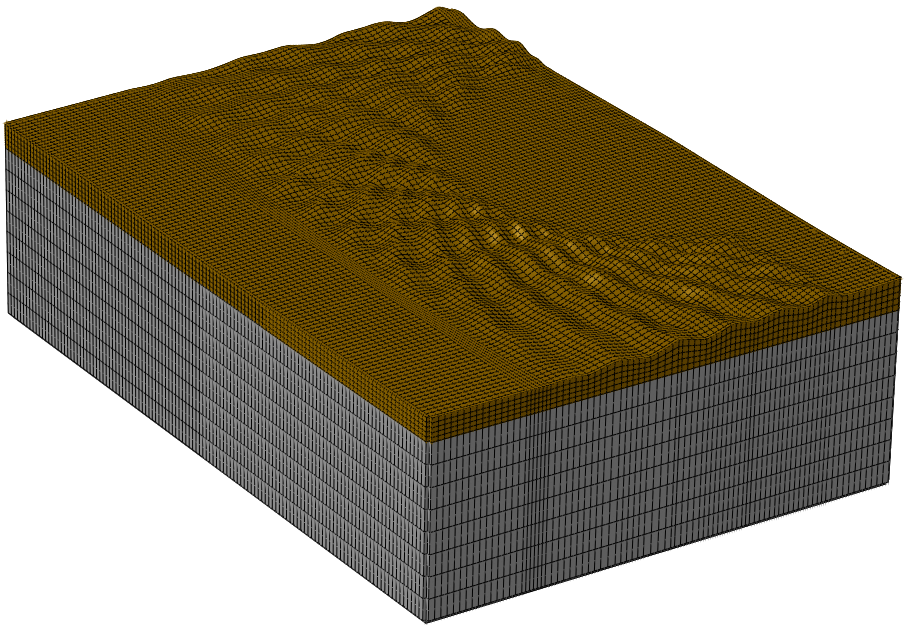

Figure 18: The FE mesh of the architectural landscape design.

landscape was approximately 90 m, its being located at the same level along the y-axis as load position 2.

A 3D FE model was developed with use of the FE software package *Abaqus 6.11*. The model was 420×290×114 m^3 (length(x)×width(y)×height(z)) in size. In the z-direction, the geometry was that of 14 m of soil and 100 m of bedrock; see Figure 18. Quadrilateral 20-node hexahedron solid elements obtained by quadric approximation using reduced integration being employed. To simulate far-field conditions and avoid reflecting boundaries, use was made of 12-node quadratic one-way infinite elements. In order to ensure that the analyses provided results of adequate accuracy, an element mesh with a minimum of seven element nodes representing the shortest wavelengths was employed. The element size in the soil was generally 4.5×4.5×4.5 m^3, so as to able to accurately describe the geometry of the hills and valleys in the shaped landscape. The bedrock was significantly stiffer than the soil, which contributed to long wavelengths being produced there, the element length in the z-direction being increased to 12.5 m in the bedrock. The model contained approximately 148,000 elements with a total of approximately 1,900,000 dofs. See Figure 18 for details regarding the FE mesh.

The FE model involved the use of a harmonic point load, representing the traffic from the nearby highway. The traffic load was applied in three different load positions, so as to be able to investigate different regions of the shaped landscape in terms of its non-symmetric design; see Figure 19a. The different load positions are each located approximately 10 m (in the direction of the x-axis) from where the shape landscape begins, just as in the parametric studies. Load position 2 corresponds to the position of the load in the 3D parametric study. The harmonic load was applied at frequencies ranging from 5 to 20 Hz in steps of 0.1 Hz.

To determine the effectiveness of the architectural landscape design, in terms of its

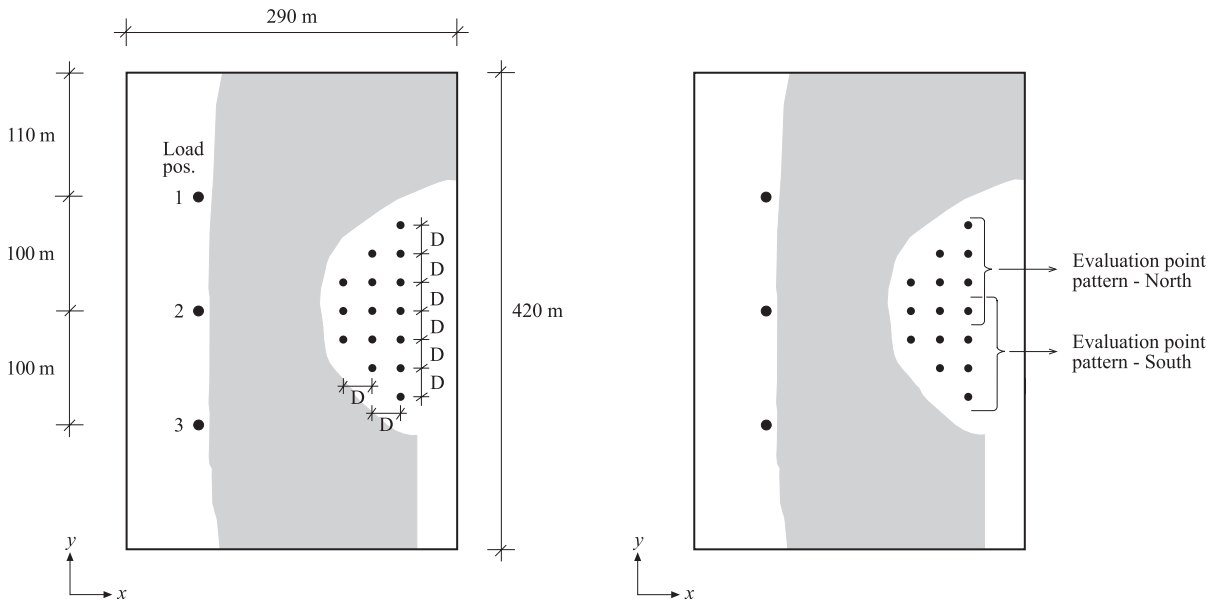

Figure 19: a) Load positions and the evaluation point pattern *All* are shown. Distance, D=25 m. b) Evaluation point patterns *North* and *South* are shown. The grey shading shows the location of the shaped landscape.

reducing the level of vibration, several evaluation points were used for evaluating the displacements that occurred at the MAX IV site. Three different patterns of evaluation points were employed. The pattern *All* included all the 15 evaluation points shown in Figure 19a. The patterns *North* and *South* included 9 evaluation points each; see Figure 19b. The first column of evaluation points is located approximately 20 m (in the direction of the x-axis) from the shaped landscape.

7.2 Results

The reduction in the vibration level obtained for different evaluation point patterns and load positions is shown in Table 10. One can note that the largest reductions in the level of vibration were for load position 1 and the lowest reductions were for load position 3, regardless of which evaluation point pattern was considered. The difference between load positions 1 and 3 in the degree of reduction achieved was one of approximately 5 % for each of the evaluation point patterns. Thus, the shaped landscapes were more effective in the region between load position 1 and the construction site than between load position 3 and the construction site.

Table 10: Reduction in the level of vibration for different patterns of evaluation points and load positions.

Evaluation point pattern	Load pos. 1 (%)	Load pos. 2 (%)	Load pos. 3 (%)
North	17.4	15.2	12.7
South	19.6	14.9	14.2
All	18.2	16.4	13.0

8 General conclusions

The degree of reduction in traffic-induced ground vibrations expected to be achieved by shaping the surrounding landscape of the high-tech facility MAX IV was investigated. The effects of the geometric parameters of such a shaped landscape were examined by means of parametric studies. An architectural design of a shaped landscape was investigated in terms of its effectiveness in reducing ground vibrations.

On the basis of the results of these investigations, the following general conclusions can be drawn.

- The most effective shaped landscape, within each configuration, was one consisting of alternating hills and valleys.
- The least effective shaped landscape (which resulted in amplification of the vibration level) within each configuration was one consisting of valleys only.

The conclusions drawn can be used at an early stage of a construction project to improve the effectiveness of an architectural landscape design through reducing incident ground vibrations.

9 Future work

The fact that the finite elements used to mesh the shapes are deformed so as to be capable of describing the geometry involved can have a certain, if slight, effect on the level of vibration achieved in the FE analyses. This was assumed, however, to not affect the conclusions drawn here. Extended analyses regarding the shape of the deformed finite elements used for the shapes involved here may thus be of interest.

Acknowledgments

The financial support for this work provided by the Silent Spaces project, a part of the EU program Interreg IVA, is gratefully acknowledged.

References

[1] Persson P. Analysis of vibrations in high-tech facility, Report TVSM-5164, Division of Structural Mechanics, Lund University, Lund, Sweden, 2010.

[2] Persson P, Persson K. Analysis of dynamic soil-structure interaction at high-tech facility. In: Eriksson A, Tibert G. editors. Proceedings of NSCM-23: the 23rd Nordic Seminar on Computational Mechanics. Stockholm, Sweden: 2010.

[3] Persson P, Persson K., Sandberg G. Reduction of traffic-induced vibrations at high-tech facility using trenches. In: Freund J, Kouhia R. editors. Proceedings of NSCM-24: the 24rd Nordic Seminar on Computational Mechanics. Helsinki, Finland: 2011.

[4] Das BM, Ramana GV. Principles of soil dynamics, Cengage Learning, Stamford, 2011.

[5] Lee V. W., Wu X., Application of the weighted residual method to diffraction by 2-D canyons of arbitrary shape: I. Incident SH waves, Soil Dynamics and Earthquake Engineering, 13, 355-364, 1994.

[6] Lee V. W., Wu X., Application of the weighted residual method to diffraction by 2-D canyons of arbitrary shape: II. Incident P, SV and Rayleigh waves, Soil Dynamics and Earthquake Engineering, 13, 365-375, 1994.

[7] Zhou H., Chen X-F., A study on the effect of depressed topography on Rayleigh surface wave, Chinese journal of geophysics, 50(4), 1018-1025, 2007.

[8] Mossessian T. K., Dravinski M., Scattering of elastic waves by three-dimensional surface topographies, Wave motion, 11, 579-592, 1989.

[9] Sánchez-Sesma F. J., Campillo M., Topographic effects for incident P, SV and Rayleigh waves, Tectonophysics, 218, 113-125, 1993.

[10] Reinoso E., Wrobel L. C., Power H., Three-dimensional scattering of seismic waves from topographical structures, Soil Dynamics and Earthquake Engineering, 16, 41-61, 1997.

[11] Nguyen K-V., Gatmiri B., Evaluation of seismic ground motion induced by topographic irregularity, Soil Dynamics and Earthquake Engineering, 27, 183-188, 2007.

[12] Zhenning B., Jianwen L., "2.5D scattering of incident plane SV waves by a canyon in layered half-space", Earthquake engineering and engineering vibration, 9, 587-595, 2010.

[13] Bouckovalas G. D., Papadimitriou A. G., Numerical evaluation of slope topography effects on seismic ground motion, Soil Dynamics and Earthquake Engineering, 25, 547-558, 2005.

[14] Ducellier A., Aochi H., "Interactions between topographic irregularities and seismic ground motion investigated using a hybrid FD-FE method", Bull Earthquake Eng, 10, 773-792, 2012.

[15] Chongbin Zhao, Valliappan S., Seismic wave scattering effects under different canyon topographic and geological conditions, Soil Dynamics and Earthquake Engineering, 12, 129-1 43, 1993.

[16] Athanasopoulos G. A., Pelekis P. C., Leonidou E. A., Effects of surface topography on seismic ground response in the Egion (Greece) 15 June 1995 earthquake, Soil Dynamics and Earthquake Engineering, 18, 135-149, 1999.

[17] Assimaki D., Kausel E., Gazetas G., Wave propagation and soilstructure interaction on a cliff crest during the 1999 Athens Earthquake, Soil Dynamics and Earthquake Engineering, 25, 513-527, 2005.

[18] Gatmiri B., Arson C., Nguyen K-V., Seismic site effects by an optimized 2D BE/FE method I. Theory, numerical optimization and application to topographical irregularities, Soil Dynamics and Earthquake Engineering, 28, 632-645, 2008.

[19] Gatmiri B., Arson C., Seismic site effects by an optimized 2D BE/FE method II. Quantification of site effects in two-dimensional sedimentary valleys, Soil Dynamics and Earthquake Engineering, 28, 632-645, 2008.

[20] Duzgun O. A., Budak A., A study on soil-structure interaction analysis in canyon-shaped topographies, Sadhana, 35(3), 255-277, 2010.

[21] Beskou N. D., Theodorakopoulos D. D., "Dynamic effects of moving loads on road pavements: A review", Soil dynamics and earthquake engineering, 31, 547-567, 2011.

[22] Jørstad P. Vibration reduction by shaping the terrain topography, Report TVSM-5183, Division of Structural Mechanics, Lund University, Lund, Sweden, 2012.

[23] Bathe KJ. Finite element procedures, Prentice Hall, New York, 2006.

[24] Zienkiewicz OC, Taylor RL. The finite element method, volume 1 and 2, MacGraw-Hill, London, 1994.

[25] Chopra AK., Dynamics of structures, Prentice Hall, Upper Saddle River, 1995.

[26] Craig Jr RR., Structural dynamics, John Wiley & Sons, New York, 1981.